(E75-10226) STUDY TO DEMONSTRATE THE FEASIBILITY OF AND DETERMINE THE OPTIMUM METHOD FOR REMOTE HAZE MONITORING BY SATELLITE Final Report (Aerospace Corp., Los Angeles, Calif.) 103 p HC $5.25

N75-21754

G3/43

Unclas
00226

THE AEROSPACE CORPORATION

STUDY TO DEMONSTRATE THE FEASIBILITY OF AND DETERMINE THE OPTIMUM METHOD FOR REMOTE HAZE MONITORING BY SATELLITE

ERTS-A Proposal Number SR 230
GSFC Identification Number PR 173

Prepared by Ernest H. Rogers
Space Physics Laboratory
The Aerospace Corporation
P. O. Box 92957
Los Angeles, California 90009

FINAL REPORT
DECEMBER 1974

Prepared for

Goddard Space Flight Center
Greenbelt, Maryland 20771

FOREWORD

This report documents the research performed under Contract Number NAS5-21719. Dr. E. H. Rogers was the Principal Investigator. Mr. D. F. Nelson and Dr. C. M. Randall were co-investigators.

The investigators are indebted to Dr. D. R. Hickman for assistance with Mie scattering calculations, to Mr. R. L. Sempek who built and operated the solar aureole brightness monitors, and to Mrs. Eda M. Rogers who piloted the airplane during many of the ground truth observations.

ABSTRACT

ERTS-1 MSS digital data from two consecutive passes over the Los Angeles area were analyzed in a variety of ways to determine the effect of haze on the data. One day, 21 Oct 1972, was quite hazy over Los Angeles. There was light haze over some of the test site and some areas were quite clear. The haze (smog) over Los Angeles was 3,500 feet thick. The visibility was about 5 miles. The particulate scattering optical depth was found to be 0.30 at 0.70 μm from analysis of solar aureole brightness measurements. The second day, 8 Nov 1972, was quite clear with about 10% of the amount of haze present on 21 Oct. The data were analyzed in a variety of ways.

The basic effect of the haze on the MSS data was found to be an overall increase in apparent brightness of the scene. The magnitude of this brightness increase was found to be approximately independent of surface reflectivity, over the range of reflectivities encountered in the test area. The magnitude of the brightness increase was found to decrease with increasing wavelength. The amount of haze present caused no significant decrease in the power spectral density, even at the highest spatial frequencies in the MSS data. It is estimated that the total amount of haze can be measured over water by analysis of the apparent brightness in MSS bands 4, 5, and 6. Only the total amount, not the vertical distribution can be determined. The accuracy is estimated to be 1/2 to 1/3 of the amount of haze present over Los Angeles on 21 Oct 1972. The amount of haze can also be determined over land with about the same or slightly better accuracy, by noting the variation in apparent brightness, if some form of ground truth for that area is known at times of previous ERTS passes over the area. This investigation was based on limited data over a single test site, however, the results are thought to be generally applicable.

CONTENTS

LIST OF TABLES

INTRODUCTION

The purpose of this investigation was to demonstrate the feasibility of and determine the optimum method for remote haze monitoring by a satellite, by analysis of ERTS-1 Multi-Spectral Scanner data.

The approach was to obtain as much ground truth as possible, at the times of ERTS-1 passes over the Test Site (the Los Angeles area), in order to choose appropriate data for the numerical analysis and to correlate the amount of haze with the magnitude of its effect on ERTS-1 MSS data. The type and magnitude of these effects pointed the way toward optimum methods for analysis of ERTS data to obtain the amount of haze present, and an estimate of the accuracy of these methods.

In many respects the ERTS-1 MSS was ideally suited for an analysis such as this. The wavelengths from 0.5 to 1.1 μm lie in a region where Rayleigh scattering is rapidly becoming less important, and where aerosols play a significant role in atmospheric scattering. The presence of four wavelength bands allows one to determine the optimum wavelength for detection of haze, and the relatively high spatial resolution allows one to determine the effects of haze on contrast at high spatial frequencies.

On the other hand, the primary motivation for flying the ERTS-1 satellite was to image the surface of the Earth. The sensor was configured to look straight down, where atmospheric effects are minimized.

GROUND TRUTH

It was necessary to determine the amount and distribution of haze over the test area at the times of ERTS-1 passes. It was also necessary to establish the presence or absence of clouds, especially high thin clouds, which might perturb the analysis. These data were required in order to choose appropriate data for numerical analysis and to correlate the amount of haze with the magntidue of its effect on ERTS multispectral imagery. Several types of ground truth data were obtained. They are described in this section. The data are compiled in Appendix A.

Four types of ground truth data were obtained.

a) Visibility and relative humidity data from airports

b) Air Pollution Control District data

c) Solar aureole brightness

d) Visual and photographic observations from a light airplane. Vertical distribution of haze. Vertical temperature profile.

The first two were obtained from outside ongoing sources. The last two were actively gathered by the investigators specifically for this analysis.

a) Visibility and Relative Humidity Data from Airports

Horizontal visibility at ground level is determined hourly, on the hour, at controlled airports and broadcast continuously for the use of private and commercial pilots.

ERTS-1 passed over our test site between 5 minutes before and one minute after the hour. Therefore, the time of visibility observations coincided nicely with ERTS-1 passes.

Visibility reports were recorded at the time of every ERTS-1 pass over our test area from the following airports, the locations of which are shown in Fig. 1.

1 Los Angeles International
2 Burbank
3 Van Nuys
4 Ontario
5 Orange County
6 Long Beach
7 Torrance
8 Palmdale
9 Palm Springs

The visibility data was not expected to be uniquely correlated with the effects of haze on the ERTS data, because it is a measure of horizontal visibility and does not reflect the vertical profile of the haze. Also, it is a semi-subjective measurement which may vary from observer to observer. It does have the advantage that it is readily available from a large number of sites and is familiar to the technical community.

The visibility data coupled with the measurements of the vertical structure of the haze layer made by the investigators (d) is thought to be a useful measure of the amount of haze.

Relative humidity measurements, which were available from many of these airports, were collected to compliment the Air Pollution Control District particulate density data, as explained below.

b) Air Pollution Control District Data

The Air Pollution Control District, County of Los Angeles, records the amounts of various pollutants at ground level hourly at 12 stations. The locations of these stations, designated by letters A–L, are shown on Fig. 1.

A	Los Angeles	G	Pomona
B	Azusa	H	Inglewood
C	Burbank	I	Whittier
D	West Los Angeles	J	Newhall
E	Long Beach	K	Lancaster
F	Reseda	L	Pasadena

The pollutants measured are:

NO	(parts per hundred million)
NO_2	(parts per hundred million)
O_3	(parts per hundred million)
Hydrocarbons	(parts per million)
CH_4	(parts per million)
CO	(parts per million)
SO_2	(parts per hundred million)
Particulate Density	(Km units x 10)

Km is a measure of particulate density based on the reduction of light reflected from filtered particulates compared with that reflected from clean filter paper.

$$Km = 10 \log_{10} \frac{R_o}{R_m}$$

where R_o is the reflectance of clean Whatman #52 filter paper at 0.40 μm.

R_m is the reflectance after one m^3 of air is filtered through an area of one cm^2.

It has been empirically determined (Ref. 1) that in the case of carbon particles:

$$\text{Carbon particulate density} \approx (7.7) \times (Km)^{1.1} \ \mu gms/m^3.$$

Km measurements alone are not sufficient to define the optical degradation of the atmosphere, because visibility has been found to be strongly dependent on relative humidity for a given value of Km (Ref. 1). Evidently, liquid water forms about the particulate contaminants to an amount determined by the relative humidity, thus significantly increasing the scattering and absorption of radiation in the atmosphere. For this reason, relative humidity measurements made at the local airports were collected along with visibility data.

c) Solar Aureole Brightness

A solar aureole monitor was designed, and two units were built. These instruments measured the brightness of the solar aureole at angles of 1.5, 3.0, and 6.0 deg from the center of the solar disc along the almucantar, i.e., parallel to the horizon, in a spectral band extending from 0.6 μm to 1.0 μm.

The brightness of the solar aureole results from small angle scattering, principally from aerosols, and is therefore a very sensitive monitor of the haze producing aerosols along the path between the observer and the sun (Refs. 2, 3, 4). The broad spectral band was chosen to approximate that of the sum of the ERTS-1 sensors, in order to maximize the correlation of these data with the effects of haze on ERTS-1 data, and to reduce the Rayleigh scattering contribution to the aureole measurements.

These data proved to be less useful than orginally envisioned because only two predetermined locations could be covered during each ERTS-1 pass, whereas the test area covers many areas of vastly different haze conditions. Even a small cloud between the observer and the sun at the time of a pass rendered the aureole monitor useless. There have been very few measurements of the brightness of the solar aureole, therefore, there is almost no base with which to compare the aureole data.

d) Visual and Photographic Observations from a Light Airplane; Vertical Distribution of Haze; Vertical Temperature Profile

Flights were made over the test area, weather permitting, at the times of ERTS-1 passes in a light plane (Cessna 172 or 150).

Visual observations, from above the haze layer, of the location, extent, and relative amounts of haze were recorded. Photographs were taken to document the visual observations and to aid in establishing relative amounts of haze from pass to pass. These photographs were taken using a Honeywell Pentax Spotmatic 35 mm camera with a 50 mm f/1.4 Super-Multi-Coated Takumar lens and a U.V. filter. The Kodachrome II film

was processed by Kodak. Photographs were taken looking both down and toward the horizon in a number of directions. Photographs were taken over a variety of locations in the test area. Time, location, altitude, direction, and camera settings (typically 1/500 Sec at f/4.9) were noted and later written on the cardboard mount of each color slide. Examples of some of these photographs, comparing the haze conditions on 21 October 1972 and 8 November 1972, are shown in Figs. 2-7. It was possible to cover a large part of the test area within 30 min of the ERTS-1 passes in this manner. Even though this method was subjective, the investigators feel that it was the best available method for establishing the haze distribution over the test area at the time of ERTS-1 passes.

The vertical distribution of haze was observed while climbing out from the airport. The top of the haze layer, if one existed, was determined by flying at the top of the layer and noting the altimeter reading.

The vertical temperature profile was taken by recording aircraft outside air temperature vs. altitude.

Summary of Ground Truth Data Obtained at the Times of ERTS-1 Passes

Table I lists the dates of ERTS-1 passes over our test area and the amount of ground truth obtained during each pass.

Through November 1972, ground truth was obtained not only for the pass over Los Angeles, which is the heart of the test area, but also for the adjacent pass (one day earlier) over San Bernardino, which is on the edge of our test area. Data over San Bernardino is less useful than that over Los Angeles and the ground truth was more difficult to obtain. However, because of the unpredictability of the weather and of the lifetime of space-borne sensors, we thought it wise to cover all possible passes until a minimum amount of data useful for our analysis was obtained.

The effort to collect ground truth was stopped on 18 July 1973, because it would not have been possible to obtain and analyze digital tapes from passes at later dates within the time frame of this contract.

The ground truth data are contained in Appendix A.

Table I. Summary of Ground Truth Data Obtained at the Time of ERTS-1 Passes

Date	Area of ERTS-1 Data*	Data Obtained**	Notes
9 Aug 72	SB	a) b)	We were not aware of these ERTS-1 passes, so no active ground truth data was obtained.
10 Aug 72	LA	a) b)	
27 Aug 72	SB	b)	Very cloudy
28 Aug 72	LA	b)	Too cloudy to obtain active ground truth
14 Sept 72	SB	a)b)c)d)	Cloud free. Heavy haze over part of the area, other parts were clear
15 Sept 72	LA	a)b)	Too cloudy to obtain active ground truth
2 Oct 72	SB	a)b)d)	Too cloudy for analysis
3 Oct 72	LA	a)b)	Very cloudy
20 Oct 72	SB	a)b)	Very cloudy
21 Oct 72	LA	a)b)c)d)	Essentially cloud free. Heavy haze over part of the area, other parts were clear
7 Nov 72	SB	a)b)	Very cloudy
8 Nov 72	LA	a)b)c)d)	Essentially cloud free. Clear day. Ideal for comparison with 21 Oct 72 data
25 Nov 72	SB	a)b)d)	High cirrus clouds, very little haze
26 Nov 72	LA	a)b)c)d)	Clear day
14 Dec 72	LA	a)b)	Cirrus clouds over test area
1 Jan 73	LA	a)b)	Clear with some dust in the air. Holiday
19 Jan 73	LA	a)b)	Partly cloudy, very little haze
6 Feb 73	LA	a)b)	Very cloudy
24 Feb 73	LA	a)b)	Very cloudy
14 Mar 73	LA	a)b)c)d)	Very clear day
1 Apr 73	LA	a)b)c)d)	Partly cloudy, very light haze
19 Apr 73	LA	a)b)c)d)	Scattered clouds, light to moderate haze

Table I (Cont.)

7 May 73	LA	a)b)c)d)	Scattered low clouds, moderate to heavy haze, some high cirrus clouds
25 May 73	LA	a)b)	Very cloudy
12 June 73	LA	a)b)	Very cloudy
30 June 73	LA	a)b)	Very cloudy
18 Jul 73	LA	a)b)d)	Broken clouds, moderate to heavy haze, high cirrus clouds

---

*ERTS-1 pass over San Bernardino SB
Los Angeles LA

**
a) Visibility and relative humidity data from airports
b) Air Pollution Control District data
c) Solar aureole brightness
d) Visual and photographic data
Vertical distribution of Haze
Vertical temperature profile

DIGITAL PROCESSING TECHNIQUES

All quantitative analysis of the ERTS data has been done from Computer Compatible Tape (CCT) sets provided by NASA. The basic program for reading these tape sets at Aerospace was made as flexible as possible. The program is modular, separating into various subroutines the different operations on the tapes, so that changing analysis procedures would require as little recoding as possible and therefore be as simple as possible. All of these programs were written in Fortran for the Control Data Computers at The Aerospace Corporation. Because they employ properties of the Aerospace operating system which are probably not generally available the programs themselves are probably not of general interest, although we would be glad to supply them, as is, to anyone who is interested. Because of this uniqueness to the Aerospace Corporation computer environment we describe what the programs do rather than details of how the programs are controlled and used. We discuss first the basic program and then the various analysis procedures developed for use with the basic program.

Basic Computer Program

The flow of operations in the basic computer program is shown in Figure 8. The names of the subroutines performing the various operations are indicated under the lower right corner of the box containing the operations description.

The spatial region to be analyzed is selected by cards read by the routine DESLOC. This is specified by giving the beginning and ending scan line numbers in the frame and the beginning and ending point numbers in the scan line. This routine also recognizes the stop directive on the input cards.

The analysis part of the program consists of 3 subroutines (or 3 entry points into one subroutine). The names of the entry points are ANPAR, LINAN and FINAN. The entry point ANPAR is called before the analysis begins and permits the input of various parameters needed for

the analysis. The program then begins to deliver, to the LINAN entry point one scan line at a time, the MSS data for all four bands. After all the desired lines have been delivered and analyzed, the entry point FINAN is called to do any summarizing needed to complete the analysis procedure.

DESLOC is called again after the call to FINAN. An attempt is made to input another spatial location and the whole procedure is repeated. Since the data is on the tapes in sequential scan line order it is much more efficient to order the locations desired for analysis in ascending order of line number. The program will handle out of order requests correctly but at the expense of rewinding the input tape files and skipping records which would not otherwise be necessary.

The difference in the computer word format between the XDS computers at the ERTS NDPF and the CDC computers available at Aerospace made the writing of these programs somewhat more difficult than it might have been otherwise. Since the XDS format is essentially the IBM 360-370 format it was deemed desirable to create a somewhat more general purpose routine for the conversion of data from XDS format to CDC format, than might have been required strictly for the ERTS analysis. This routine is described in Appendix C.

RESULTS

On the basis of ground truth information, the data from the ERTS-1 passes on 21 Oct 1972 and 8 Nov 1972 were picked for extensive digital analysis. The "observation identifier" for these frames are 1090-18012 and 1108-18014. During the 21 Oct 1972 pass much of the test area was quite hazy. (See Fig. 2, 4, 6 and Appendix A). There were also regions of moderate and light haze as well as clear areas. At the time of the 8 Nov 1972 pass, most sections of the test area, including regions that were hazy on 21 Oct, were quite clear (see Fig. 3, 5, 7 and Appendix A). We had complete ground truth for both passes, and both were essentially cloud free. Differences in terrain features and solar elevation angle are minimal, because these were consecutive passes. These images were compared in various ways to determine the effects of haze on ERTS-1 images.

Quantitative Assessment of Haze

A quantitative assessment of the amount of haze present at various locations on 21 Oct 72 and 8 Nov 72 from the ground truth data listed in Table A- II, pp A-13 and A-15.

First, the particulate density measurements, Km, made at ground level by the Air Pollution Control District were studied. In an attempt to determine the relative importance of solid particulates and water droplets, all available data from Table A-11 were used to make a least squares fit to the form

$$\text{visibility (miles)} = \frac{a}{Km(b+R.H.)}$$

to determine the parameters a and b. R.H. is the relative humidity, in percent. The data from Table A-II, cover ranges of 29 to 88% relative humidity, 2.5 to 40 miles in visibility, and Km values from 0.9 to 4.5. The best fit values were

$$a = 927 \text{ miles}$$

$$b = 0.10$$

b is negligibly small compared with reasonable values of relative humidity. Thus the atmospheric scattering becomes very small when either Km or the relative humidity becomes very small. This implies that water droplets are the primary scattering material and that solid particulates play the role of condensation centers. We don't see any way to determine aerosol concentration from the Km measurements.

The solar aureole brightness measurements may be used to obtain aerosol concentrations; however, some assumptions about materials and size distributions must be made. For reasons discussed in the preceding paragraph, water was chosen as the material. Deirmendjian (Ref. 5) has calculated the scattering of light of wavelength 0.70μm (near the peak response of the aureole monitor, 0.75 μm) by water droplets. He made these calculations for two particle size distributions M (marine) and L (continental). The normalized total phase functions are shown as a function of scattering angle in Fig. 9. The relative aureole brightness values at 1 1/2, 3, and 6 deg. measured on 21 Oct 72 agree reasonably well with the L-type scattering phase function. Therefore the following calculations will be made using Deirmendjian's L-type particle size distribution (Ref. 5).

Following the nomenclature of Ward et al. (Ref. 4),

$$B_T(\lambda,\psi) = H(\lambda)\exp[-\tau(\lambda)\sec\theta][\tau_R(\lambda)R(\psi) + \tau_p(\lambda)P(\psi,\lambda)]\sec\theta$$

where:

B_T ≡ Aureole brightness

H_λ ≡ unattenuated solar brightness (same units as B_t, e.g., Watts/cm^2 · sr · μm)

θ ≡ solar angle from the zenith

ψ ≡ scattering angle

λ ≡ wavelength

$R(\psi)$ ≡ the normalized Rayleigh scattering phase function = $3/8\,(1 + \cos^2\psi)$

$P(\psi,\lambda)$ ≡ The normalized particulate scattering phase function (Fig. 9)

$\tau_R(\lambda)$ ≡ The Rayleigh optical depth, .0292 at 0.75 μm (Ref. 6)

$\tau_p(\lambda)$ ≡ The Particulate scattering optical depth.

$\tau(\lambda)$ ≡ Total optical depth.

The values of τ_p obtained in this way were:

$$\tau_p(21 \text{ Oct } 72) = 0.30$$

$$\tau_p(8 \text{ Nov } 72) = 0.03$$

From these values of particulate optical depth, the total number of particulates in an atmospheric column of one cm^2 area, N_T can be obtained from Deirmendjian's calculations of the extinction coefficient (Ref. 5) (still with L-type particle size distribution). The results are:

$$N_T(21 \text{ Oct } 72) = 7.6 \times 10^5 \text{ particles/cm}^2$$

$$N_T(8 \text{ Nov } 72) = 0.8 \times 10^5 \text{ particles/cm}^2$$

These particle number data can be used to calculate the expected visibility. The investigators observed that the haze on 21 Oct 72 was composed of a layer of approximately uniform density and about 3,500 feet thick. If the total amount of haze on 21 Oct is spread uniformly along a 3,500 ft. thick layer, the number density is

$$n(21 \text{ Oct } 72) = 710 \text{ particles/cm}^3.$$

The extinction coefficient β can again be obtained from Deirmendjian's calculations, now for visible light (0.45 μm), instead of the extinction coefficient calculated at 0.7 μm used to obtain number density from the aureole data.

$$\beta = 0.34 \text{ km}^{-1}$$

From this value of the extinction coefficient, β, the visibility can be calculated (Ref. 7) as,

$$\text{visibility} = \frac{3.912}{\beta}$$

Thus, calculated visibility for 21 Oct 72 is found to be 11.5 km = 7 miles. This is thought to be quite good agreement with the reported visibilities of 5 and 6 miles.

The ERTS-1 Multi-Spectral Scanner Digital Data

The key characteristics of the digital data are listed in Table II. The analysis was carried out in units of the lease significant bit of the digital data word. They may be converted to radiometric units by multiplication with the values given in the last column of Table II.

Images

The first analysis package allowed the investigators to produce images of selected areas of a frame for a particular MSS band. The images were produced by the Calcomp 835 film plotter associated with the CDC 7600 computer. Thirty-two gray shades were available; 35mm Panatomic-x film was used. Four minutes in D-96 at 70°F was found to yield optimum processing. These images were somewhat skewed because the effect of the rotation of the earth, as the MSS scanned the scene, was not removed. Stripes were placed at certain scan lines in order to precisely locate these scan lines geographically.

This pictoral capability was developed in order to view the effect of haze on the image, to precisely geographically locate the pixels included in the various digital analyses, and to display the results of numerical manipulation, e.g., ratios or differences of two frames of data.

Figures 10 and 11 show photographs of an area in the western part of the Los Angeles basin made by the investigators from MSS Band 5 digital tapes. The area was quite hazy at the time of Fig. 10 and quite clear at the time of Fig. 11. The exposure times were slightly different, and a slightly higher contrast grade of paper was used to make the print of the hazy day, but the image quality appears quite comparable. Similar results were obtained for MSS bands 4, 6, and 7.

Line Plots of Intensity

Plots of the intensity of all four MSS bands along a large number of selected lines were made from the 21 Oct frame and the 8 Nov frame.

Table II. Description of ERTS-1 MSS Digital Data

Channel Designation	Spectral Bandpass (μm)	Number of Gray Shades (linear with brightness)	Radiometric Equivalent of Least Significant Bit (watts/$cm^2 \cdot sr$)
MSS 4	0.5 - 0.6	128 (7 bits)	1.95×10^{-5}
MSS 5	0.6 - 0.7	128 (7 bits)	1.57×10^{-5}
MSS 6	0.7 - 0.8	128 (7 bits)	1.39×10^{-5}
MSS 7	0.8 - 1.1	64 (6 bits)	7.30×10^{-5}

These line plots were quite useful in precisely geographically locating picture elements along scan, as well as in examining the data to determine the effects of haze. Figures 13 and 14 show examples of the plots for part of one line from the 21 Oct frame and the corresponding line from the 8 Nov data. There appears to be very little difference between the line plots for the two days except that 21 Oct data (hazy day) appear to be shifted up by a nearly constant amount. The amount of this shift decreases as wavelength (i.e., MSS band number increases. This shift seems to disappear when areas that were clear on both days are compared.

Intensity Value Distributions

Brightness value distributions were computed for several areas from the 21 Oct frame and for the same geographical areas from the 8 Nov frame. Figure 15 shows a histogram plot of the brightness values of one area from both the 21 Oct and 8 Nov data for MSS band 4. Figures 16 - 18 are similar plots of MSS band 5, 6, and 7 data. The area for which data is shown in Fig. 15 - 18 includes ocean, beach, harbor, vacant land, city, and parkland. It was hazy over this area on 21 Oct and clear on 8 Nov. This area lies between the top pair of white lines in Figs. 10, 11, and 12 and extends from the ocean to about the prominent white streak on the right of these pictures formed by the Los Angeles river. These histograms show a double peak. The brighter peak is associated with terrain, the darker peak with water.

The distribution is clearly shifted toward brighter values on 21 Oct. The amount of this shift decreases with the increasing wavelength. It appears that the shift is greater, in absolute value, for the brighter peak than for the darker one.

The fine structure in these histograms, i.e., dips and humps in adjacent intensity values, must be discounted. This is because the ERTS digital data has missing values. In the range of brightness values say 20-45, about one half of the values are unpopulated (forbidden) in a certain line of data. The particular missing numbers are correlated with a particular detector, that is, they repeat every six lines. About the same number of values are missing for the other detectors, but the

particular values which are forbidden vary from detector to detector. The histograms shown in Figs. 15 - 18 are averaged over eleven adjacent lines. However, these are values which are forbidden for as many as five of the six detectors. These values show dips in the histograms. Other values are forbidden in as few as one detector; these values show peaks in the histogram plots. This phenomena was not present in MSS band 7.

Mean values of brightness of both water and terrain were computed from the data shown in Figs. 15 - 18. This area includes the city of Inglewood (Location H on Fig. 1) and is referred to as the Inglewood area. Similar mean values were derived from brightness distributions around San Pedro (between locations 6 and 7 on Fig. 1) including part of the harbor area, and Palmdale (just south of Location 8 on Fig. 1), where it was clear on both 21 Oct and 8 Nov. The terrain data are tabulated in Table III. The mean values of brightness over water are shown in Table IV. The differences in the mean values, Δ, is also listed. The high apparent brightness of water in MSS band 4, and to a lesser extent in band 5, even during clear times is caused by reflection of the incident sunlight into the ERTS sensor by the clear atmosphere (Rayleigh scattering) rather than a high reflectivity of water at these wavelengths. The Rayleigh scattering into the ERTS sensor is nearly independent of solar elevation angle over the range of elevation angles encountered in this investigation.

Table IV shows that there was a significant increase in the apparent brightness of water in MSS bands 4, 5, and 6 during hazy conditions at Inglewood and San Pedro, caused by the haze scattering incident sunlight toward the ERTS sensor. Palmdale, which was clear on both days, showed about the same apparent brightness for water on the two days. The magnitude of this effect decreases with increasing wavelength. For example, at San Pedro, the Δ's for MSS bands 4, 5, 6, and 7 are: 5.8, 4.8, 3.4, and 0.4, in units of the least significant bit of the ERTS MSS data words. When converted to radiometric units using the data from Table II, these Δ's become 11.3, 7.5, 4.7, and 2.9×10^{-5} watts/cm^2. sr.

Table III. Mean Values of Brightness Distributions Over Terrain*

Inglewood	21 Oct 72 (Hazy)	8 Nov 72 (Clear)	Δ
MSS Band 4	35.6 (35.1)	27.7	7.9 (6.4)
5	30.9 (29.7)	24.7	6.2 (5.0)
6	31.4 (30.5)	26.1	5.3 (4.4)
7	13.4 (13.2)	12.0	1.4 (1.2)
San Pedro	**21 Oct 72 (Hazy)**	**8 Nov 72 (Clear)**	**Δ**
MSS Band 4	35.5 (33.8)	29.0	6.5 (4.8)
5	30.8 (29.5)	25.3	5.5 (4.2)
6	25.9 (25.1)	22.7	3.2 (2.4)
7	9.4 (9.3)	8.7	0.7 (0.6)
Palmdale	**21 Oct 72 (Clear)**	**8 Nov 72 (Clear)**	**Δ**
MSS Band 4	39.7 (37.0)	37.0	2.7 (0)
5	43.8 (41.5)	41.5	2.3 (0)
6	40.6 (39.2)	39.2	1.4 (0)
7	17.7 (17.4)	17.4	0.3 (0)

*Values in parentheses are the brightness values after normalizing the same solar elevation angle as 8 Nov 72. The observed variations in the Palmdale data were used to make the corrections at Inglewood and San Pedro.

Table IV. Mean Values of Brightness Distributions Over Water

Inglewood	21 Oct 72 (Hazy)	8 Nov 72 (Clear)	Δ
MSS Band 4	21.0	15.8	5.2
5	10.5	5.9	4.6
6	5.9	2.5	3.4
7	0.3	0	0.3
San Pedro	**21 Oct 72 (Hazy)**	**8 Nov 72 (Clear)**	**Δ**
MSS Band 4	23.4	17.6	5.8
5	12.1	7.3	4.8
6	6.6	3.2	3.4
7	0.4	0	0.4
Palmdale	**21 Oct 72 (Clear)**	**8 Nov 72 (Clear)**	**Δ**
MSS Band 4	18.1	17.9	0.2
5	9.3	10.2	-0.9
6	4.4	5.9	-1.5
7	0.1	0.4	-0.3

If bands 5, 6, and 7 are normalized to the same amount of incident sunlight as band 4, the relative values of these Δ's become 11.3, 8.9, 7.1, and 2.3. The haze, therefore, is monotonically less effective in scattering incident sunlight into the ERTS sensor as the center wavelength of the band becomes larger. This is a reasonable behavior. Deirmenjian's calculations of scattering by water droplets with an L-type particle size distribution shows a decrease of the extinction coefficient from 0.04797 km^{-1} to 0.03953 km^{-1}. When the wavelength is increased from 0.45 μm to 0.70 μm (Ref. 5). (These extinction coefficients are calculated for 100 particles/cm^3.) Plass and Katlawar (Ref. 9) have calculated the amount of sunlight scattered away from the earth for different amounts of haze at wavelengths of 0.7 and 0.9 μm for an ocean surface. They find less backscatter per unit incident sunlight at 0.9 μm than at 0.7 μm, but not nearly as much less as we observe in comparing MSS bands 6 and 7. The results then look quite reasonable, except that the observed Δ in band 7 appears anomalously small when compared with bands 4, 5, and 6.

Table III shows that there was an increase in apparent brightness of terrain at Inglewood and San Pedro on the hazy day. These Δ also decrease with increasing wavelength in a reasonable way, except for band 7, which again shows a smaller Δ relative to the other bands than expected.

A correction for solar elevation angle should be made in comparing terrain brightnesses on these two days. The magnitude of this variation, as well as that caused by variations in the terrain, has been minimized by analyzing data from consecutive passes. It is not possible to accurately made this correction for a scene containing such a variety of shapes and materials; however, as the correction is small, an approximate correction should suffice. The Palmdale area was clear on both days, therefore, it was possible to use the observed variation in terrain brightness at Palmdale to approximately correct the Inglewood and San Pedro data. The corrected apparent brightness values and the associated Δ's are shown in parenthesis in Table III.

We have here a very significant result. That is, haze causes an overall increase in scene brightness, Δ, which is approximately

independent of scene reflectivity over typical (not highly reflective) terrain. The magnitude of Δ decreases with increasing wavelength.

Minimum Brightness Values

One of the easiest parameters to determine from a set of data is the apparent brightness of the picture element with the smallest apparent brightness of the set. Table V shows the results of such an analysis of the same areas treated in the previous section. These values can be determined from the histograms shown in Figs. 15 - 18 for the Inglewood area. The advantage of this analysis is that the entire histogram need not be produced or analyzed to obtain the minimum brightness value.

The values of the differences, Δ's, of minimum brightness values on the hazy and the clear days, listed in Table V, are seen to be nearly equal to the mean brightness differences over water and terrain (Tables III and IV). for bands 4 and 5.

Table V. Minimum Populated Values of the Brightness Distribution

Inglewood	21 Oct 72 (Hazy)	8 Nov 72 (Clear)	Δ
MSS Band 4	19	13	6
5	9	4	5
6	3	1	2
7	0	0	0

San Pedro	21 Oct 72 (Hazy)	8 Nov 72 (Clear)	Δ
MSS Band 4	20	15	5
5	10	5	5
6	3	1	2
7	0	0	0

Palmdale	21 Oct 72 (Clear)	8 Nov 72 (Clear)	Δ
MSS Band 4	16	16	0
5	8	9	-1
6	3	4	-1
7	0	0	0

Power Spectral Density

The power spectral density was computed as a function of spatial frequency over the Inglewood area (same geographical area used in the brightness distribution) from the 21 Oct and the 8 Nov data for all MSS bands. For each band for every line selected the data was reformated into the correct form for input to a fast Fourier transform program originally developed at Aerospace for interferometric spectroscopy (Ref. 10). This reformated data was copied to tape and then used as input to the Fourier transform program which was used to compute the power spectrum. The program computed the power spectral density, $P(\nu)$ as a function of spatial frequency, from the $I(x)$, the difference between the observed intensity and the average intensity on that line. x is distance along the scan line.

$$P(\nu) = 2\Delta x \sum_{n=-N}^{N} I(n\Delta x)\, e^{-2i\pi n\Delta x}$$

The units of P are (intensity units/km^{-1}). The intensity units in this case are again the magnitude of the least significant bit in the ERTS-1 MSS digital data tapes.

The power spectral density was computed for the appropriate segment of each line, then averaged over the 11 lines included in the Inglewood area. The results are plotted in Figs. 19–22.

The results were essentially negative. The power spectral density may be slightly higher on 8 Nov than 21 Oct for MSS band 4 (Fig. 19), however, for all other bands the two days look the same. We conclude that there is essentially no difference in power spectral density between the hazy 21 Oct data and the clear 8 Nov data.

This result is consistent with an approximately constant difference in brightness in the data for these two days, because a baseline shift has no effect on power spectral density except to the zero spatial frequency point, which is not included in our calculation.

The motive for making the power spectral density calculations was to look for a possible effect of small angle scattering of light by haze after it has been reflected by the ground toward the ERTS sensor. Such small angle scattering causes light to appear as if reflected from a point on the ground which is slightly displaced from the actual point of reflection. This effect reduces resolution, contrast and power spectral density for high spatial frequencies. This effect becomes quickly less important for large spatial frequencies, because scattering from aerosols is strongly forward peaked (Fig. 9). Our analysis shows that for the amount of haze present over Inglewood on 21 Oct 72, for a nadir looking sensor and for the maximum resolution of the ERTS Multi-Spectral Scanner this small angle scattering of the reflected light is negligible. This effect is, of course, minimized in the case of the ERTS-1 Multi-Spectral Scanner, by its nadir looking geometry, because sunlight reflected from terrain passes through a minimum amount of atmosphere before reaching the sensor.

Contrast Reduction

Image contrast has been defined in many different ways, as the difference or ratio of intensities I_1 and I_2, normalized in a variety of ways, between two points in a scene. For example

$$C_1 = I_1 - I_2$$

$$C_2 = \frac{I_1}{I_2} \equiv R$$

$$C_3 = \frac{I_1 - I_2}{I_2} = R - 1$$

$$C_4 = \frac{I_1 - I_2}{I_1 + I_2} = \frac{R - 1}{R + 1}$$

The power spectral density, described in the previous section, is an elegant way of describing the unnormalized difference contrast as a function of spatial frequency.

Photographic contrast usually involves the ratio of two intensities, because the logarithmic response of film results in a constant density difference for a given ratio, R, otherwise independent of the magntidues of I_1 and I_2.

C_3 is usually used in the literature concerning contrast reduction by the atmosphere, where a target intensity I_1 is treated against a uniform background I_2. The contrast reduction is found to be a function of I_2 for a given atmosphere (Ref. 11). Of course, the real world seldom provides a constant background intensity.

We have found that the most significant effect of haze on ERTS-1 MSS data is an overall increase in brightness, Δ, which is approximately independent of scene reflectivity (over typical, not highly reflective terrain). The magnitude of Δ was found to decrease with increasing wavelength. C_1 is not changed by this effect, whereas the magnitude of C_2, C_3 and C_4 are all decreased. For example,

$$C_3' = \frac{I_1 + \Delta - I_2 - \Delta}{I_2 + \Delta} = \frac{I_1 - I_2}{I_2 + \Delta} \quad .$$

The constrast C_3, of mean harbor water against mean city background is listed for the San Pedro area from both the 21 Oct and 8 Nov data in Table VI.

It appears fruitless to pursue this line of approach in this investigation. There is reduction in contrast, C_2, C_3, or C_4, caused by haze. But there is no apparent gain in monitoring one of these contrast functions rather than the overall increase in brightness, Δ, which is the primary cause of the contrast reduction.

Image of the Difference of Two Frames

The analysis of the 21 Oct and 8 Nov data has shown that the principal effect of haze on the ERTS-1 MSS data is an overall increase in brightness, which is approximately independent of terrain reflectivity.

Table VI. Contrast Between Mean Apparent Water Brightness and Mean Apparent Terrain Brightness Over San Pedro for 21 Oct 72 and 8 Nov 72

	21 Oct 72 (hazy)	8 Nov 72 (clear)
MSS Band 4	$\frac{23.4 - 35.5}{35.5} = -0.341$	$\frac{17.6 - 29.0}{29.0} = -0.393$
MSS Band 5	$\frac{12.1 - 30.8}{30.8} = -0.607$	$\frac{7.3 - 25.3}{25.3} = -0.711$
MSS Band 6	$\frac{6.6 - 25.9}{25.9} = -0.745$	$\frac{3.2 - 22.7}{22.7} = -0.859$
MSS Band 7	$\frac{0.4 - 9.4}{9.4} = -0.957$	$\frac{0.0 - 8.7}{8.7} = -1.00$

The mean apparent brightness intensities are from Tables III and IV.

This suggests a method of accurately locating the geographical extent of haze by imaging the difference fo two frames.

The data of 8 Nov was subtracted from the 21 Oct data on a point by point basis, and an image of the difference was made in such a way that zero difference was imaged as neutral gray. We expect this image to show the geographical extent of the haze on 21 Oct as slightly lighter feature. Fig. 23 shows the image of the difference for MSS Band 4. The light region over land corresponds quite well with the geographical extent of haze on 21 Oct as determined by the investigators. There is no ground truth data concerning the haze distribution over the ocean to compare with the subtracted image. An area of about 45 x 100 miles is covered in Fig. 23. The most prominent features are clouds. Those present on 21 Oct are white, those on 8 Nov are black. The coastline is visible because the surf was heavier, i.e., brighter, on 8 Nov than 21 Oct.

The grid of picture elements on one pass will generally not exactly geographically overlap the grid obtained on another pass. Therefore, the data from 21 Oct and 8 Nov were geographically registered to the nearest line number and element number at several points. Then the data were smoothed by averaging each 10 x 10 array of picture elements. This produced a lower resolution image, but one that was registered much more accurately relative to picture element size. The smoothed data were then subtracted on a point by point basis.

SUMMARY AND CONCLUSIONS

ERTS-1 MSS digital data from two consecutive passes over the Los Angeles area were analyzed in a variety of ways to determine the effect of haze on the data. One day, 21 Oct 1972 was quite hazy over Los Angeles, but clear in other parts of the test site. The haze (smog) over Los Angeles was 3,500 feet thick. The visibility was about 5 miles (the visibility must be 3 miles or greater in order for aircraft to operate under visual flight rules). The particulate scattering optical depth was found to be 0.30 at 0.7 μm, from analysis of solar aureole brightness measurements. This corresponds to a number of 7.6×10^5 particles/cm^2 in a total column of atmosphere, assuming Deirmendjian's (Ref. 5) L-type particle size distributions. The amount of haze on the clear day 8 Nov 1972, was about 1/10 of the amount present over Los Angeles on 21 Nov.

The most pronounced effect, indeed the only independent effect, of haze on the ERTS MSS data was found to be an overall increase in apparent brightness of the scene, caused by scattering of incident sunlight toward the ERTS sensor by the haze. The magnitude of this brightness increase was found to be approximately independent of surface reflectivity, over the range of reflectivities encountered in our test area. The magnitude of this increase in scene brightness was found to decrease with increasing wavelength. The absolute values of this brightness increase were 11.3, 7.5, 4.7, and 1.0×10^{-4} watts/cm$^2 \cdot$ sr$\cdot$μm for MSS bands 4, 5, 6, and 7, respectively. When normalized to equal amounts of incident sunlight, the relative values become 11.3, 8.9, 7.1 and 2.3.

We found no decrease in power spectral density, even at the highest spatial frequencies in ERTS MSS data, caused by the amount of haze present on 21 Oct 1972.

The optimum method for analysis depends upon one's requirements. We next discuss two methods, which seem feasible as a result of this investigation.

One can determine the amount of haze, using only the data from a particular pass, over water. The scene reflectivity is quite low. The Rayleigh scattering contribution is constant. Thus one can determine the total amount of haze from the apparent brightness in bands 4, 5, and 6. Many more measurements correlating measured amount of haze with apparent water brightness, and calculations such as those of Plass and Kattawar (Ref. 9) at the ERTS wavelengths, would be necessary before the technique could become operational, but it is nearly certain that it could be done. The question is, how accurate could this method be? It is not possible to make a statistical analysis from such a limited number of observations, but some estimates can be made. The accuracy will probably be limited by systematic errors, rather than detector noise or sensor calibration, etc. The systematic errors would include variations in the reflectivity of water, caused by sediments, waves, foam, etc., and by perhaps such parameters as the size of the body of water and the reflectivity of the surrounding terrain. From Table IV we see that the ratio of the variation of apparent water brightness, for different bodies of water, on the haze-free day to the increase in brightness caused by the haze of 21 Oct is 0.38, 0.91, 1.00 for bands 4, 5, and 6, respectively. Thus we conclude that the absolute accuracy of the total column of haze would be about 1/2 or 1/3 of the amount of haze present on 21 Oct 1972.

If one is willing to follow the brightness history of an area for some time, and if he has some kind of retroactive ground truth to establish brightness distributions vs. amount of haze, then a near real time assessment of the amount of haze would be possible from analysis of the brightness distributions of the area in bands 4, 5, and 6. Our data show more consistency in Δ brightness caused by haze, than in absolute brightness over the water. It can also be applied to areas where there is no water, because the increase in scene brightness was found to be independent of scene reflectivity over a reasonably wide range of reflectivity. Of course one would concentrate on the variation of the areas of lowest reflectivity because variations caused by changing solar elevation angle, etc., would be minimized. A similar technique is the determination of minimum brightness value for a given area. The

variation of the minimum brightness was found to agree quite well with the shift of mean brightness values for bands 4 and 5. The accuracy would be degraded somewhat, by looking only at minimum brightness, rather than the entire distribution, but the required processing time would be significantly reduced.

The effects of haze would be more pronounced, and therefore the sensitivity of both of the above techniques increased, if the sensor looked several degrees away from the nadir, rather than straight down as it does.

This analysis was based on limited data. However, the results are thought to be generally applicable.

REFERENCES

1. S. R. Hall, Anal. Chem. 24, 996 (1952).

2. Reiner Eiden, Tellus, XX, 380 (1968).

3. A.E.S. Green, A. Deepak, and B. J. Lipofsky, Appl. Opt. 10, 1263 (1971).

4. Gray Ward, K. M. Cushing, R. D. McPeters, A. E. S. Green, Appl. Opt. 12, 2585 (1973).

5. D. Deirmendjian, Electromagnetic Scattering on Spherical Polydispersions (American Elsevier Publishing Company, 1969), pp. 75, 78, 152, 167.

6. Shea L. Valley, ed., Handbook of Geophysics and Space Environments (Air Force Cambridge Research Laboratories, 1965), p. 7-27.

7. Seibert Q. Duntley, J. Opt. Soc. Am. 38, 179 (1948).

8. ERTS Data Users Handbook: NASA Document 71SD4249, Page G-14 (revised September 1972).

9. Gilbert N. Plass and George W. Kattawar, Appl. Opt. 11, 1598 (1972).

10. C. M. Randall, "Users Guide to Computer Programs for Fourier Spectroscopy," The Aerospace Corporation Technical Report TR-0073(9260-01)-8, 30 November 1972.

11. Seibert Q. Duntley, Appl. Opt. 3, 551 (1964).

12. Max Born and Emil Wolf, Principles of Optics (Pergamon Press, 1959), pp. 394-397.

FIGURE CAPTIONS

Fig. 1 Map of the Test Area showing airports where visibility and humidity data were obtained (1–9), and the locations where air pollutants were monitored (A–L).

Fig. 2 The Virginia Country Club, Long Beach (near location 6 on Fig. 1). Looking NNE from 4,500' altitude, 43 minutes before the pass of ERTS-1 on 21 Oct 72.

Fig. 3 The Virginia Country Club, Long Beach (near location 6 on Fig. 1). Looking ENE from 4,500' altitude, 30 minutes before the pass on ERTS-1 on 21 Oct 72.

Fig. 4 Hollywood Park, Inglewood (between locations 1 and H on Fig. 1). Looking ENE from 4,500' altitude, 30 minutes before the pass of ERTS-1 on 21 Oct 72.

Fig. 5 Hollywood Park, Inglewood (between locations 1 and H on Fig. 1). Looking NE from 4,500' altitude, 9 minutes before the pass of ERTS-1 on 8 Nov 72.

Fig. 6 Looking ENE from an altitude of 4,500' over Santa Monica (near location D on Fig. 1) 25 minutes before the ERTS-1 pass on 21 Oct 72. The distance to the nearest mountain range is 23 miles.

Fig. 7 Looking NE from an altitude of 3,500' over Culver City (between locations 1 and D on Fig. 1) 5 minutes before the ERTS-1 pass on 8 Nov 72. The distance to the nearest mountain range, the same as that shown in Fig. 8, is 26 miles.

Fig. 8 Flow chart of the ERTS-1 program.

Fig. 9 Normalized, total phase functions for scattering from water droplet haze with both marine and continental particle size distributions for $\lambda = 0.70$ μm, from Deirmendjian (Ref. 5). The lower curves represent scattering angles from 0 to 180 deg, as shown along the bottom of the figure. The upper curves depict the small angle part of the same curves on an expanded scale, shown at the top of the figure.

Figure Captions (Cont.)

Fig. 10 ERTS-1 MSS Band 5 image produced from digital tapes by the investigators. A 12 x 24 mile area in the western part of the Los Angeles basin is shown from the 21 Oct 72 pass. The area shown was quite hazy at the time of the ERTS-1 pass. White lines are included to precisely locate specific frame lines in order to correlate the digital analysis with the visual image.

Fig. 11 ERTS-1 MSS Band 5 image produced by the investigators from digital tapes of the 8 Nov 72 pass. The area shown is roughly the same as that in Fig. 10. The area was quite clear (haze free) at the time of the ERTS-1 pass. The white strips are included to precisely locate specific frame lines.

Fig. 12 Similar to Fig. 10 except for MSS Band 7.

Fig. 13 Intensity plots for all MSS bands along line 1871, from the same frame of data as Fig. 10. Lines 1865 and 1875 are marked on Fig. 10, thus line 1871 can be accurately located. The east-west extension, i.e., point numbers is the same as for Fig. 10, MSS bands 4, 5, 6 and 7 are plotted in order from bottom to top.

Fig. 14 Intensity plots for the line (1788) of the 8 Nov 72 data that most nearly coincides with the line plotted in Fig. 13 from the 21 Oct 72 data. There is an along scan shift, because the frames from these two passes do not exactly overlap. These plots are from the same frame of data shown in Fig. 11. Lines 1780 and 1790 are marked in Fig. 11, therefore line 1788 can be accurately located.

Fig. 15 Histograms of brightness values from ERTS-1 MSS Band 4 digital tapes. Data from lines 1783 to 1793 and points 1813 to 2363 were included from the 8 Nov 72 frame. This area can be located on Fig. 11. This area includes ocean, beach, harbor, vacant land, city, and parkland. The same geographical area was included from the 21 Oct 72 frame, i.e., lines 1866 and 1876 and points 1735 to 2285. This area can be located on Fig. 10.

Fig. 16 Similar to Fig. 15, except for MSS Band 5.

Fig. 17 Similar to Fig. 15, except for MSS Band 6.

Figure Captions (Cont.)

Fig. 18 Similar to Fig. 15, except for MSS Band 7.

Fig. 19 Power, spectra from the same data defined in Fig. 15.

Fig. 20. Similar to Fig. 19, except for MSS Band 5.

Fig. 21 Similar to Fig. 19, except for MSS Band 6.

Fig. 22 Similar to Fig. 19, except for MSS Band 7.

Fig. 23 Image of the difference in point by point brightness of two frames. The digital data of 21 Oct 72 minus the data of 8 Nov 72, covering an area of approximately 45 x 100 miles, is pictured. Areas of zero difference are imaged as middle gray. The most prominent features are clouds. Clouds present on 21 Oct appear white, while those present on 8 Nov are black. The coastline is visible because the surf was more prominent (brighter) on 8 Nov than 21 Oct. The slightly brighter area corresponds quite well with the region observed to be hazy on 21 Oct.

Fig. 24 Drawing of the essential elements of the solar aureole monitor.

Fig. 25 Photograph of the solar aureole monitor in operation.

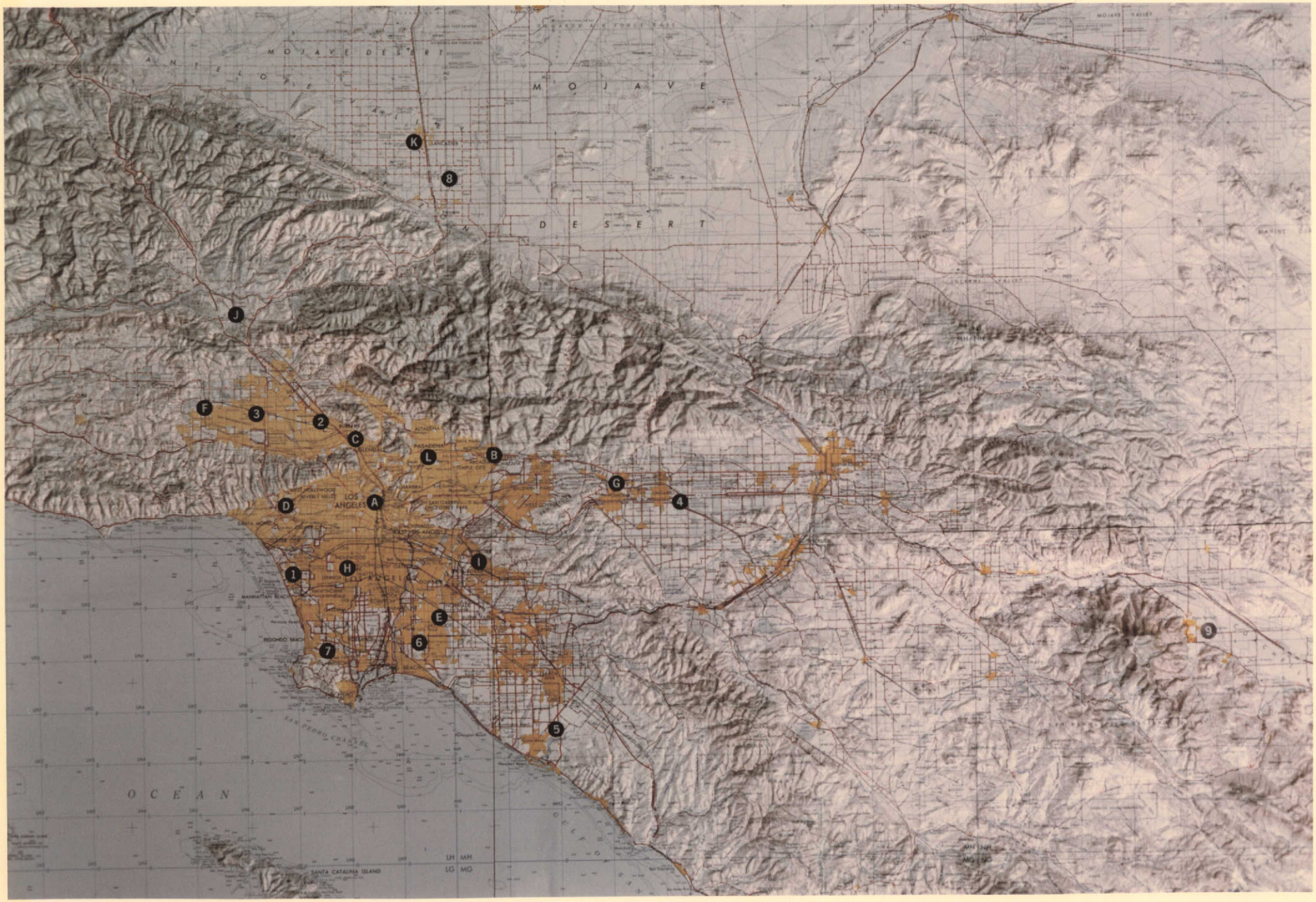

FIG. 1

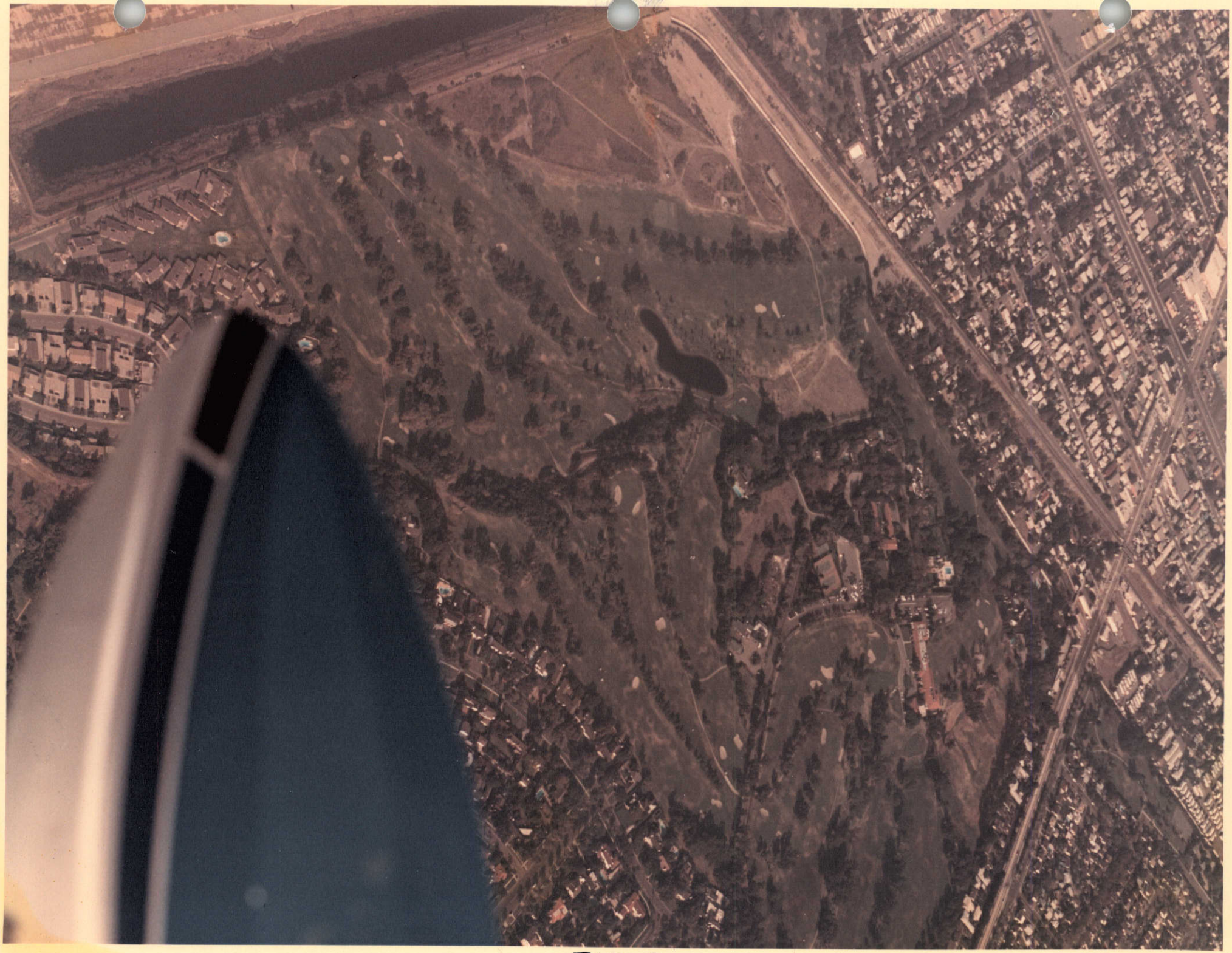

FIG. 2

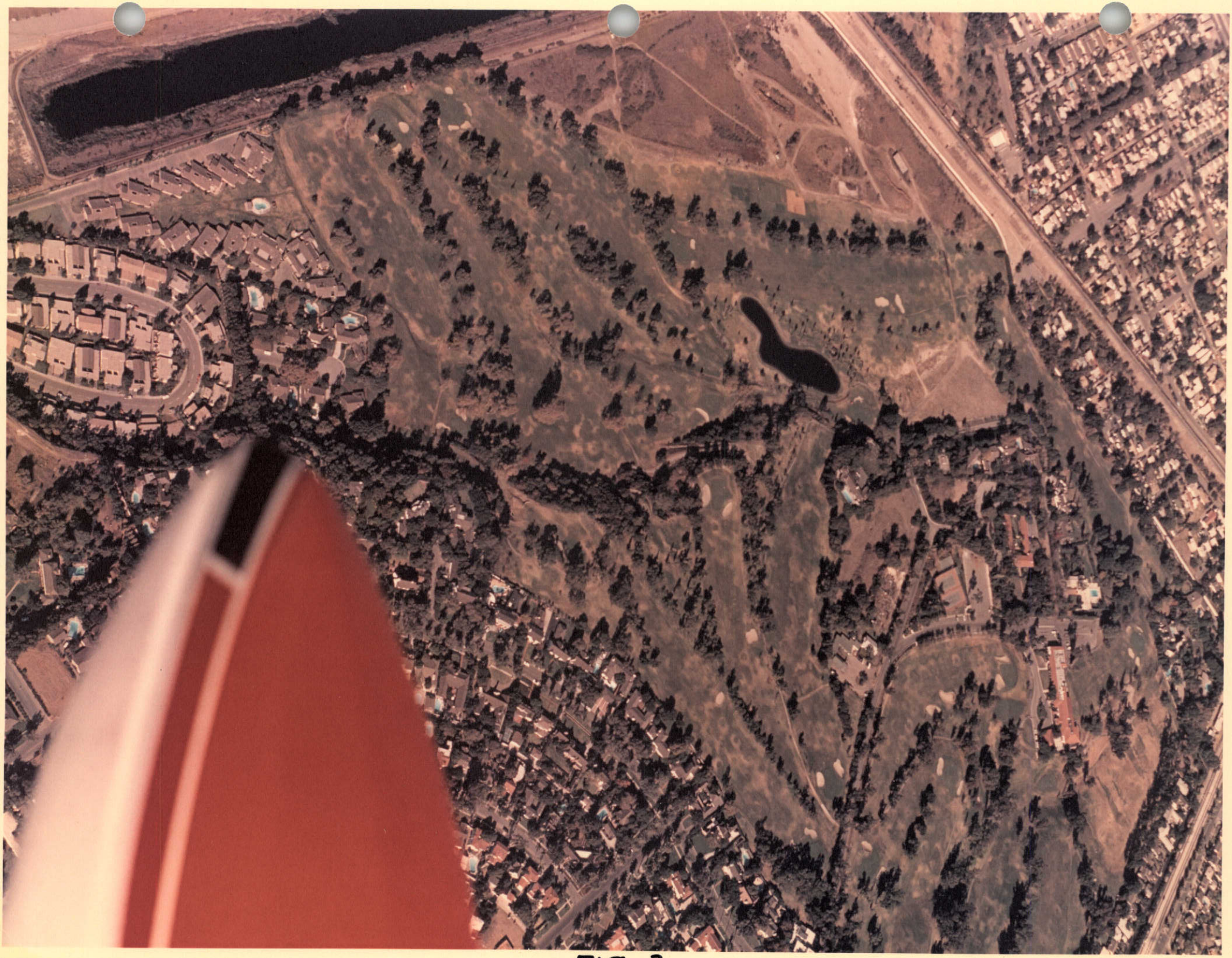

FIG. 3

FIG. 4

FIG. 5

FIG. 6

FIG. 7

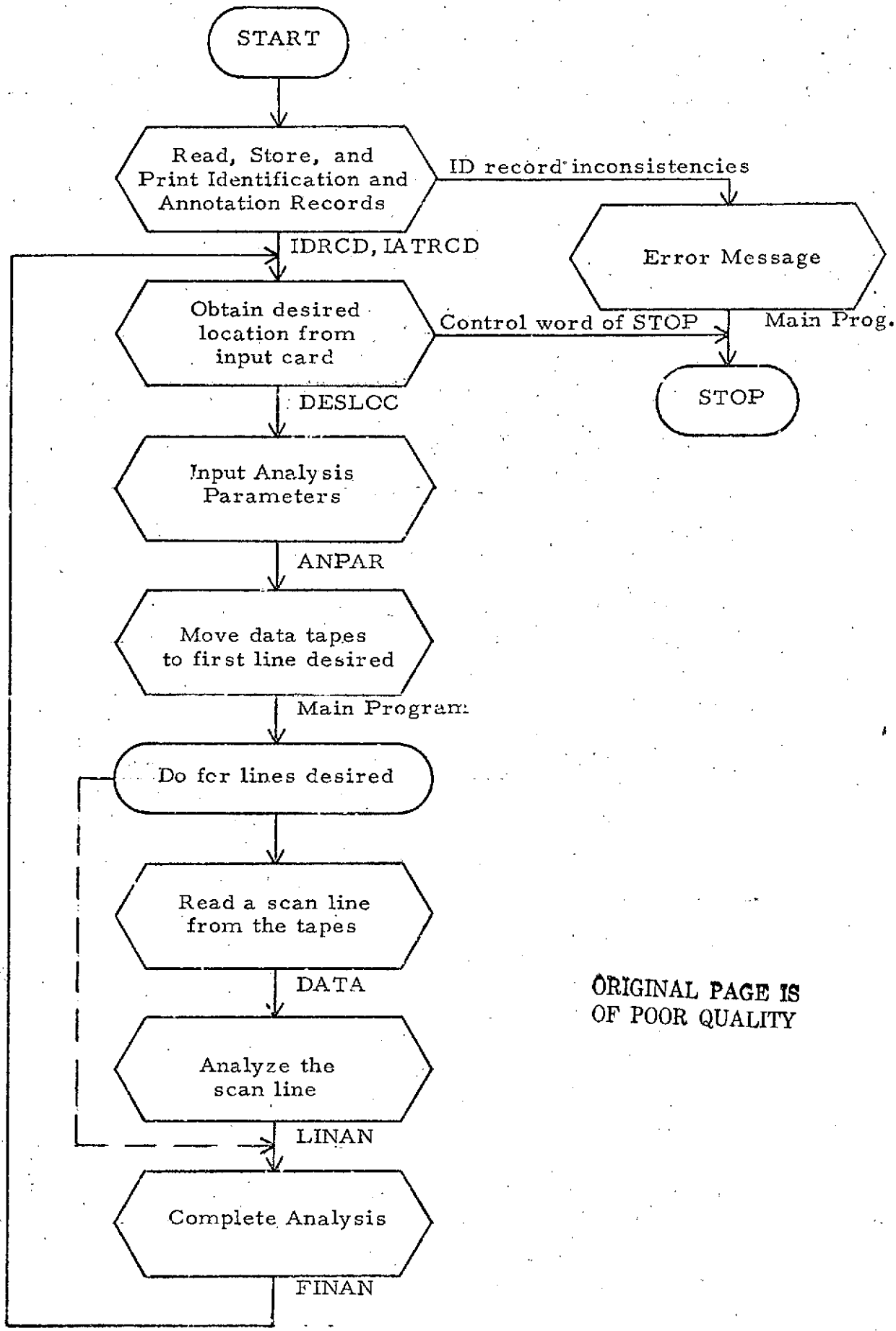

ORIGINAL PAGE IS
OF POOR QUALITY

Figure 8. Flow chart of the ERTS1 program.

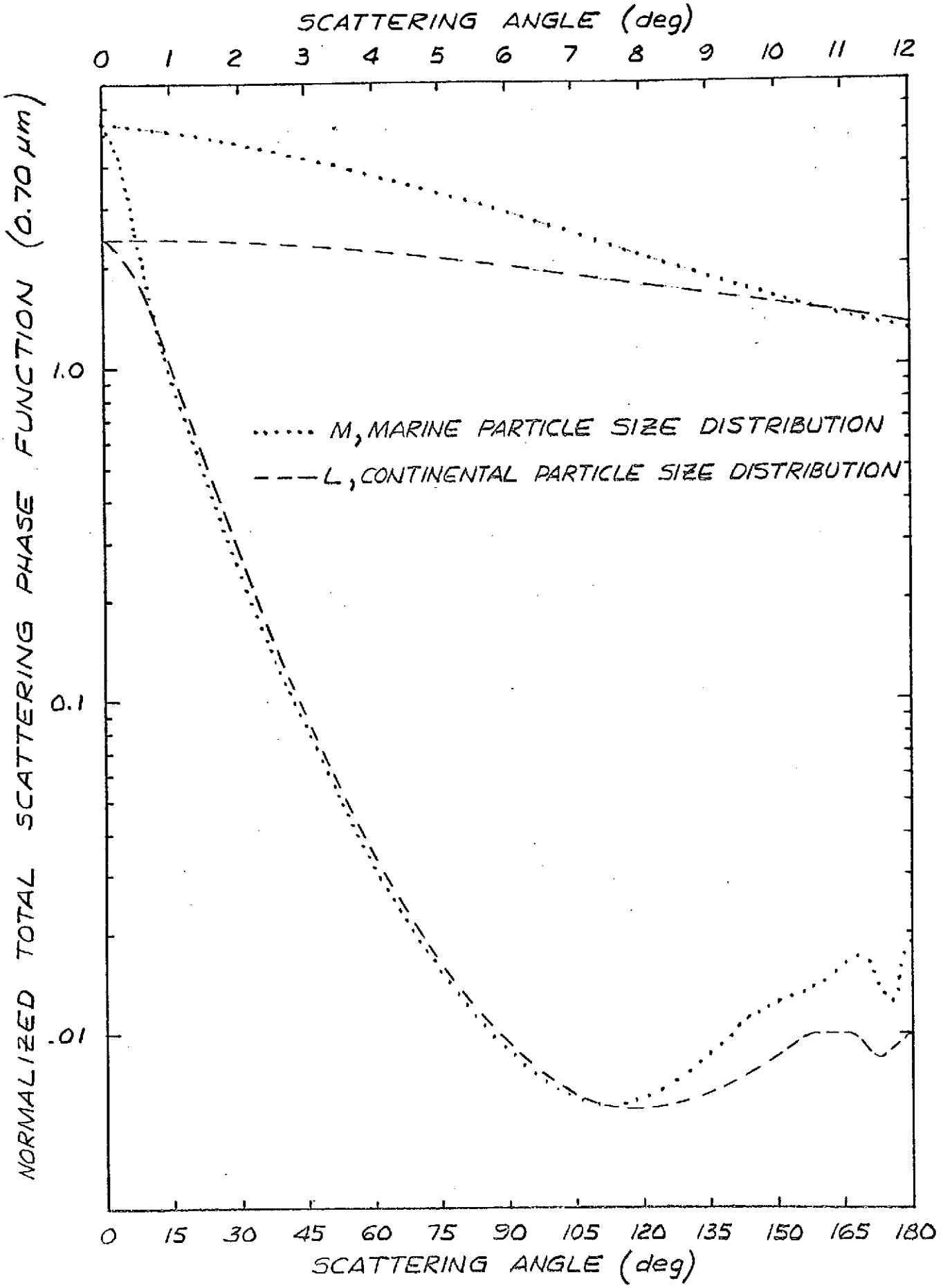

FIG. 9

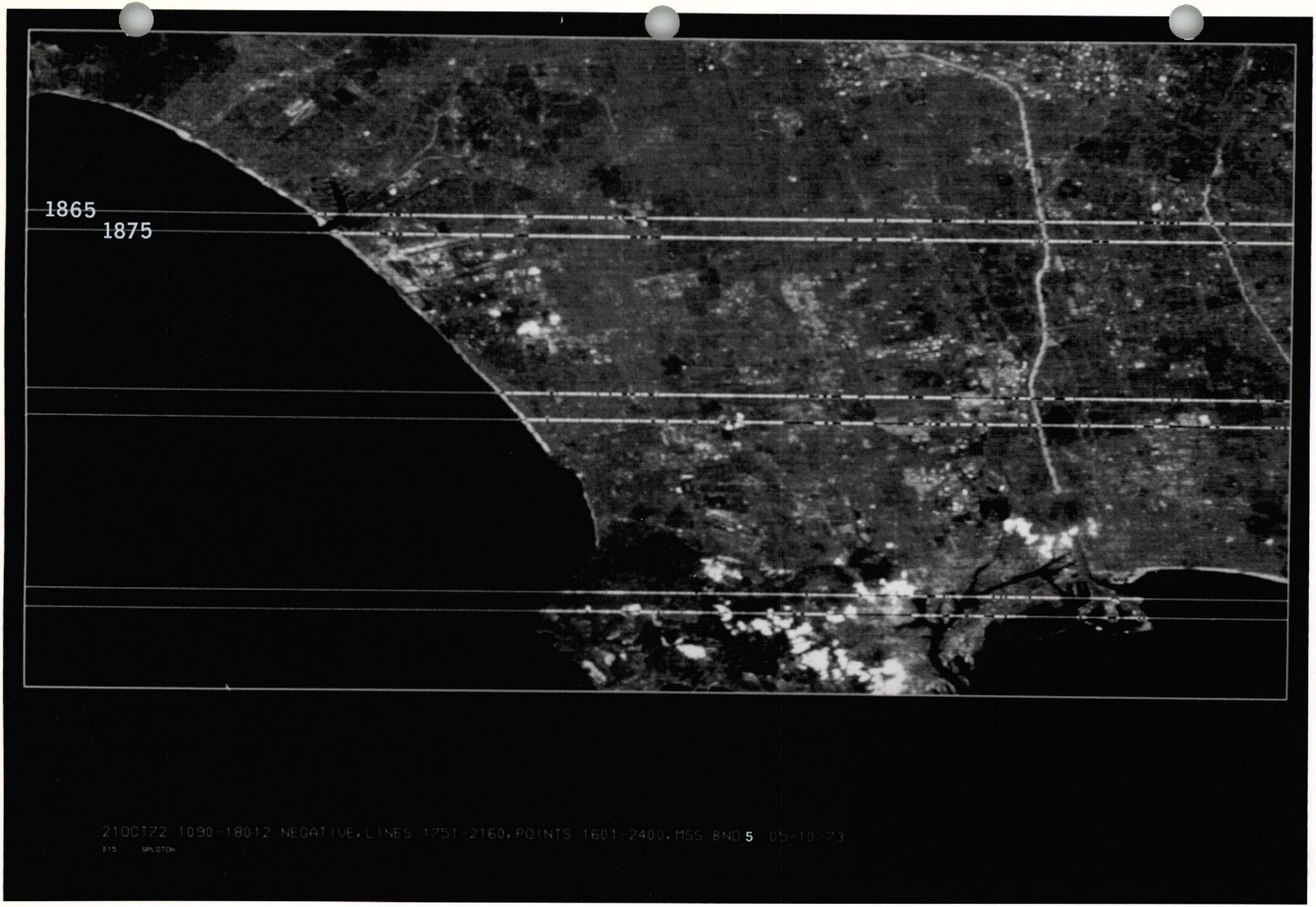
1865
1875
21OCT72 1090-18012 NEGATIVE. LINES 1251-2160. POINTS 1601-2400. MSS BND 5 05/10/73

FIG. 10

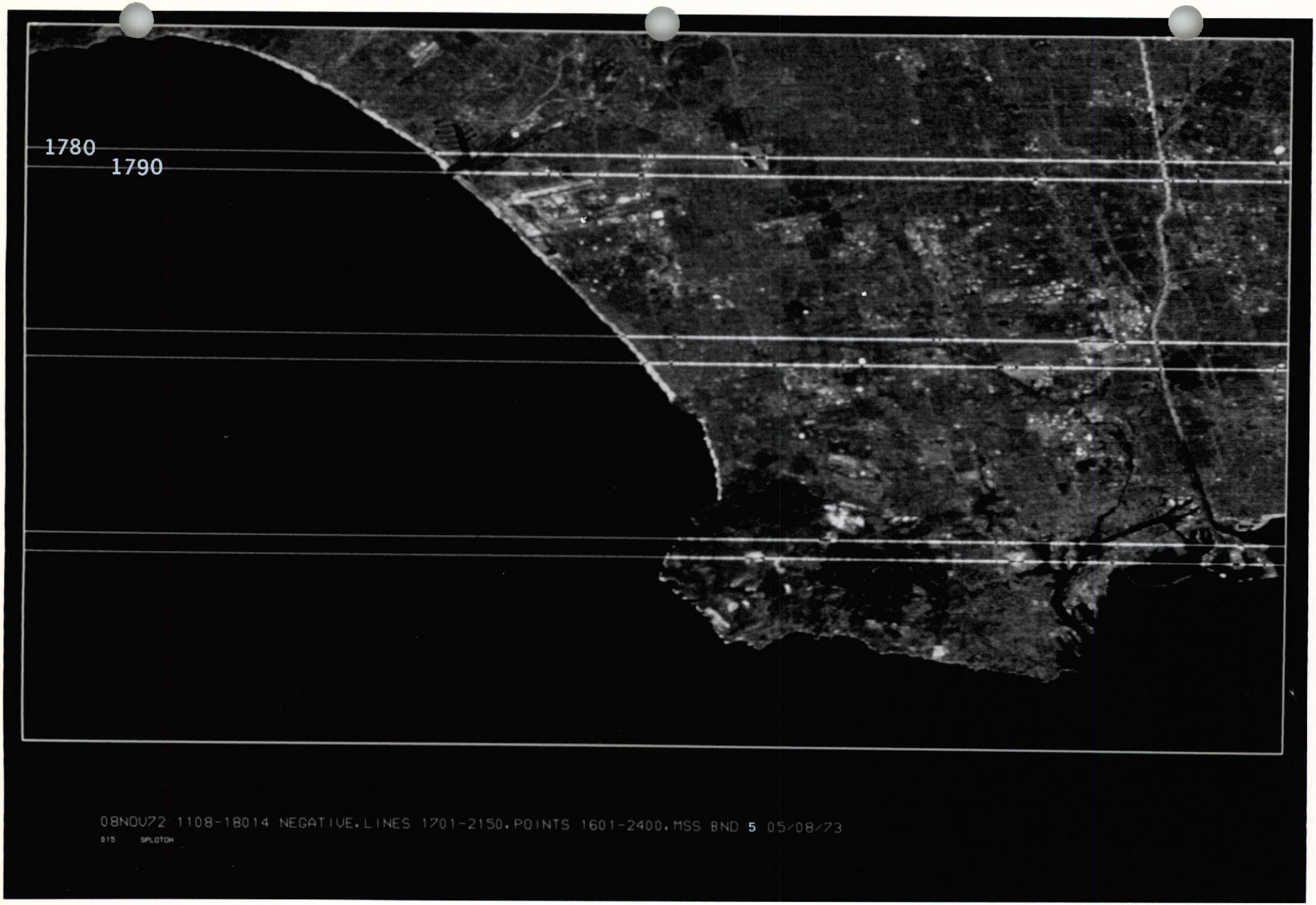
1780
1790
08NOV72 1108-18014 NEGATIVE. LINES 1701-2150. POINTS 1601-2400. MSS BND 5 05/08/73
015 SPLOTCH

FIG. 11

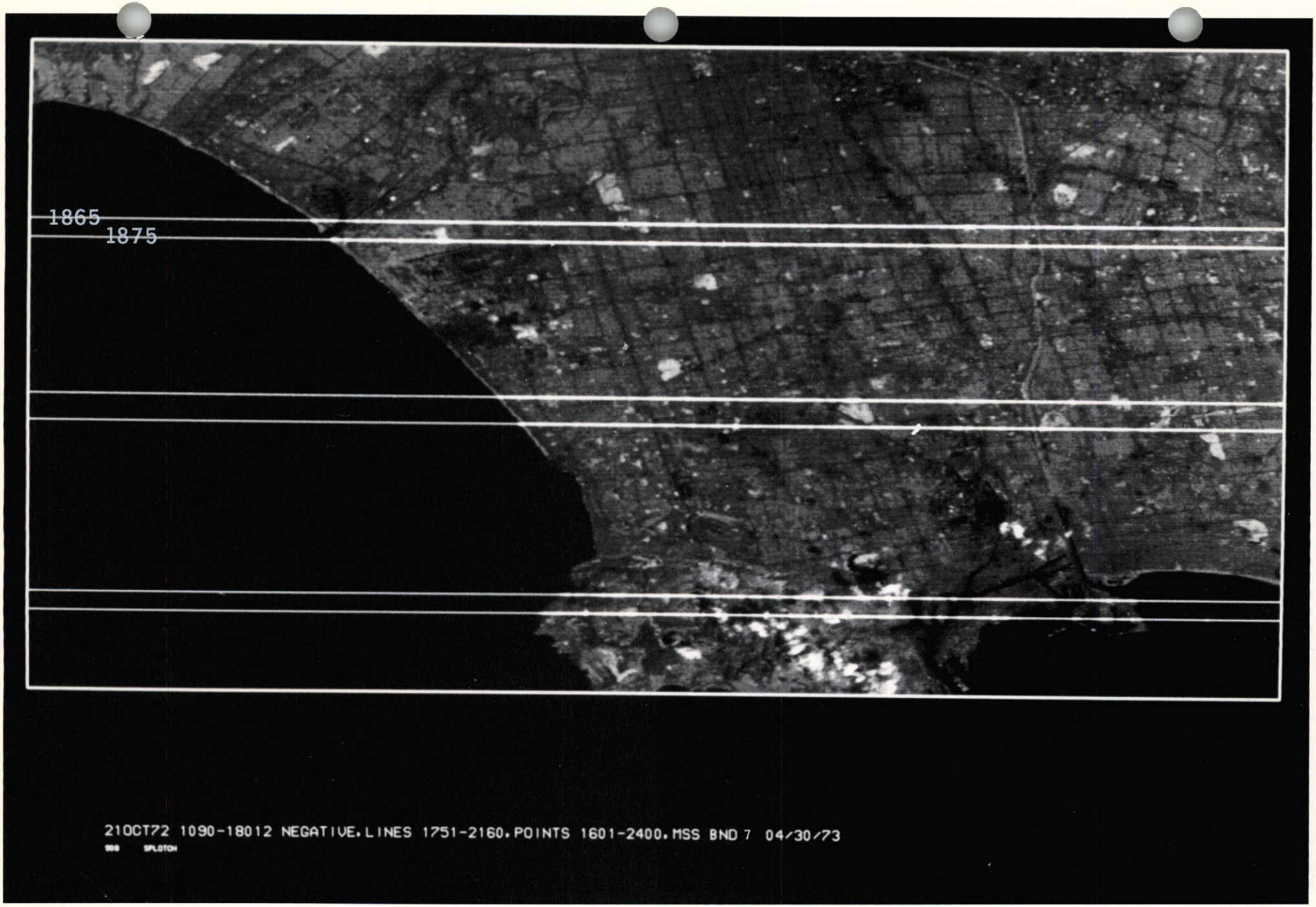
1865
1875
21OCT72 1090-18012 NEGATIVE. LINES 1751-2160. POINTS 1601-2400. MSS BND 7 04/30/73
900 SPLOTCH

FIG. 12

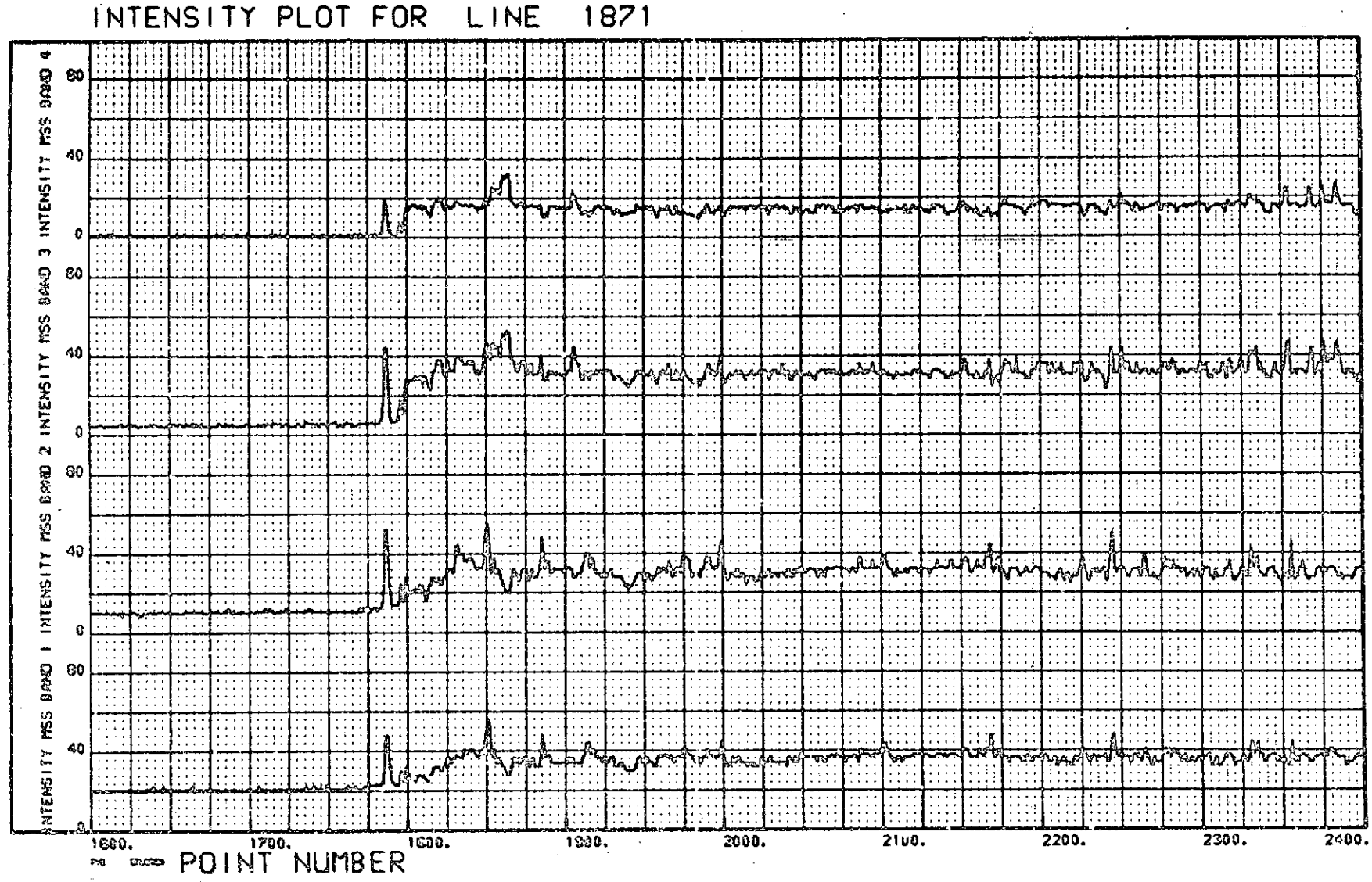
INTENSITY PLOT FOR LINE 1871
INTENSITY MSS BAND 1
INTENSITY MSS BAND 2
INTENSITY MSS BAND 3
INTENSITY MSS BAND 4
80
40
0
80
40
0
80
40
0
80
40
0
1600.
1700.
1800.
1900.
2000.
2100.
2200.
2300.
2400.
POINT NUMBER

FIG. 13

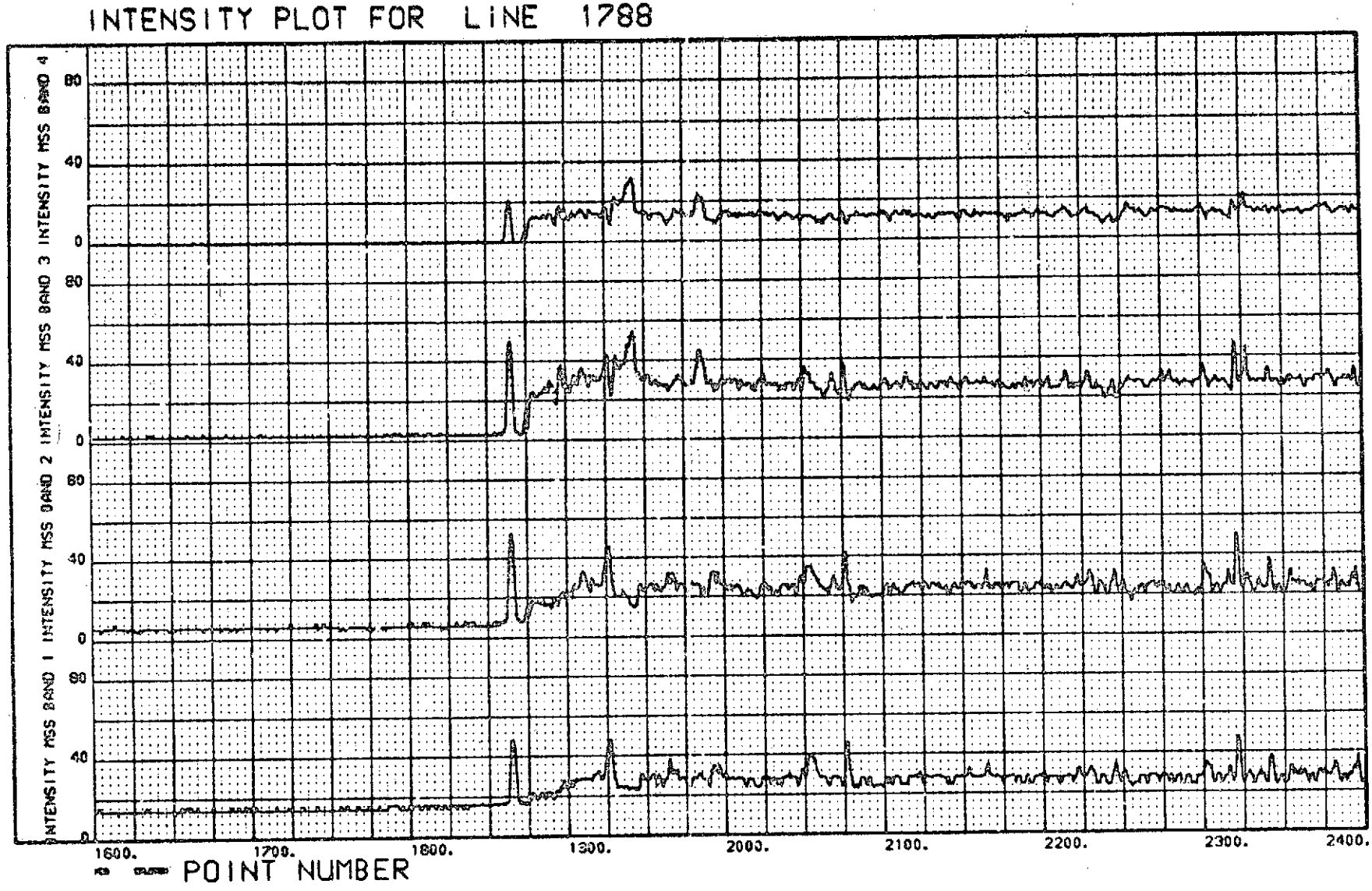
INTENSITY PLOT FOR LINE 1788
INTENSITY MSS BAND 1 INTENSITY MSS BAND 2 INTENSITY MSS BAND 3 INTENSITY MSS BAND 4
80
40
0
1600.
1700.
1800.
1900.
2000.
2100.
2200.
2300.
2400.
POINT NUMBER

FIG. 14

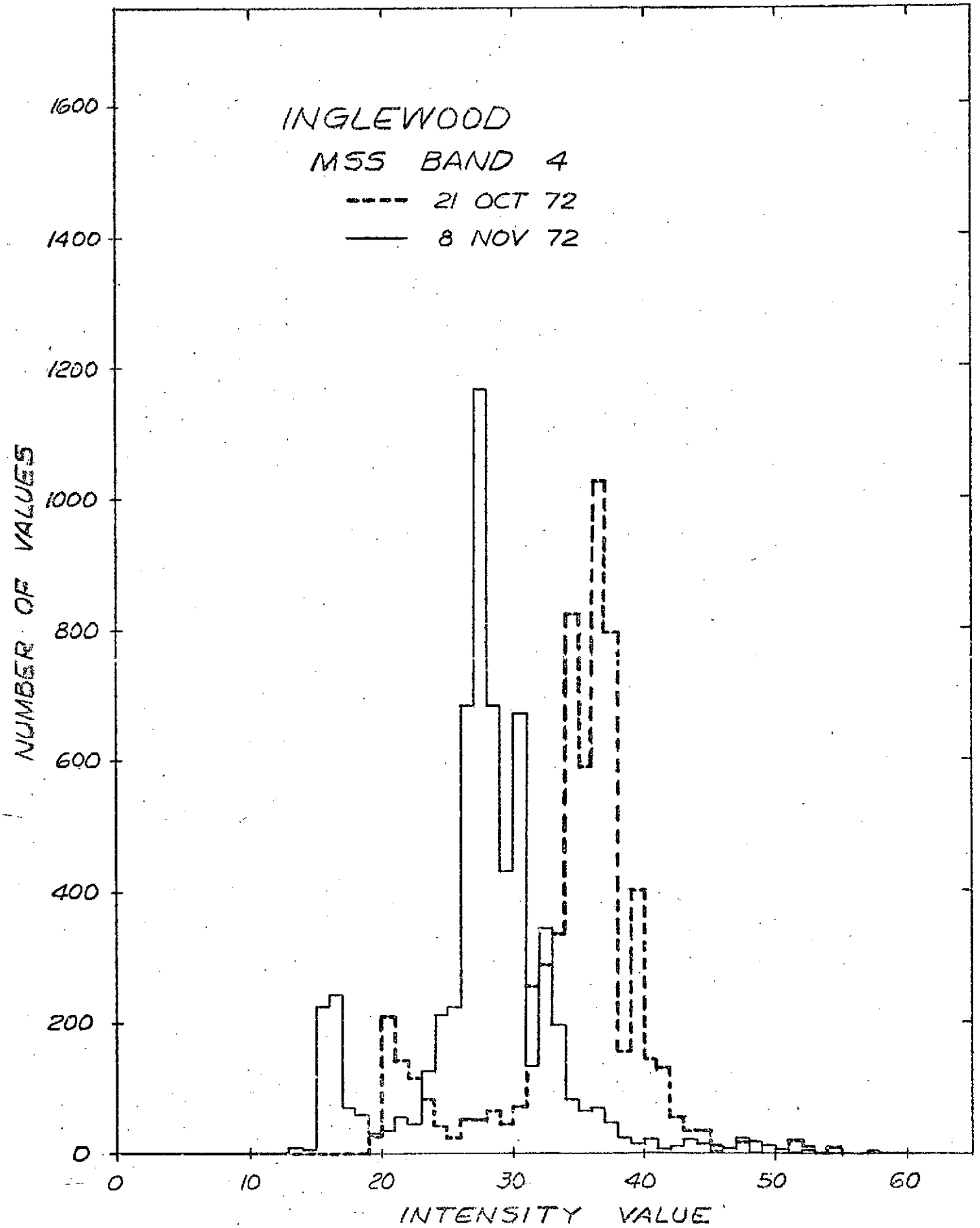
INGLEWOOD
MSS BAND 4
21 OCT 72
8 NOV 72
NUMBER OF VALUES
1600
1400
1200
1000
800
600
400
200
0
0
10
20
30
40
50
60
INTENSITY VALUE

FIG. 15

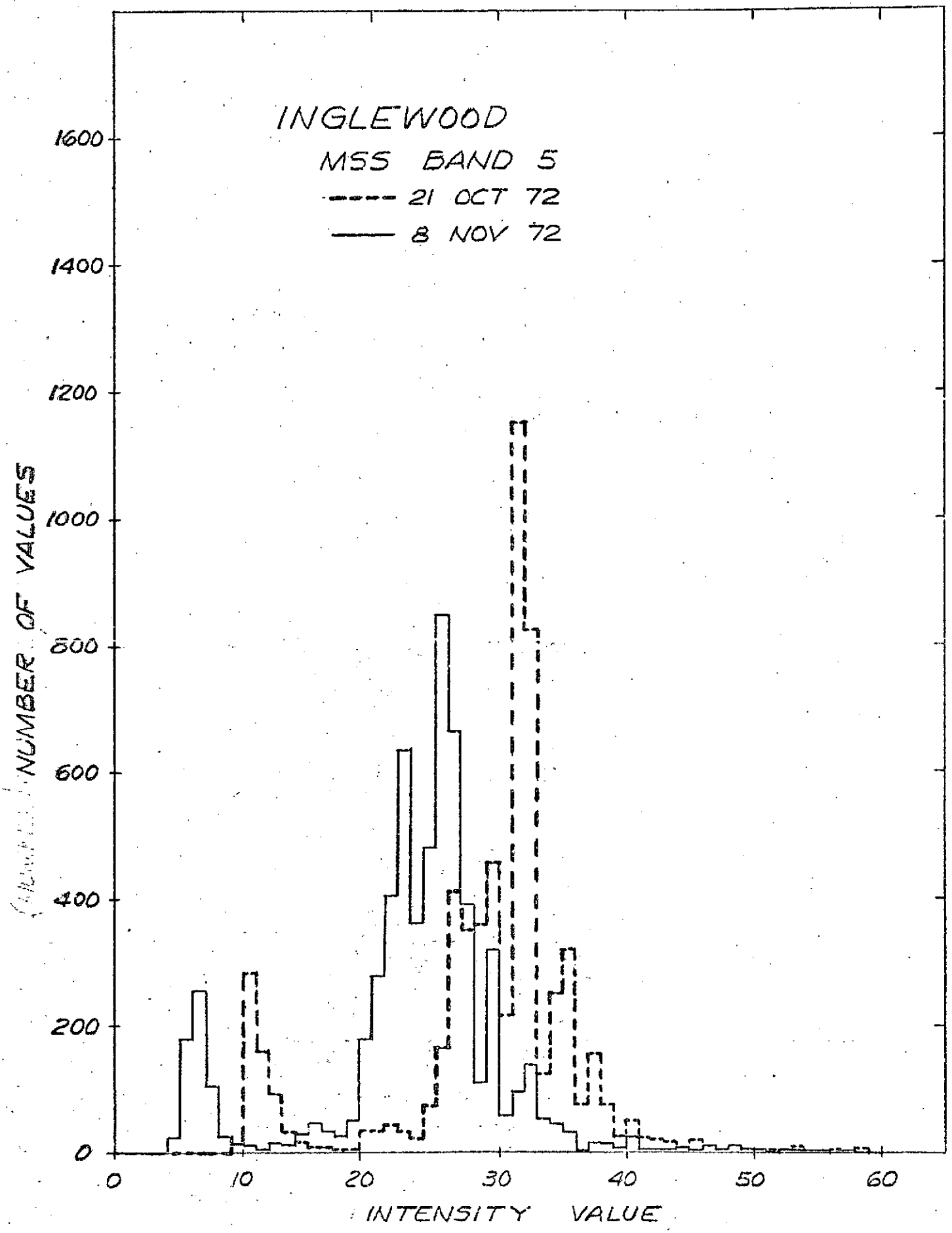
INGLEWOOD
MSS BAND 5
21 OCT 72
8 NOV 72
NUMBER OF VALUES
1600
1400
1200
1000
800
600
400
200
0
0
10
20
30
40
50
60
INTENSITY VALUE

FIG. 16

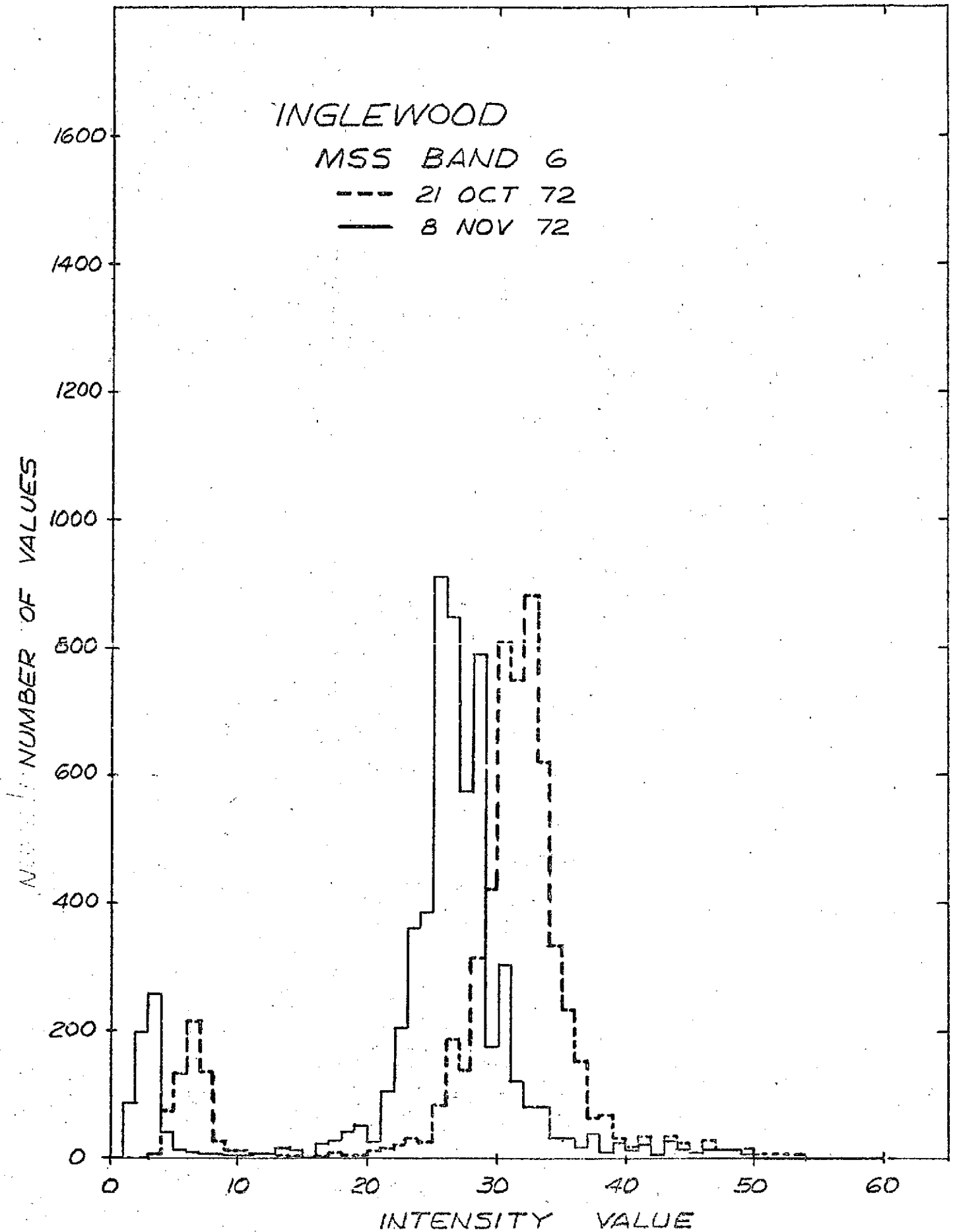
INGLEWOOD
MSS BAND 6
21 OCT 72
8 NOV 72
NUMBER OF VALUES
1600
1400
1200
1000
800
600
400
200
0
0
10
20
30
40
50
60
INTENSITY VALUE

FIG. 17

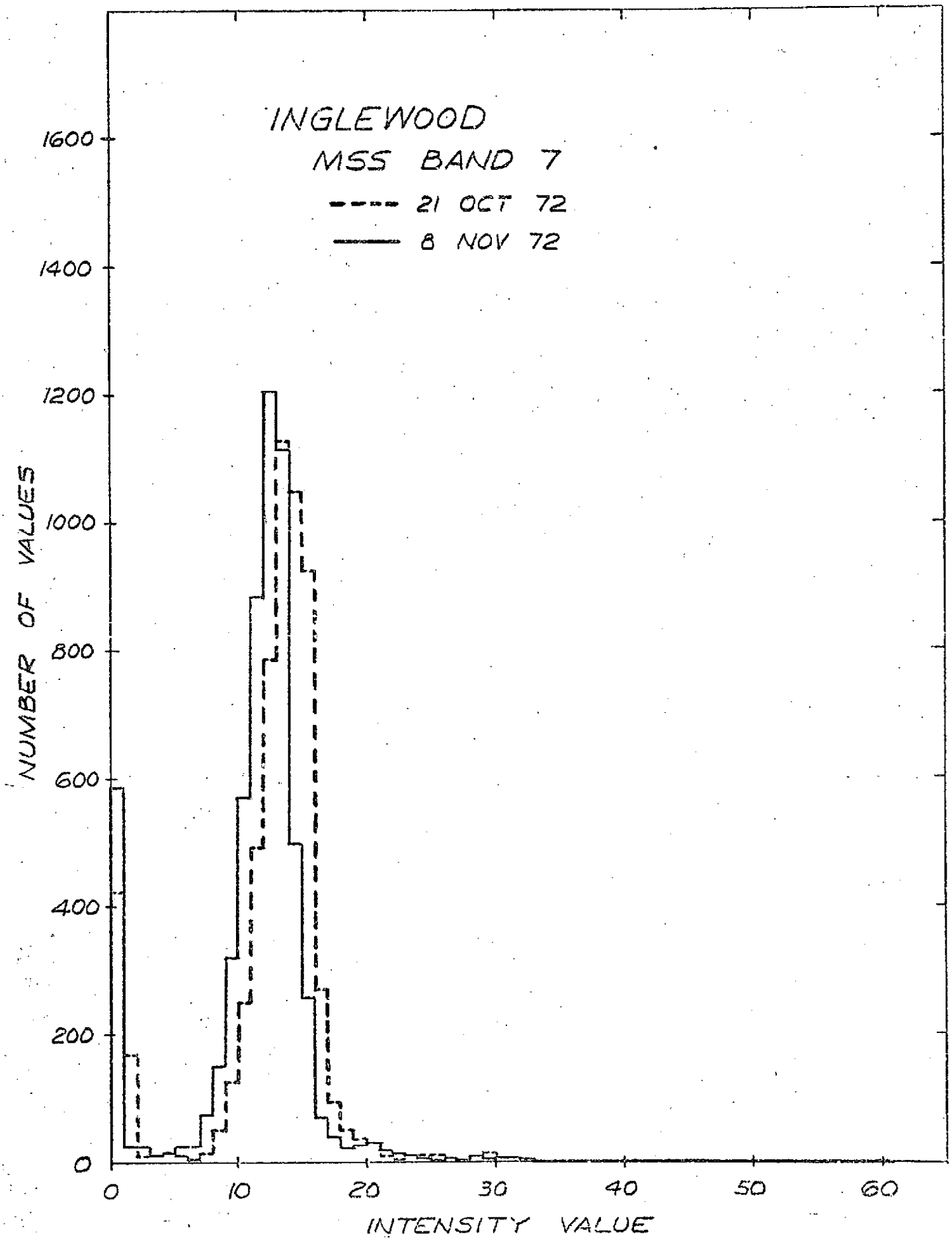
INGLEWOOD
MSS BAND 7
21 OCT 72
8 NOV 72
NUMBER OF VALUES
0
200
400
600
800
1000
1200
1400
1600
0
10
20
30
40
50
60
INTENSITY VALUE

FIG. 18

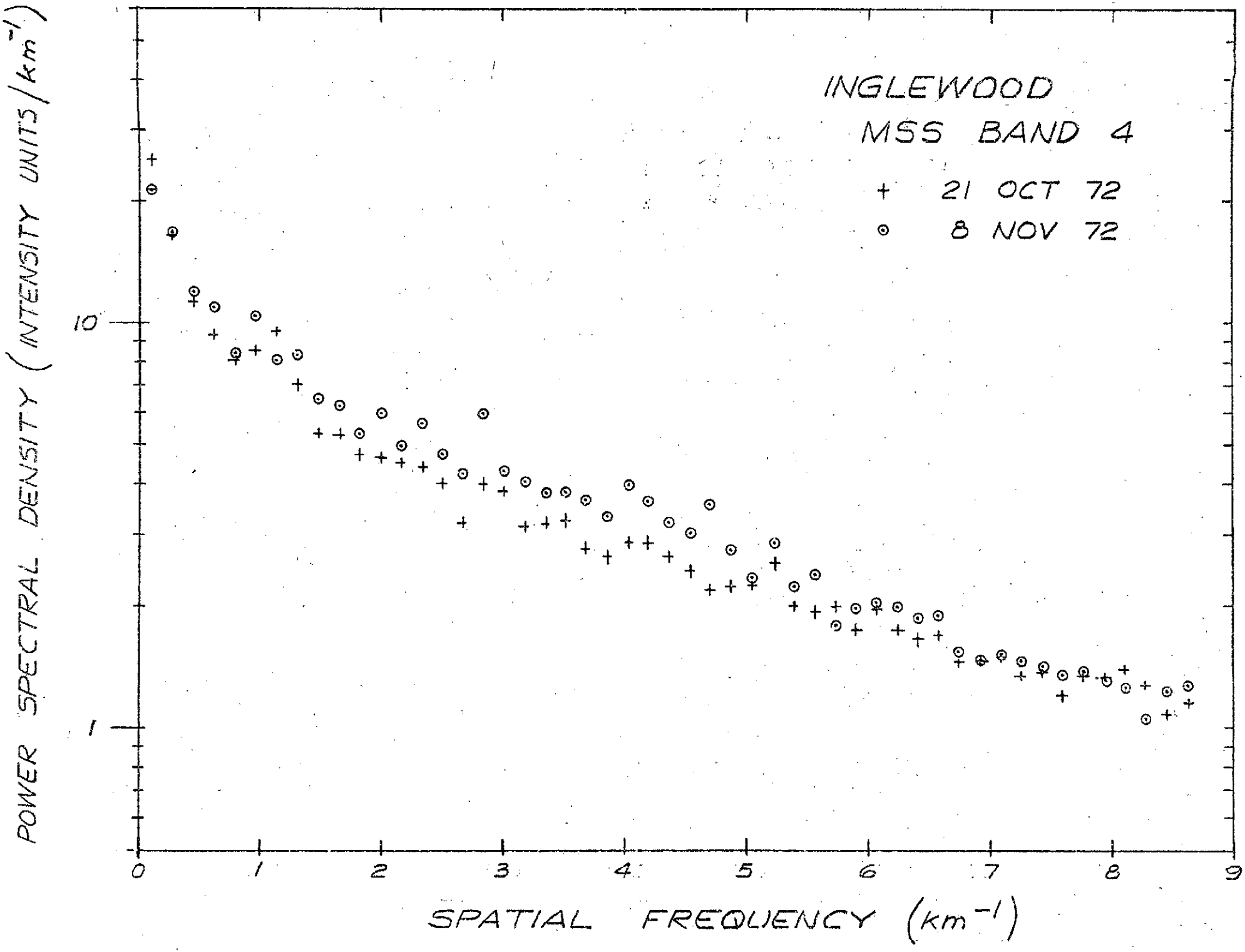
INGLEWOOD
MSS BAND 4
+ 21 OCT 72
⊙ 8 NOV 72
POWER SPECTRAL DENSITY (INTENSITY UNITS/km⁻¹)
10
1
0
1
2
3
4
5
6
7
8
9
SPATIAL FREQUENCY (km⁻¹)

FIG. 19

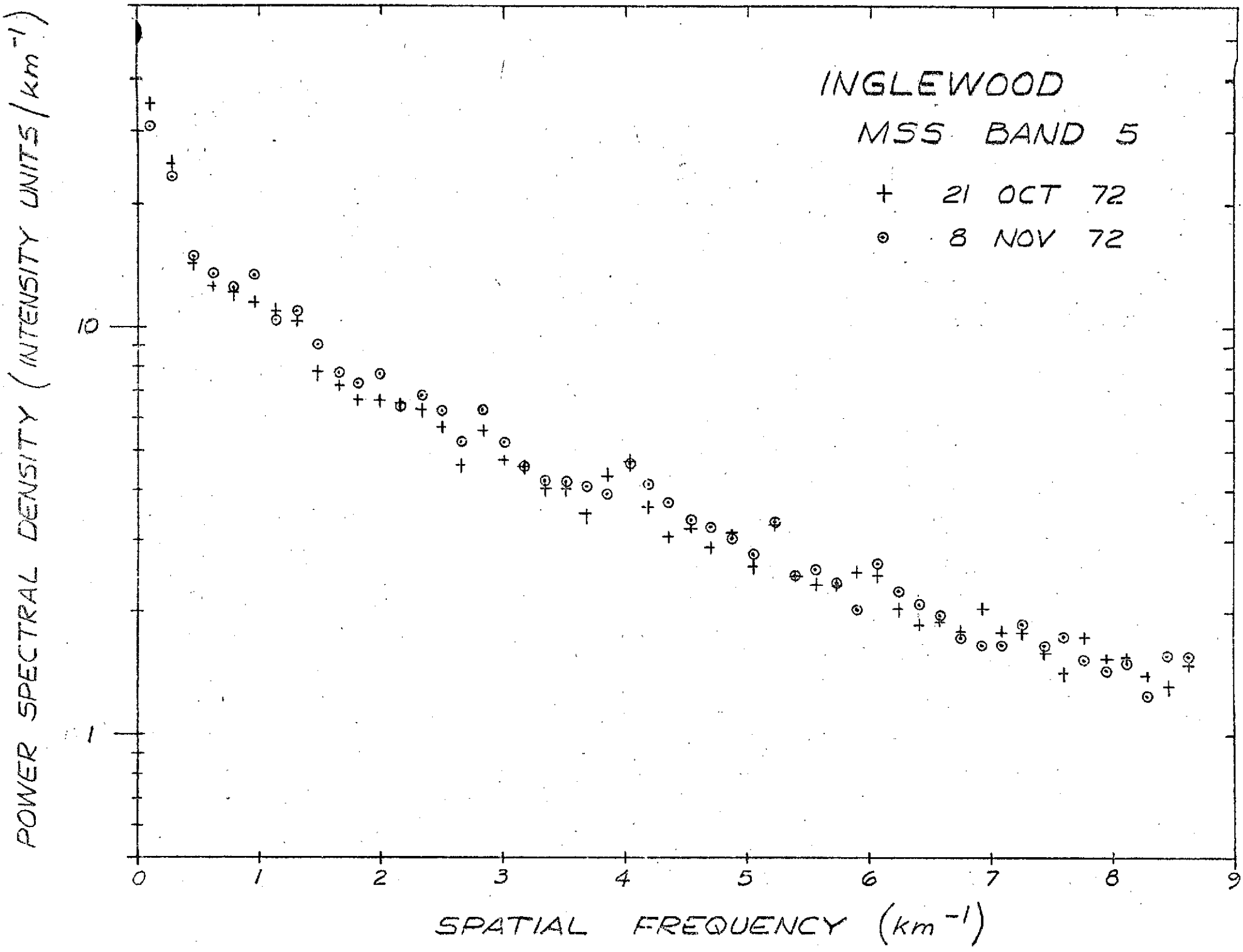
INGLEWOOD
MSS BAND 5
+ 21 OCT 72
⊙ 8 NOV 72
POWER SPECTRAL DENSITY (INTENSITY UNITS/km⁻¹)
10
1
0
1
2
3
4
5
6
7
8
9
SPATIAL FREQUENCY (km⁻¹)

FIG. 20

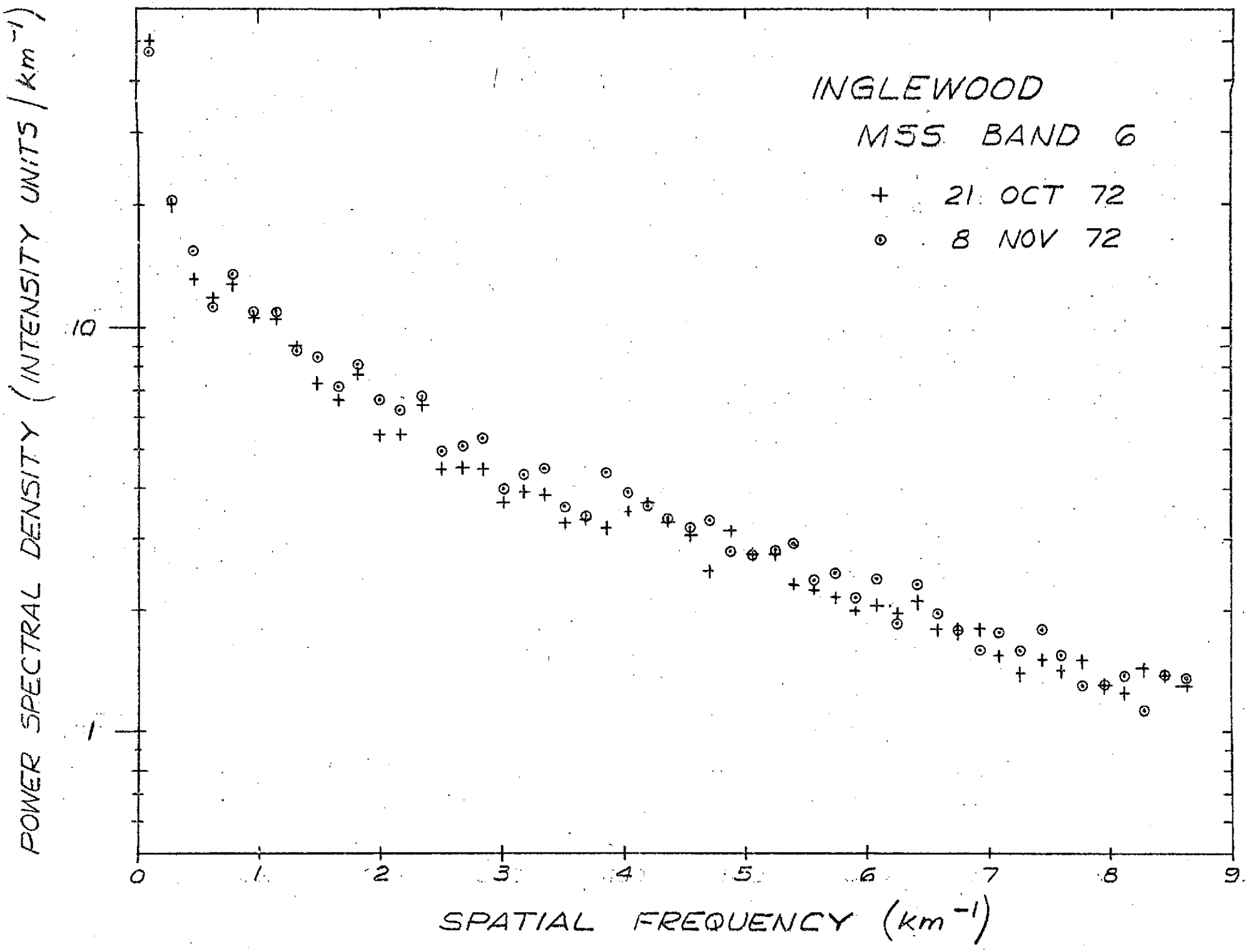
INGLEWOOD
MSS BAND 6
+ 21 OCT 72
⊙ 8 NOV 72
POWER SPECTRAL DENSITY (INTENSITY UNITS / km⁻¹)
10
1
0
1
2
3
4
5
6
7
8
9
SPATIAL FREQUENCY (km⁻¹)

FIG. 21

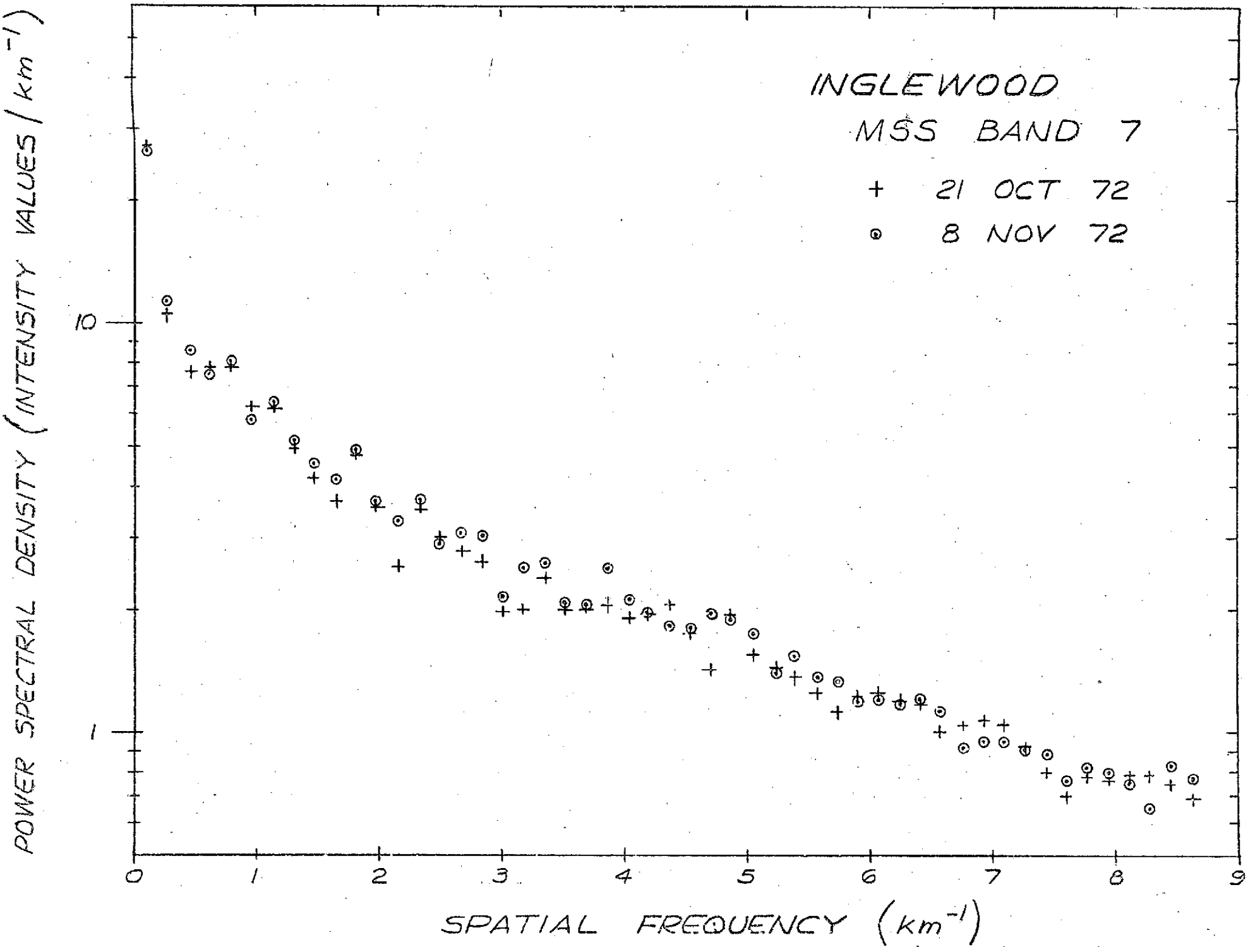
INGLEWOOD
MSS BAND 7
+ 21 OCT 72
⊙ 8 NOV 72
POWER SPECTRAL DENSITY (INTENSITY VALUES / km⁻¹)
10
1
0
1
2
3
4
5
6
7
8
9
SPATIAL FREQUENCY (km⁻¹)

FIG. 22

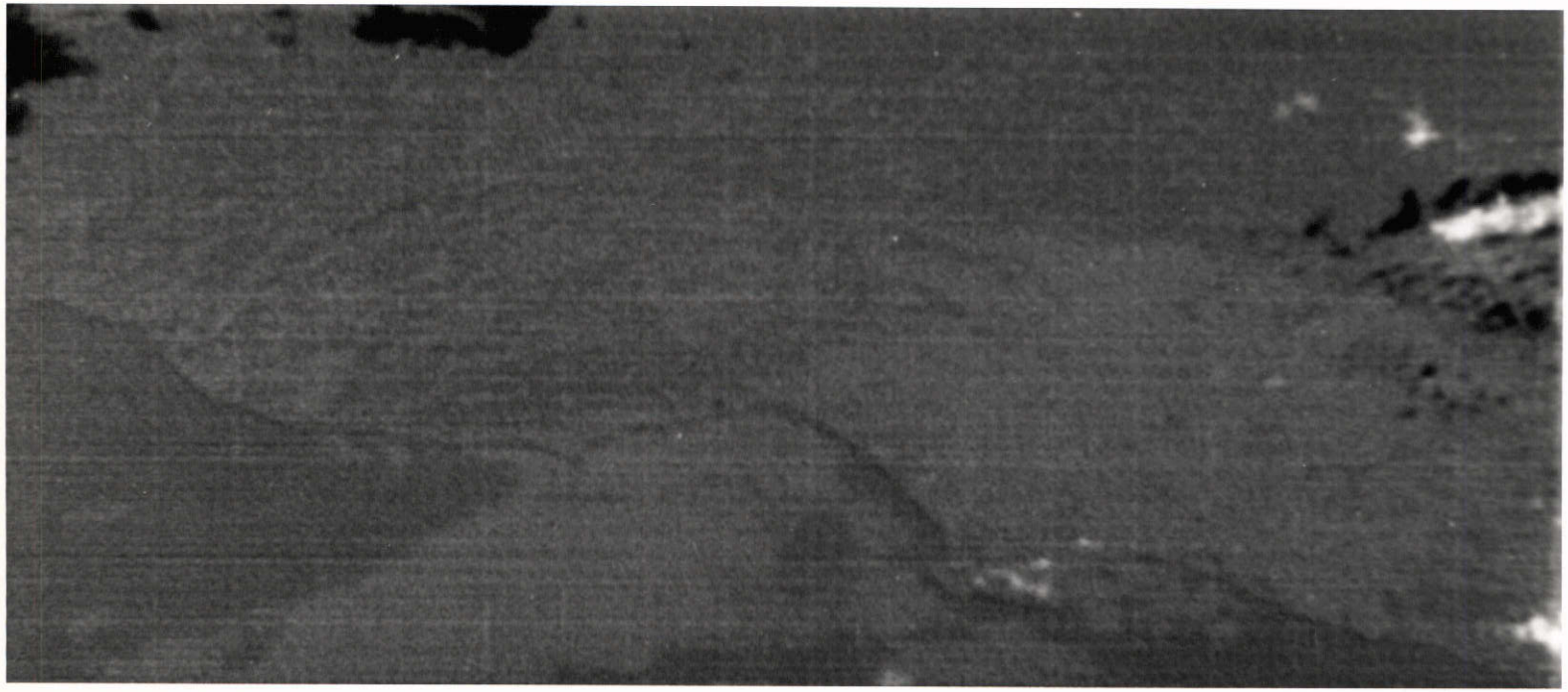

FIG. 23

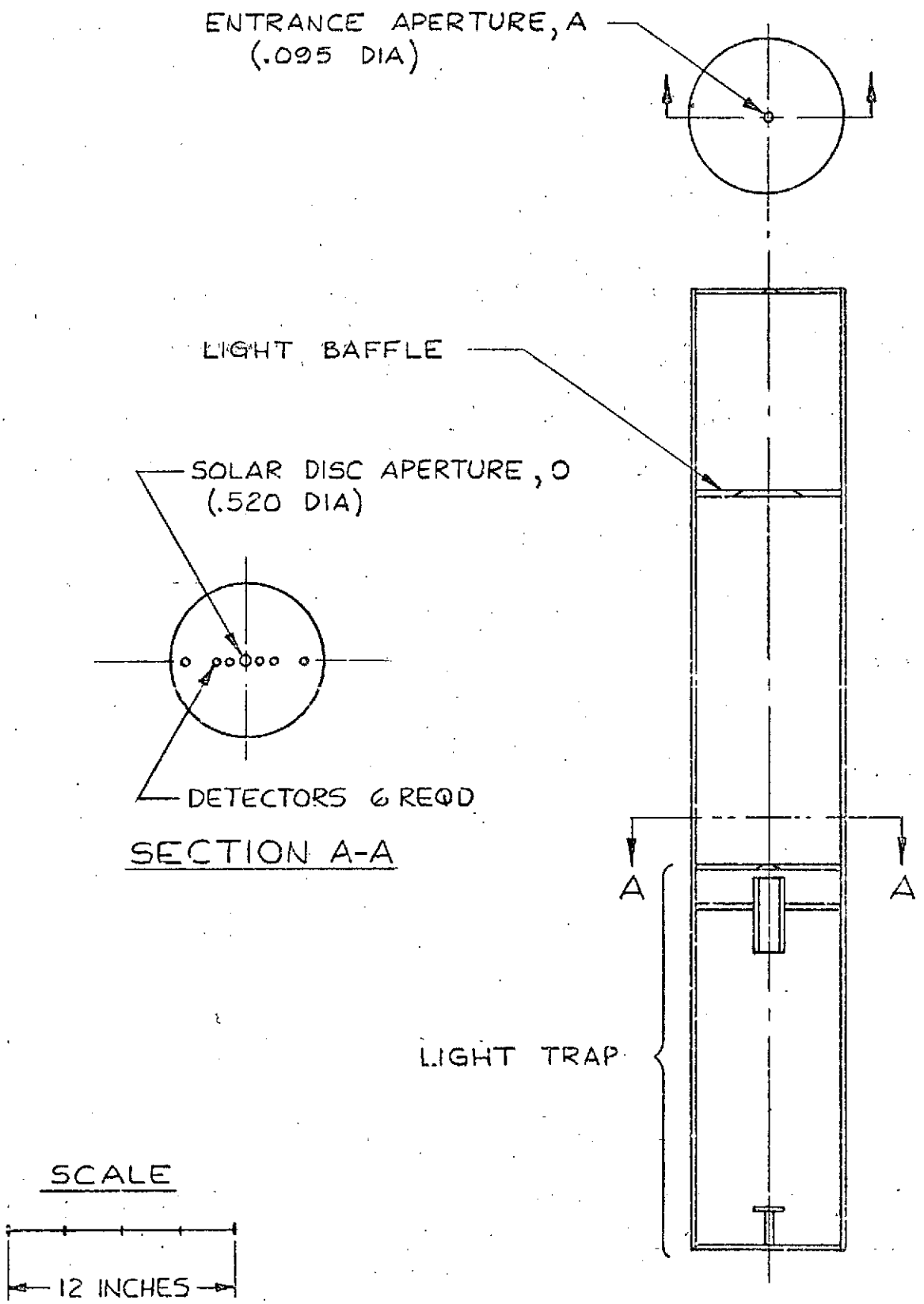
ENTRANCE APERTURE, A
(.095 DIA)
LIGHT BAFFLE
SOLAR DISC APERTURE, O
(.520 DIA)
DETECTORS 6 REQD
SECTION A-A
A
A
LIGHT TRAP
SCALE
12 INCHES

FIG. 24

FIG. 25

APPENDIX A

GROUND TRUTH DATA

Table A-I. Visual Observations of the Haze Conditions, Including the Altitude of the Top of the Haze Layer Over the Test Area at the Times of ERTS-1 Passes

Letters and numbers in parentheses refer to locations shown in Fig. 1.

In order of increasing haziness the haze conditions are described as: clear, very light, light, moderate, moderate to heavy, heavy, very heavy, extremely heavy.

14 Sept 1972 - Pass over San Bernardino. Cloud free. Moderate to heavy haze (smog) over the Los Angeles basin (A, B, D, E, H, I, L, 1, 6, 7). Haze top at 2,500 ft. over Torrance (7) and Inglewood (H). Heavy haze (smog) over San Bernardino and Ontario (4). Clear north of the San Bernardino mountains in Antelope Valley and Lucerne Valley. Clear at Big Bear and Arrowhead (high in the San Bernardino mountains).

2 Oct 1972 - Pass over San Bernardino. Broken clouds, bottoms around 2,500 ft, tops about 5,500 ft. over the Los Angeles basin. Very light haze tops at 5,500 ft. over the Los Angeles basin (A, D, E, H, 1, 6). Too cloudy over San Bernardino and Ontario (4) for analysis.

21 Oct 1972 - Pass over Los Angeles. Heavy haze (smog) over the entire Los Angeles basin (A, B, D, E, G, H, I, L, 1, 4, 5, 6, 7). Haze tops at 3,500 ft. over Torrance (7) and LAX (1), slightly higher inland. There is moderate to heavy haze (smog) over the southern part of the San Fernando Valley decreasing to light haze at the northern side of the Valley. There is a clear area around

Table A-1 (Cont.)

the Van Norman reservoir. It is clear in the Newhall area (J). It is clear over Palmdale (8) and Lancaster (K). There are a few small low clouds over the Palos Verdes Peninsula (near 7), Orange County (5), and Ontario (4).

8 Nov 1972 - Pass over Los Angeles. A very clear day. It is clear over the Los Angeles basin west of Whittier (I) and Arcadia (B). There is very light haze over Orange County (5). Light to moderate haze (smog) and scattered clouds over Pomona (G) and Ontario (4). It is clear over the San Fernando Valley (F, 2, 3). It is clear around Newhall (J) and over Palmdale (8) and Lancaster (K). It is very cloudy northwest of Newhall (J).

25 Nov 1972 - Pass over San Bernardino. There are scattered cirrus clouds which might well confuse a haze analysis. There is light haze, which tops at 1,000 ft. over the Los Angeles basin. The haze is patchy around Anaheim because it settles in low areas. Clear over Riverside and San Bernardino. Light haze over Pomona (G) and Ontario (4) similar to the Los Angeles basin.

26 Nov 1972 - Pass over Los Angeles. Smog has been blown out to sea. Clear over the San Fernando Valley. Clear over the Los Angeles basin except for a very thin layer of smog, 100 to 200 ft. thick. In some places this layer is at ground level, in other places as much as 1,000 ft. above ground level. It looks slightly hazier over Orange County (5) than over the Los Angeles basin.

14 Mar 1973 - Pass over Los Angeles. A very clear day. Just a hint of haze over Anaheim and Long Beach (6). Some clouds over the San Gabriel mountains.

Table A-1 (Cont.)

1 Apr 1973 - Pass over Los Angeles. Very light haze (marine type not smog) over the Los Angeles basin (A, B, D, E, H, I, 1, 6, 7). Haze tops at 5, 500 ft. A few clouds also top at 5, 500 ft. No cirrus above. There are heavy clouds northwest of Newhall (J).

19 Apr 1973 - Pass over Los Angeles. Very light haze along the coast (D, 1, 7) and over the San Fernando Valley (F, 2, 3). Moderate haze and some low scattered clouds over the remainder of the Los Angeles basin (A, B, E, H, I, L, 6). The top of the haze layer is at 4, 000 ft. No cirrus.

7 May 1973 - Pass over Los Angeles. Heavy haze (fog and smog) over Los Angeles basin (A, D, E, H, 1, 7, 6). Top of haze layer and some scattered clouds at 2, 800 ft. Light fog over the ocean. There are cirrus north of Santa Monica (D), but none south of Santa Monica. There is moderate to heavy haze over the San Fernando Valley (F, 2, 3).

18 July 1973 - Pass over Los Angeles. Moderate to heavy haze (fog) over the Los Angeles basin. The haze layer tops at 2, 100 ft. Broken clouds top at the same altitude. There are high cirrus clouds over the area.

Table A-II. Airport Visibility and Humidity Data, Air Pollution Control District Data, Vertical Temperature Profile and Solar Aureole Brightness

DATE: 9 AUG 1972 TIME: 10:00 AM P.S.T.

LOCATION	VISIBILITY (MILES)	RELATIVE HUMIDITY (%)	PARTICULATE DENSITY (Km x 10)	NO (PPHM)	NO_2 (PPHM)	O_3 (PPHM)	HYDRO-CARBONS (PPM)	CH_4 (PPM)	CO (PPM)	SO_2 (PPHM)
1	7	76								
2	5	54								
3										
4	3	56								
5										
6	7	70								
7										
8	25	25								
9										
A	4	59	27			7	4	3	4	3
B			32	1	9	6	3	3	3	2
C			41	6	14	6	3	3	6	2
D			17	1	3	3			2	2
E			22	8	7	1			5	1
F			33	4	14	6	3	3	4	1
G			23	3	10		3	2	5	1
H			11	2	3	1	2	1	3	5
I				2	7	4	2	2	3	2
J			33	1	9	10	3	2	5	
K			7	1	1	8	2	2	1	1
L			35	1	12	7	3	3	5	1

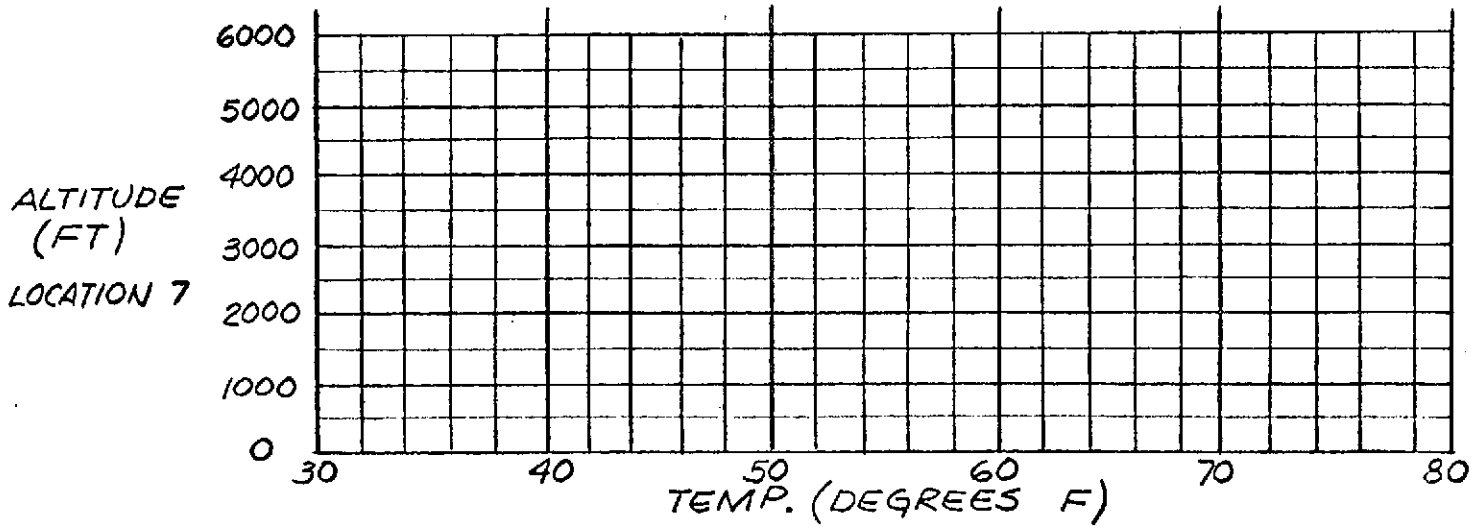

SOLAR AUREOLE BRIGHTNESS (WATTS/ cm^2 STER)					
LOCATION	SOLAR ELEVATION ANGLE (DEG)	DISTANCE FROM THE CENTER OF THE SOLAR DISC ALONG THE ALMUCANTAR			
		0 DEG	1 1/2 DEG	3 DEG	6 DEG

Table A-II (Cont.)

DATE: 10 AUG 1972 TIME: 10:00 AM P.S.T.

LOCATION	VISIBILITY (MILES)	RELATIVE HUMIDITY (%)	PARTICULATE DENSITY (Km x 10)	NO (PPHM)	NO2 (PPHM)	O3 (PPHM)	HYDRO-CARBONS (PPM)	CH4 (PPM)	CO (PPM)	SO2 (PPHM)
1	4	73								
2	3	55								
3										
4	2	51								
5										
6	5	66								
7										
8	10	22								
9										
A	4	58	44	4	17	5	4	3	5	3
B			47	2	11	6	4	3	5	3
C			43	2	19	10	4	3	7	1
D			17	1	4	5			3	2
E			28	6	9	1			4	5
F			30	3	14	7	3	3	4	2
G			29	4	14	5	3	2	6	1
H			23	3	6	1	2	1	5	7
I				5	11	2	2	2	3	4
J			35	1	6	1	3	2	4	
K			7	1	1	6	2	2	1	2
L			49	2	19	9	4	3	6	1

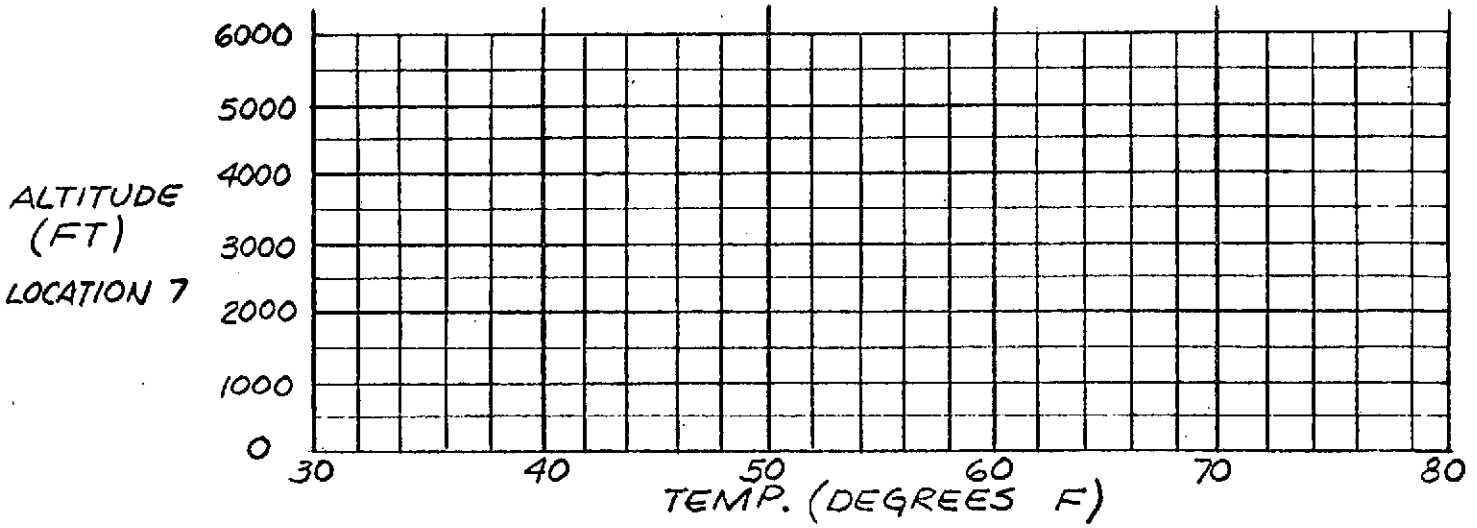

SOLAR AUREOLE BRIGHTNESS (WATTS/cm² STER)					
LOCATION	SOLAR ELEVATION ANGLE (DEG)	DISTANCE FROM THE CENTER OF THE SOLAR DISC ALONG THE ALMUCANTAR			
		0 DEG	1 1/2 DEG	3 DEG	6 DEG

Table A-II (Cont.)

DATE: 27 AUG 1972 TIME: 10:00 AM P.S.T.

LOCATION	VISIBILITY (MILES)	RELATIVE HUMIDITY (%)	PARTICULATE DENSITY (Km x 10)	NO (PPHM)	NO2 (PPHM)	O3 (PPHM)	HYDRO-CARBONS (PPM)	CH4 (PPM)	CO (PPM)	SO2 (PPHM)
1		81								
2		79								
3										
4		73								
5										
6		76								
7										
8		43								
9										
A		66	22	2	7	3	3	3	3	2
B			17	2	5	4	3	3	2	2
C			15	2	6	3	2	2	2	2
D			11	1	3	4			3	2
E			16	5	7	1			4	5
F			15	1	6	6	3	3	2	1
G			16	3	7	3	2	2	5	1
H			23	2	3	2	2	2	2	1
I				2	5	3	2	2	2	3
J			15	1	7	8	2	2	3	
K			5	1	1	4	2	2	2	1
L			21	1	6	4	2	2	3	2

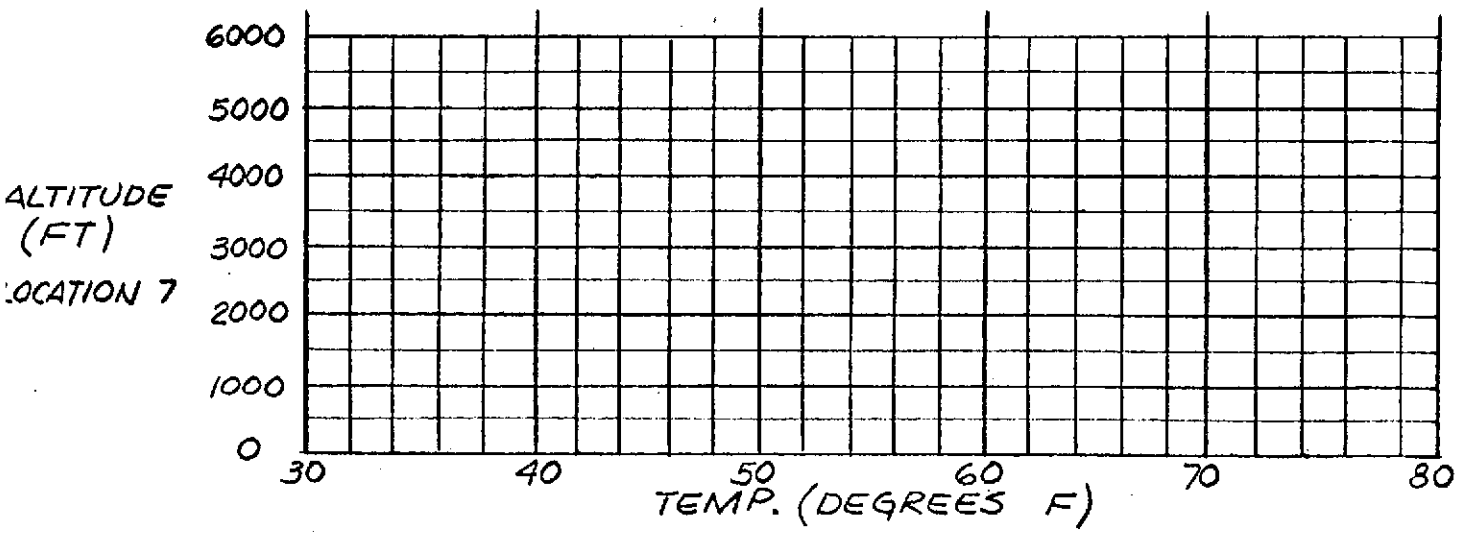

SOLAR AUREOLE BRIGHTNESS (WATTS/cm² STER)					
LOCATION	SOLAR ELEVATION ANGLE (DEG)	DISTANCE FROM THE CENTER OF THE SOLAR DISC ALONG THE ALMUCANTAR			
		0 DEG	1 1/2 DEG	3 DEG	6 DEG

Table A-II (Cont.)

DATE: 28 AUG 1972 TIME: 10:00 AM P.S.T.

LOCATION	VISIBILITY (MILES)	RELATIVE HUMIDITY (%)	PARTICULATE DENSITY (Km x 10)	NO (PPHM)	NO_2 (PPHM)	O_3 (PPHM)	HYDRO-CARBONS (PPM)	CH_4 (PPM)	CO (PPM)	SO_2 (PPHM)
1		62								
2		56								
3										
4		56								
5										
6		55								
7										
8		38								
9										
A		50		3	22	13	4	3	7	2
B				3	12	9	4	3	6	3
C				2	13	8			5	2
D				1	6	5			5	1
E				6	16	5				3
F				1	6	11	3	3	2	2
G				3	8	8	2	2	5	2
H				3	7	5	3	3	6	1
I				1	12	11	3	2	6	4
J				1	2	5	2	2	2	
K				1	1	4	2	2	2	
L				1	6	12	3	2	4	2

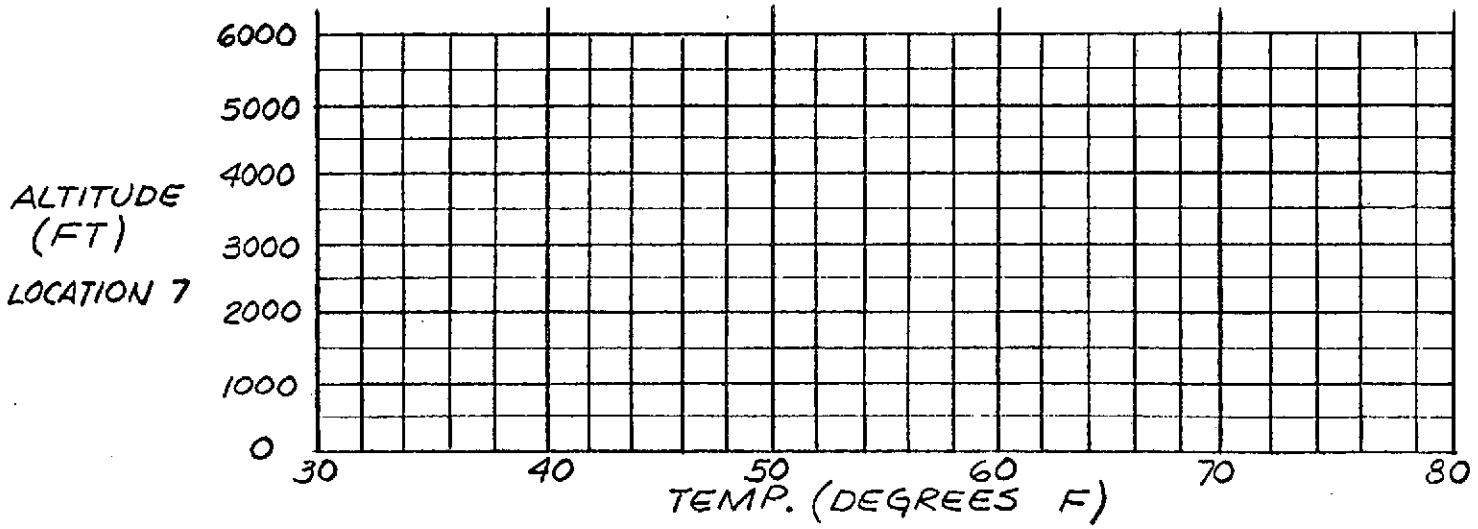

SOLAR AUREOLE BRIGHTNESS (WATTS/cm² STER)					
LOCATION	SOLAR ELEVATION ANGLE (DEG)	DISTANCE FROM THE CENTER OF THE SOLAR DISC ALONG THE ALMUCANTAR			
		0 DEG	1 1/2 DEG	3 DEG	6 DEG

Table A-II (Cont.)

DATE: 14 SEPT 1972 TIME: 10:00 AM P.S.T.

LOCATION	VISIBILITY (MILES)	RELATIVE HUMIDITY (%)	PARTICULATE DENSITY (Km x 10)	NO (PPHM)	NO_2 (PPHM)	O_3 (PPHM)	HYDRO-CARBONS (PPM)	CH_4 (PPM)	CO (PPM)	SO_2 (PPHM)
1	7	70								
2	6	47								
3	7									
4	3	43								
5	5									
6	6	64								
7										
8	20	19								
9	25	55								
A	7		25	1	10	6	3	2	3	1
B			50	2	15	10	5	4	6	4
C			35	2	16	9	4	2	6	2
D			13	1	4	4			2	1
E			23	6	14	1			3	7
F			28	1	14	10	4	2	4	1
G			38	3	13	10	4	3	6	2
H			14	4	6	1	2	1	1	5
I				4	18	4	4	2	4	4
J			27	1	6	10	3	2	6	
K			12	1	1	5	2	2	3	4
L			57	2	17	11	4	2	7	1

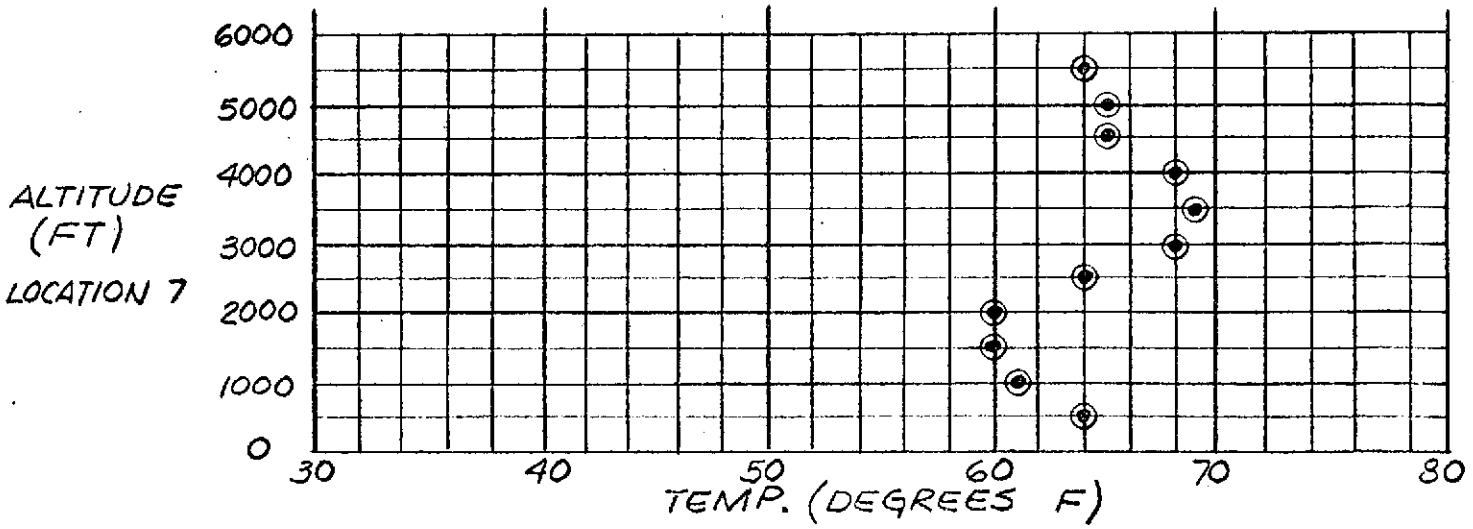

SOLAR AUREOLE BRIGHTNESS (WATTS/cm² STER)					
LOCATION	SOLAR ELEVATION ANGLE (DEG)	DISTANCE FROM THE CENTER OF THE SOLAR DISC ALONG THE ALMUCANTAR			
		0 DEG	1 1/2 DEG	3 DEG	6 DEG
1	50	3.5×10^{2}	1.6×10^{-2}	1.3×10^{-2}	1.1×10^{-2}

Table A-II (Cont.)

DATE: 15 SEPT 1972 TIME: 10:00 AM P.S.T.

LOCATION	VISIBILITY (MILES)	RELATIVE HUMIDITY (%)	PARTICULATE DENSITY (Km x 10)	NO (PPHM)	NO_2 (PPHM)	O_3 (PPHM)	HYDRO-CARBONS (PPM)	CH_4 (PPM)	CO (PPM)	SO_2 (PPHM)
1	2.5	73								
2	3	75								
3										
4	1.5	61								
5										
6	2.5	73								
7										
8	30	22								
9										
A	2	54	45	2	16	7	4	2	6	4
B			52	3	17	3	4	3	5	5
C			43	4	19	4	3	2	6	3
D			41	1	9	4			4	3
E			43	9	15	2			5	4
F			33	1	9	9	3	3	2	3
G			45	6	16	6	4	3	7	3
H			35			1	4	2	4	
I				2	12	7	4	2	4	10
J			25	1	9	11	2	2	7	
K			10	1	1	7	2	2	2	3
L			60	2	14	9	4	2	7	2

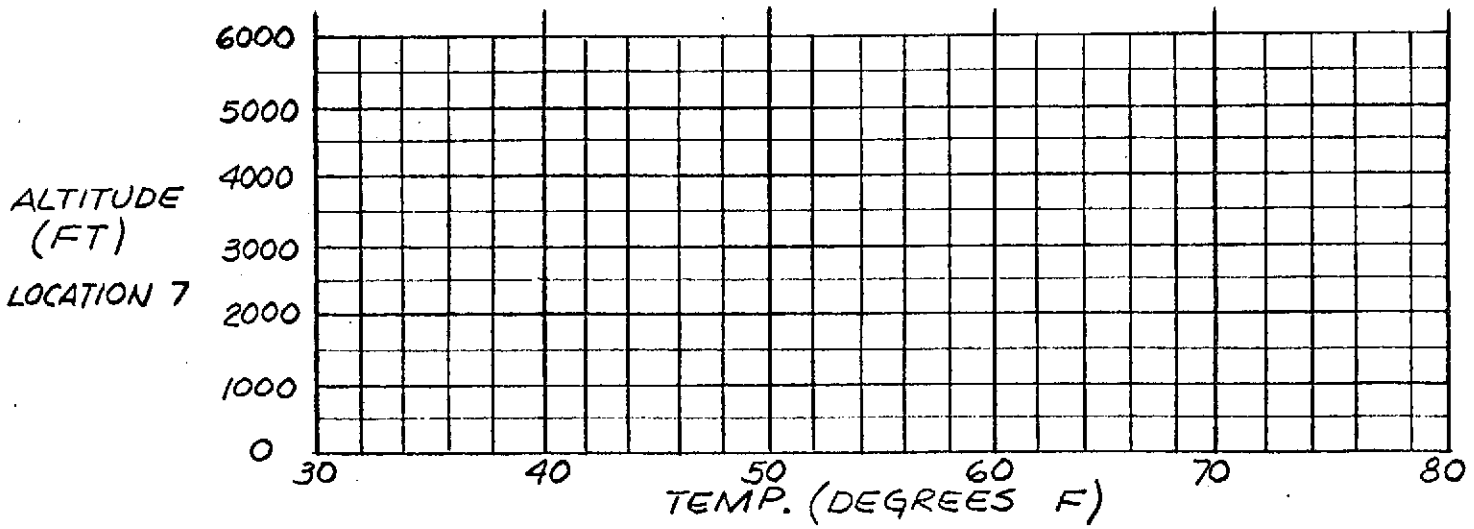

SOLAR AUREOLE BRIGHTNESS (WATTS/cm² STER)					
LOCATION	SOLAR ELEVATION ANGLE (DEG)	DISTANCE FROM THE CENTER OF THE SOLAR DISC ALONG THE ALMUCANTAR			
		0 DEG	1 1/2 DEG	3 DEG	6 DEG

Table A-II (Cont.)

DATE: 2 OCT 1972 TIME: 10:00 AM P.S.T.

LOCATION	VISIBILITY (MILES)	RELATIVE HUMIDITY (%)	PARTICULATE DENSITY (Km x 10)	NO (PPHM)	NO2 (PPHM)	O3 (PPHM)	HYDRO-CARBONS (PPM)	CH4 (PPM)	CO (PPM)	SO2 (PPHM)
1	20	57								
2	10	70								
3	10									
4	15	54								
5	15									
6	20	55								
7										
8	25	38								
9	40									
A	20	54	18	2	8	1	3	3	2	1
B			11	1	1	2	4	3	2	1
C			13	2	6	2	2	2	4	1
D			13	1	5	1			2	1
E			15	4	2	2			6	1
F			20	1	4	3	3	3	1	1
G			10	4	3	3	2	2	4	1
H			11	8	6	1	2	2	1	1
I				2	3	2	2	2	3	2
J			13	1	4	2	2	2	4	
K			5	1	1	3	2	2	2	
L			10	2	4	2	2	2	2	1

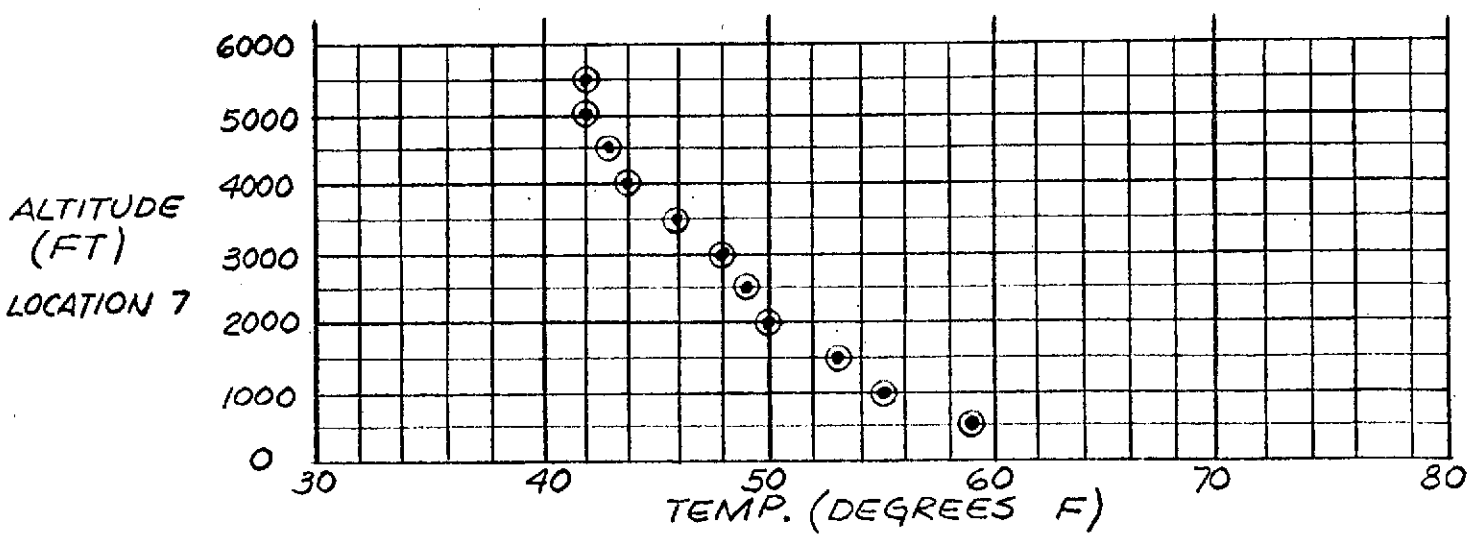

SOLAR AUREOLE BRIGHTNESS (WATTS/cm² STER)					
LOCATION	SOLAR ELEVATION ANGLE (DEG)	DISTANCE FROM THE CENTER OF THE SOLAR DISC ALONG THE ALMUCANTAR			
		0 DEG	1 1/2 DEG	3 DEG	6 DEG

Table A-II (Cont.)

DATE: 3 OCT 1972 TIME: 10:00 AM P.S.T.

LOCATION	VISIBILITY (MILES)	RELATIVE HUMIDITY (%)	PARTICULATE DENSITY (Km x 10)	NO (PPHM)	NO2 (PPHM)	O3 (PPHM)	HYDRO-CARBONS (PPM)	CH4 (PPM)	CO (PPM)	SO2 (PPHM)
1	6	78								
2	10	68								
3										
4	7	49								
5										
6	7	65								
7										
8	15	44								
9										
A	6	62	36	10	8	4	4	3	4	3
B			29	5	7	3	3	2	4	1
C			25	11	7	4	4	3	4	2
D			42	9	7				5	1
E			35	12	11				6	2
F			33	8	5	4	4	4	4	1
G			20	4	6	2	2	2	4	1
H			33			3	3	3	6	5
I				7	9	3	3	2	8	4
J			17	4	6	2	2	2	4	3
K			11	1	1	2	2	2	3	
L			28	7	9	3	3	2	5	1

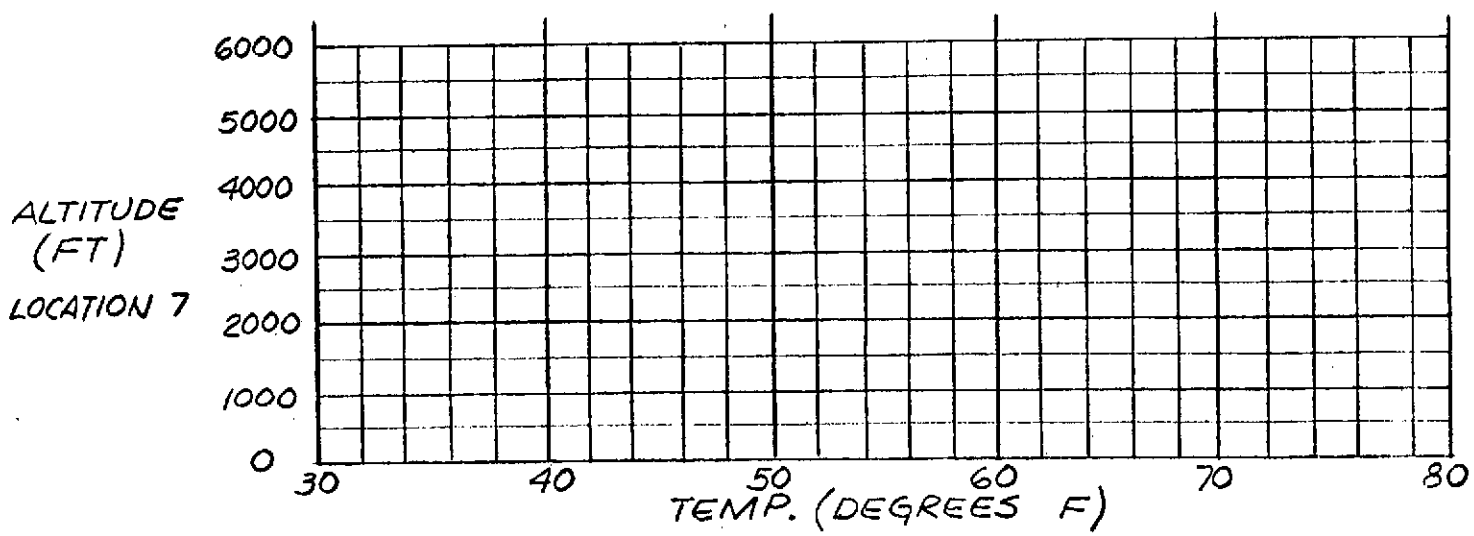

SOLAR AUREOLE BRIGHTNESS (WATTS/cm² STER)					
LOCATION	SOLAR ELEVATION ANGLE (DEG)	DISTANCE FROM THE CENTER OF THE SOLAR DISC ALONG THE ALMUCANTAR			
		0 DEG	1 1/2 DEG	3 DEG	6 DEG

Table A-II (Cont.)

DATE: 20 OCT 1972 TIME: 10:00 AM P.S.T.

LOCATION	VISIBILITY (MILES)	RELATIVE HUMIDITY (%)	PARTICULATE DENSITY (Km x 10)	NO (PPHM)	NO_2 (PPHM)	O_3 (PPHM)	HYDRO-CARBONS (PPM)	CH_4 (PPM)	CO (PPM)	SO_2 (PPHM)
1	10	75								
2	5	81								
3	3									
4	4	83								
5	10									
6	12	68								
7										
8	20	67								
9	15									
A	6	60	45	11	7	3	3	2	5	1
B			13	1	3	3	3	2	2	2
C			23	6	5	3	3	3	4	
D			30						4	2
E			35	19	7				3	3
F			32	6	8	4	4	4	3	1
G			23	6	6	2	2	2	5	1
H			45			3	3	2	5	1
I				11	7	3	3	3	4	2
J			15	5	5	2	2	2	3	4
K			7	1	1	2	2	2	2	1
L			34	7	6	3	3	2	5	1

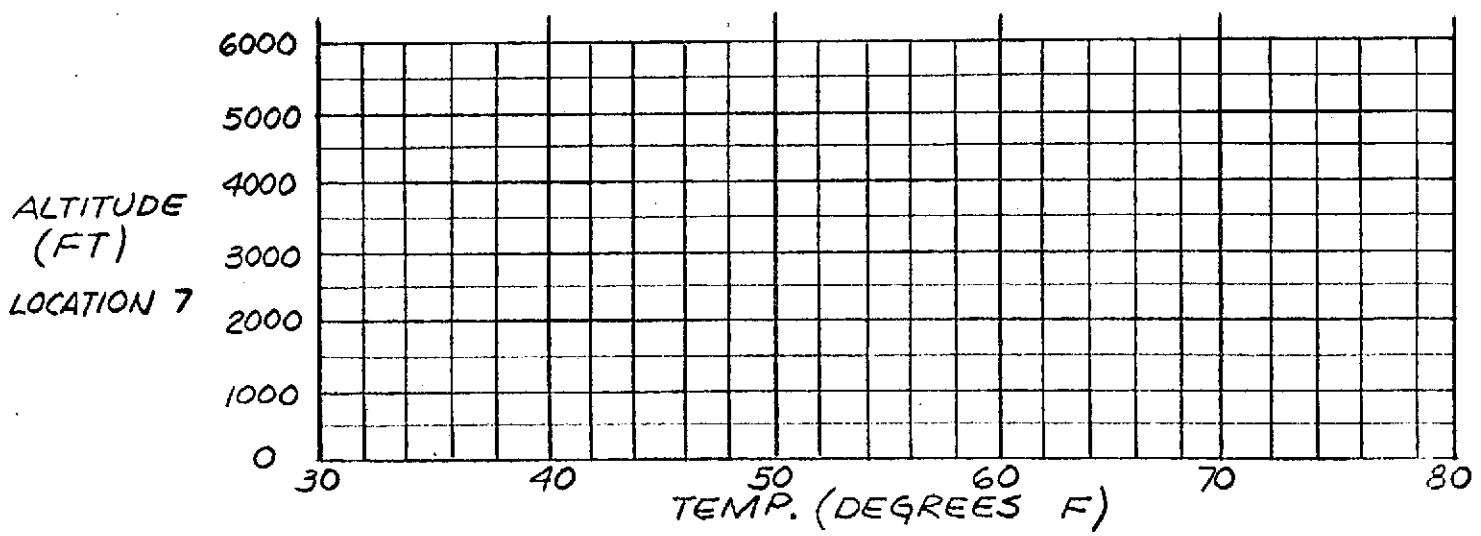

SOLAR AUREOLE BRIGHTNESS (WATTS/cm² STER)					
LOCATION	SOLAR ELEVATION ANGLE (DEG)	DISTANCE FROM THE CENTER OF THE SOLAR DISC ALONG THE ALMUCANTAR			
		0 DEG	1 1/2 DEG	3 DEG	6 DEG

Table A-II (Cont.)

DATE: 21 OCT 1972 TIME: 10:00 AM P.S.T.

LOCATION	VISIBILITY (MILES)	RELATIVE HUMIDITY (%)	PARTICULATE DENSITY (Km x 10)	NO (PPHM)	NO_2 (PPHM)	O_3 (PPHM)	HYDRO-CARBONS (PPM)	CH_4 (PPM)	CO (PPM)	SO_2 (PPHM)
1	6	65								
2	5	61								
3	3									
4	1.5	81								
5	4									
6	3	61								
7	5									
8	30	44								
9	20									
A		54	34			4	2	2	4	2
B			23	2	6	4	3	2	3	1
C			28	2	8	5	3	3	5	1
D			21	5	10	4			3	2
E			28	10	13	1			3	31
F			26	1	5	5	3	3	1	1
G			19	4	7	4	2	2	5	2
H			20	8	8	1	3	3	3	10
I				4	11	2	3	2	4	3
J			8	2	3	2	2	2	1	1
K			12	1	1	3	2	2	2	
L			22	1	7	5	3	2	3	1

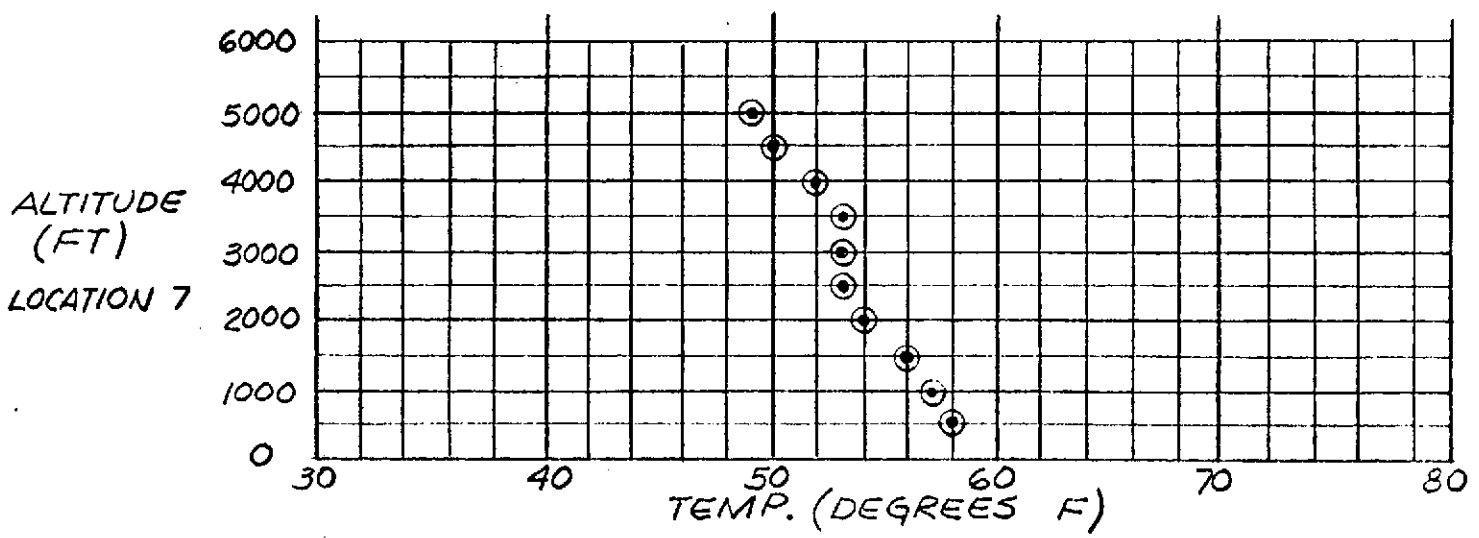

SOLAR AUREOLE BRIGHTNESS (WATTS/cm² STER)					
LOCATION	SOLAR ELEVATION ANGLE (DEG)	DISTANCE FROM THE CENTER OF THE SOLAR DISC ALONG THE ALMUCANTAR			
		0 DEG	1 1/2 DEG	3 DEG	6 DEG
1	40	2.6×10^{2}	2.2×10^{-2}	2.0×10^{-2}	1.9×10^{-2}

Table A-II (Cont.)

DATE: 7 NOV 1972 TIME: 10:00 AM P.S.T.

LOCATION	VISIBILITY (MILES)	RELATIVE HUMIDITY (%)	PARTICULATE DENSITY (Km x 10)	NO (PPHM)	NO2 (PPHM)	O3 (PPHM)	HYDRO-CARBONS (PPM)	CH4 (PPM)	CO (PPM)	SO2 (PPHM)
1	10	81								
2	3	56								
3										
4	4	67								
5										
6	3	70								
7										
8	25	33								
9										
A	6	78	38	8	9	3	3	2	5	2
B			50	6	12	7	7	6	5	3
C			31	4	11				3	2
D			15	3	7				3	2
E			30	12	9				3	3
F			52	14	21	5	5	4	7	3
G			27			3	3	2	6	2
H			20	7	7	2	2	2	3	2
I				4	11	3	3	3	5	3
J			30	4	8	3	3	2	5	1
K			15	1	5	3	3	2	3	4
L			37	6	10	4	4	3	6	3

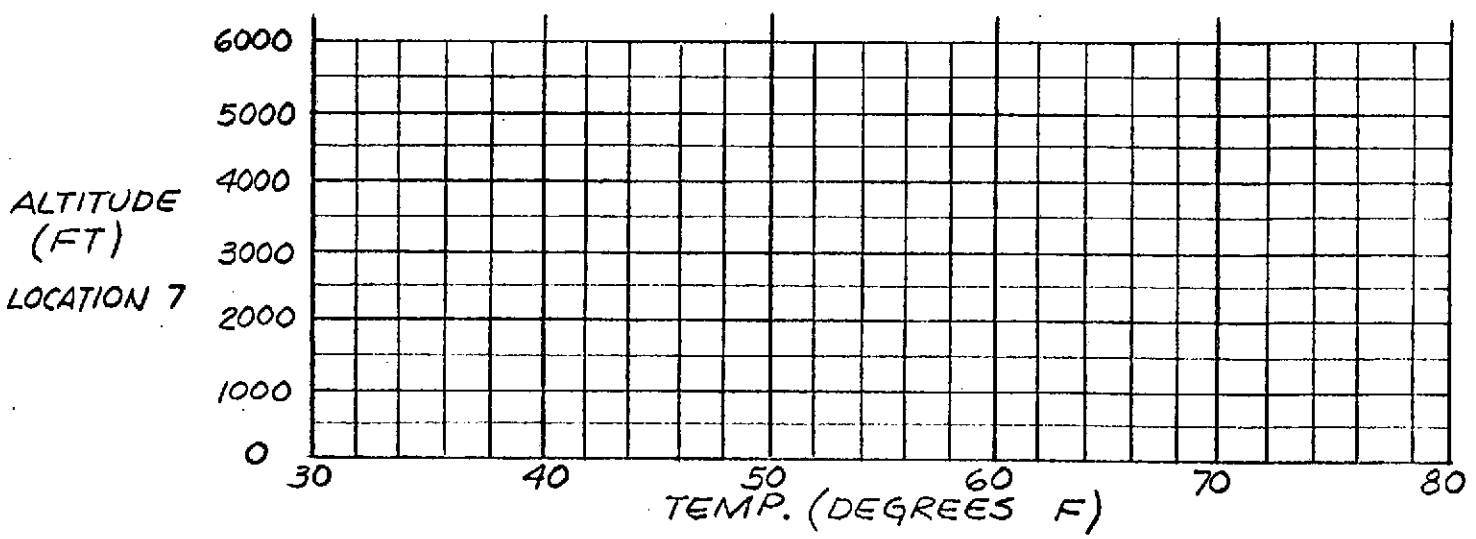

SOLAR AUREOLE BRIGHTNESS (WATTS/cm² STER)					
LOCATION	SOLAR ELEVATION ANGLE (DEG)	DISTANCE FROM THE CENTER OF THE SOLAR DISC ALONG THE ALMUCANTAR			
		0 DEG	1 1/2 DEG	3 DEG	6 DEG

Table A-II (Cont.)

DATE: 8 NOV 1972 TIME: 10:00 AM P.S.T.

LOCATION	VISIBILITY (MILES)	RELATIVE HUMIDITY (%)	PARTICULATE DENSITY (Km x 10)	NO (PPHM)	NO_2 (PPHM)	O_3 (PPHM)	HYDRO-CARBONS (PPM)	CH_4 (PPM)	CO (PPM)	SO_2 (PPHM)
1	30	36								
2	40	40								
3	25									
4	4	75								
5	15									
6	30	35								
7	>15									
8	20	61								
9	40									
A	8	42	15	1	3	3	1	1	1	1
B			19	1	6	3	3	3	3	1
C			11	2	3	2	2	2	2	1
D			8	4	4	2			2	1
E			20	7	8	2			3	2
F			8	1	1	3	3	3	1	1
G			28			3	2	2	4	1
H			13	6	5	2	2	1	2	2
I				1	2	2	2	2	1	1
J			9	1	1	2	2	2	1	1
K			8	1	1	2	2	2	2	
L			5	1	2	3	2	2	2	1

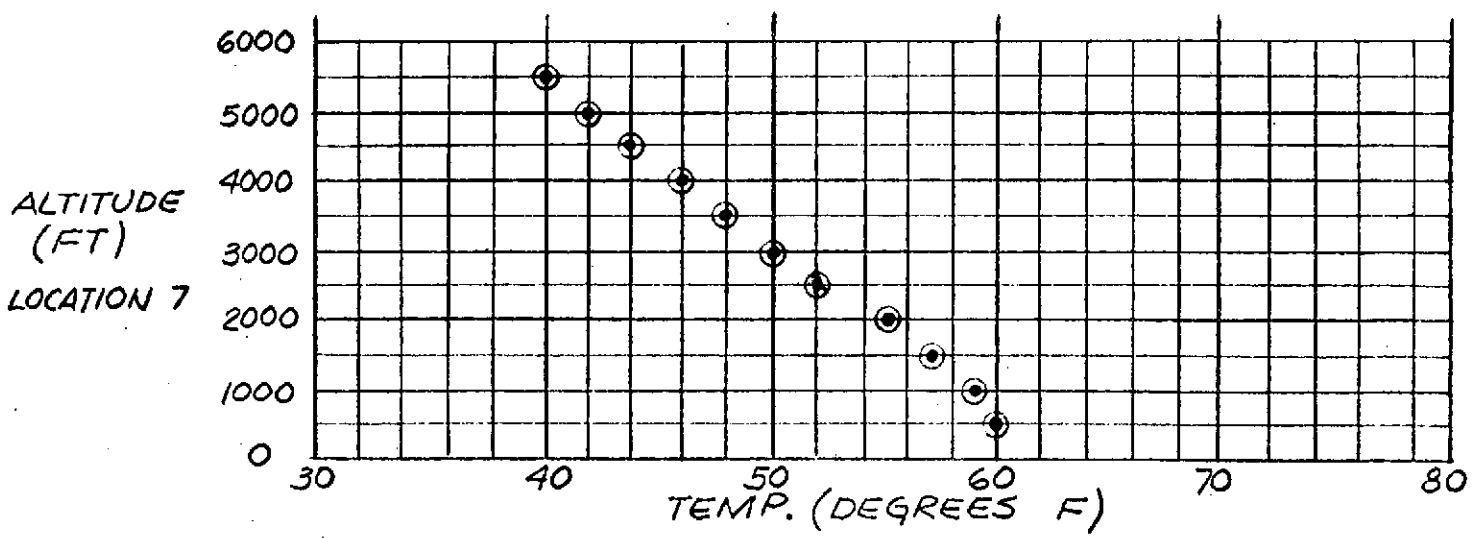

SOLAR AUREOLE BRIGHTNESS (WATTS/cm² STER)					
LOCATION	SOLAR ELEVATION ANGLE (DEG)	DISTANCE FROM THE CENTER OF THE SOLAR DISC ALONG THE ALMUCANTAR			
		0 DEG	1 1/2 DEG	3 DEG	6 DEG
1	34	4.0×10^{2}	4.7×10^{-3}	4.4×10^{-3}	4.1×10^{-3}

Table A-II (Cont.)

DATE: 25 NOV 1972 TIME: 10:00 AM P.S.T.

LOCATION	VISIBILITY (MILES)	RELATIVE HUMIDITY (%)	PARTICULATE DENSITY (Km x 10)	NO (PPHM)	NO2 (PPHM)	O3 (PPHM)	HYDRO-CARBONS (PPM)	CH4 (PPM)	CO (PPM)	SO2 (PPHM)
1	5	47								
2	40	26								
3	>50									
4	3	41								
5	6									
6	4	54								
7										
8	35	43								
9	40									
A	10	41	35	11	12	3	3	2	7	1
B			20	2	8	3	3	3	2	
C			21	4	11	3	3	3	2	1
D			33	7	16	2			5	2
E			47	12	15	3			4	2
F			21	5		2	4	4	4	2
G			26	3	7	3	2	2	6	2
H			55	29	18	3	5	4	5	4
I				16	18	2			7	31
J			10	2	1	2	1	1	4	1
K			15	1	1	1	2	2	2	
L			17	2	7	4	3	2	3	2

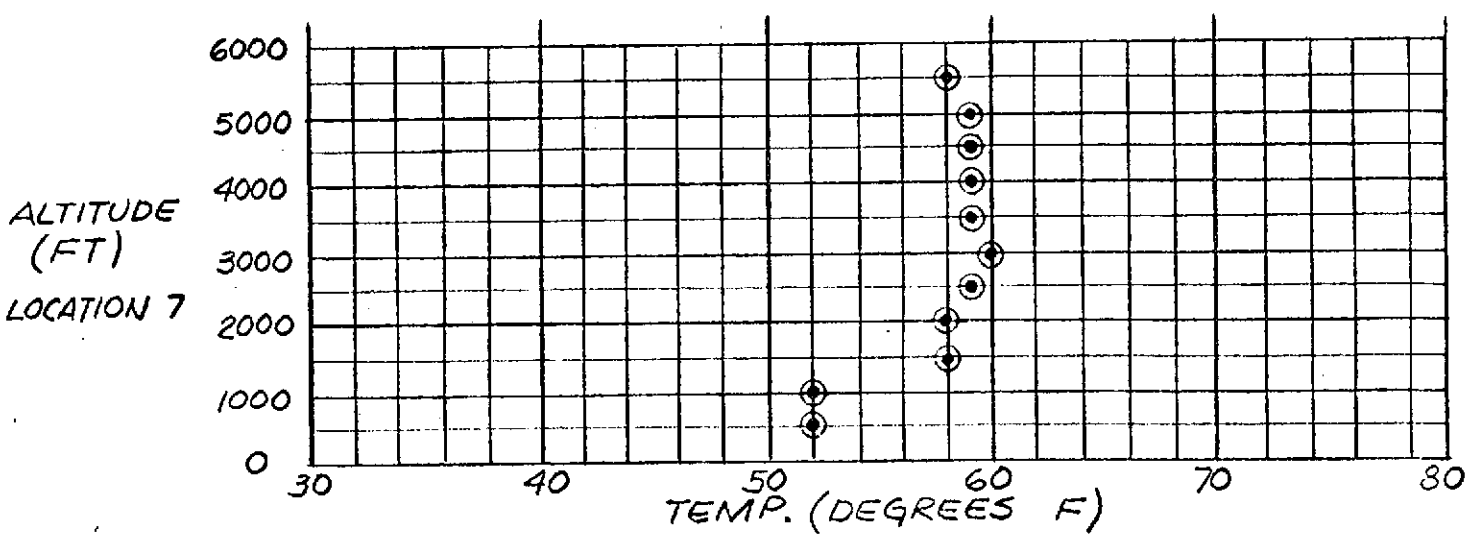

SOLAR AUREOLE BRIGHTNESS (WATTS/cm² STER)					
LOCATION	SOLAR ELEVATION ANGLE (DEG)	DISTANCE FROM THE CENTER OF THE SOLAR DISC ALONG THE ALMUCANTAR			
		0 DEG	1 1/2 DEG	3 DEG	6 DEG

Table A-II (Cont.)

DATE: 26 NOV 1972 TIME: 10:00 AM P.S.T.

LOCATION	VISIBILITY (MILES)	RELATIVE HUMIDITY (%)	PARTICULATE DENSITY (Km x 10)	NO (PPHM)	NO_2 (PPHM)	O_3 (PPHM)	HYDRO-CARBONS (PPM)	CH_4 (PPM)	CO (PPM)	SO_2 (PPHM)
1	12	37								
2	50	37								
3	>50									
4	55	30								
5	3									
6	5	47								
7	>15									
8	35	42								
9	40									
A		38	15	2	5	1	2	2	3	1
B			9	1	2	2	2	2	1	
C			20	5	12	4	4	3	3	1
D			24	4	15	4			4	1
E			58	11	25	5			7	1
F			13	4		2	4	4	1	
G			17	3	7	3	2	2	5	2
H			22	36	22	3	6	5	3	2
I				4	22	5			7	5
J			2	1	1	2	1	1	5	1
K			11			2	2	2	3	
L			12	1	2	2	2	2	3	1

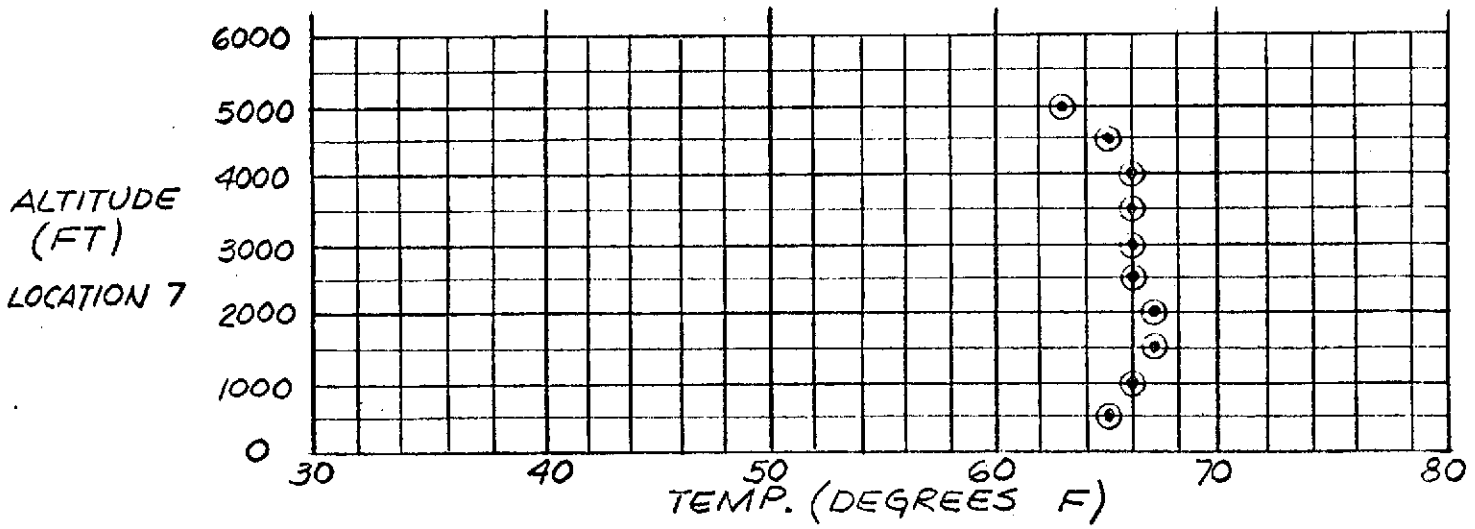

SOLAR AUREOLE BRIGHTNESS (WATTS/cm² STER)					
LOCATION	SOLAR ELEVATION ANGLE (DEG)	DISTANCE FROM THE CENTER OF THE SOLAR DISC ALONG THE ALMUCANTAR			
		0 DEG	1 1/2 DEG	3 DEG	6 DEG
1	30	3.3×10^{2}	1.6×10^{-2}	9.2×10^{-3}	8.0×10^{-3}

Table A-II (Cont.)

DATE: 14 DEC 1972 TIME: 10:00 AM P.S.T.

LOCATION	VISIBILITY (MILES)	RELATIVE HUMIDITY (%)	PARTICULATE DENSITY (Km x 10)	NO (PPHM)	NO2 (PPHM)	O3 (PPHM)	HYDRO-CARBONS (PPM)	CH4 (PPM)	CO (PPM)	SO2 (PPHM)
1	7	42								
2	30	39								
3										
4	25	39								
5										
6	7	36								
7										
8										
9										
A	8	29	43	14	10	1	2	2	5	2
B			24	4	4	2	2	2	3	2
C			52	16	16	2	3	3	9	2
D			45	18	15	2			13	3
E			60	14	13	3			4	1
F			35	11	12	1	5	4	5	1
G			30	3	4	2	2	2	4	1
H			55	33	12		4	3	13	2
I				6	7	2	4	3	4	1
J			16	3	4	2	2	2	3	1
K			23	5	1	1	2	2	3	1
L			20	4	6	2	3	2	2	1

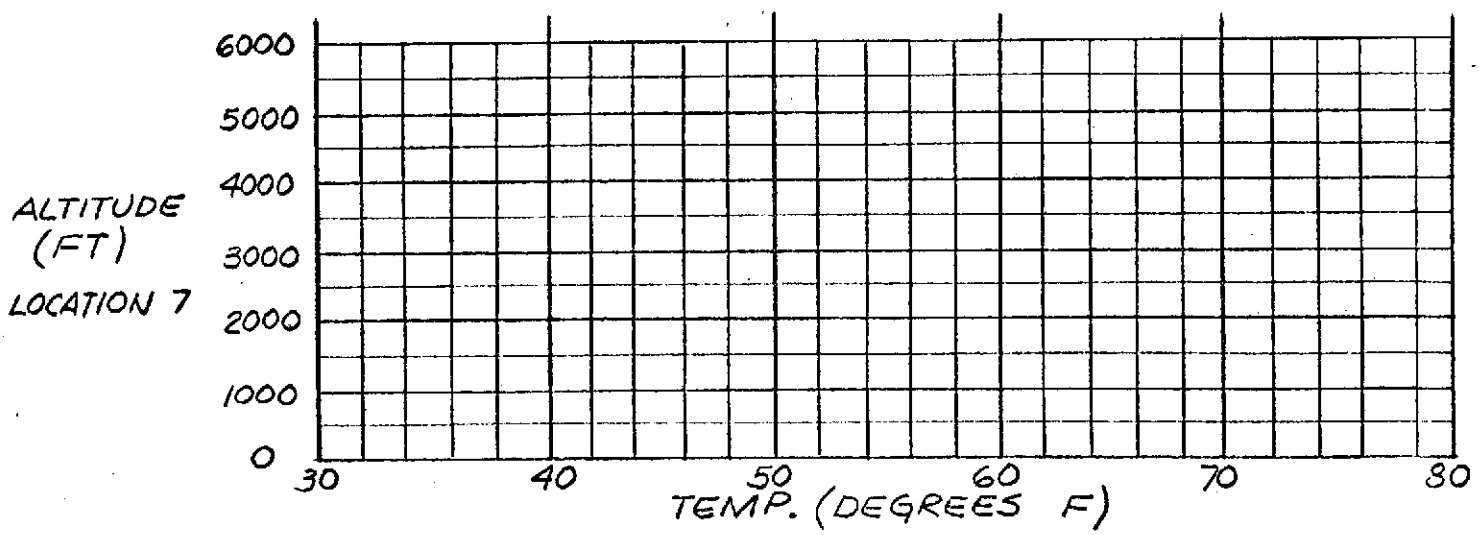

SOLAR AUREOLE BRIGHTNESS (WATTS/cm² STER)					
LOCATION	SOLAR ELEVATION ANGLE (DEG)	DISTANCE FROM THE CENTER OF THE SOLAR DISC ALONG THE ALMUCANTAR			
		0 DEG	1 1/2 DEG	3 DEG	6 DEG

Table A-II (Cont.)

DATE: 1 JAN 1973 TIME: 10:00 AM P.S.T.

LOCATION	VISIBILITY (MILES)	RELATIVE HUMIDITY (%)	PARTICULATE DENSITY (Km x 10)	NO (PPHM)	NO_2 (PPHM)	O_3 (PPHM)	HYDRO-CARBONS (PPM)	CH_4 (PPM)	CO (PPM)	SO_2 (PPHM)
1	30	15								
2	50	13								
3										
4	3	20								
5										
6	15	12								
7										
8	20	21								
9										
A		18	3	1	1	2	1	1	2	1
B			15	1	1	5	2	2	2	6
C			6	1	1	2	2	2	1	2
D			8	1	1	3			1	1
E			15	1	1	3			1	2
F			15	1	1	3	3	3	1	1
G			7	1	1	3	1	1	3	1
H			5	4	3	3	3	3	3	1
I				1	1	4	2	2	1	1
J			6	2	1	3	2	2	2	1
K			2	1	1	3	2	2	2	
L			15	1	1	3	2	2	1	1

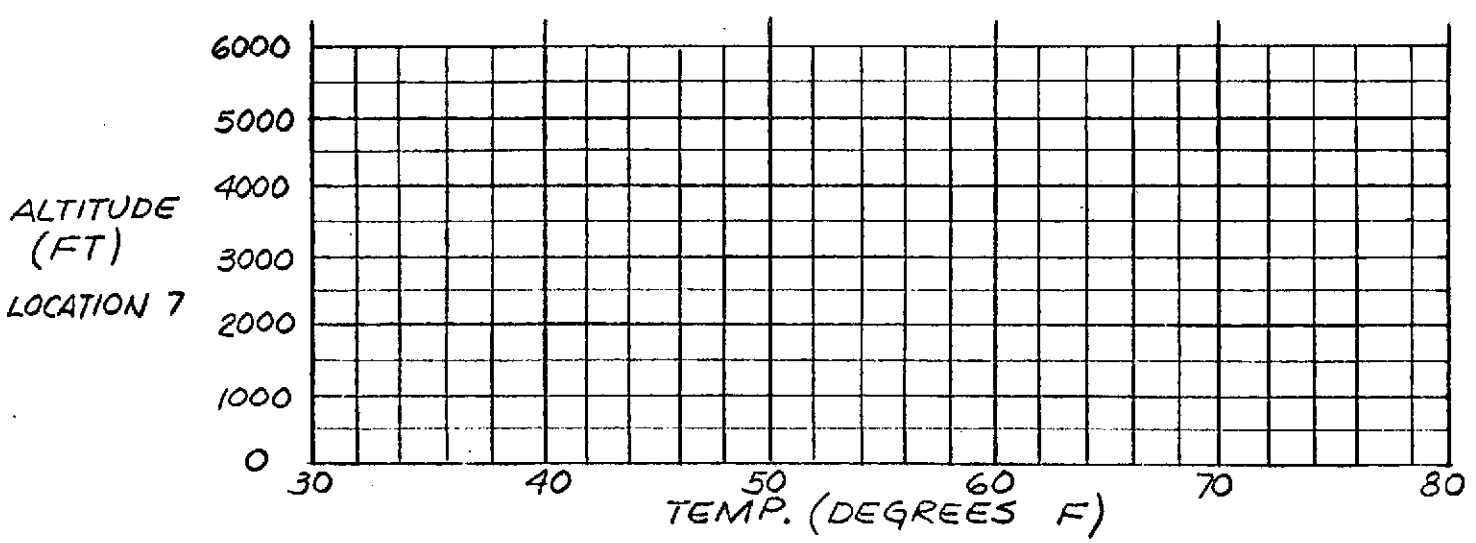

SOLAR AUREOLE BRIGHTNESS (WATTS/cm² STER)					
LOCATION	SOLAR ELEVATION ANGLE (DEG)	DISTANCE FROM THE CENTER OF THE SOLAR DISC ALONG THE ALMUCANTAR			
		0 DEG	1 1/2 DEG	3 DEG	6 DEG

Table A-II (Cont.)

DATE: 19 JAN 1973 TIME: 10:00 AM P.S.T.

LOCATION	VISIBILITY (MILES)	RELATIVE HUMIDITY (%)	PARTICULATE DENSITY (Km x 10)	NO (PPHM)	NO2 (PPHM)	O3 (PPHM)	HYDRO-CARBONS (PPM)	CH4 (PPM)	CO (PPM)	SO2 (PPHM)
1	50	47								
2	40	38								
3										
4	30	72								
5										
6	45	45								
7										
8	20	75								
9										
A	40	32	9	2	3	3	1	1	2	
B			7	1	1	5	3	3	2	1
C			5	2	2	1	2	2	2	1
D			8	7	6	2			3	
E			16	5	4	4			1	1
F			10	2	4	2	3	3	2	1
G			12	4	3	2	2	2	3	1
H			15			1	2	2	3	
I				1	2	2	2	2	2	1
J			6	3	2	2	2	2	2	1
K			5	1	1	3	2	2	3	
L			13	3	3	3	2	2	2	1

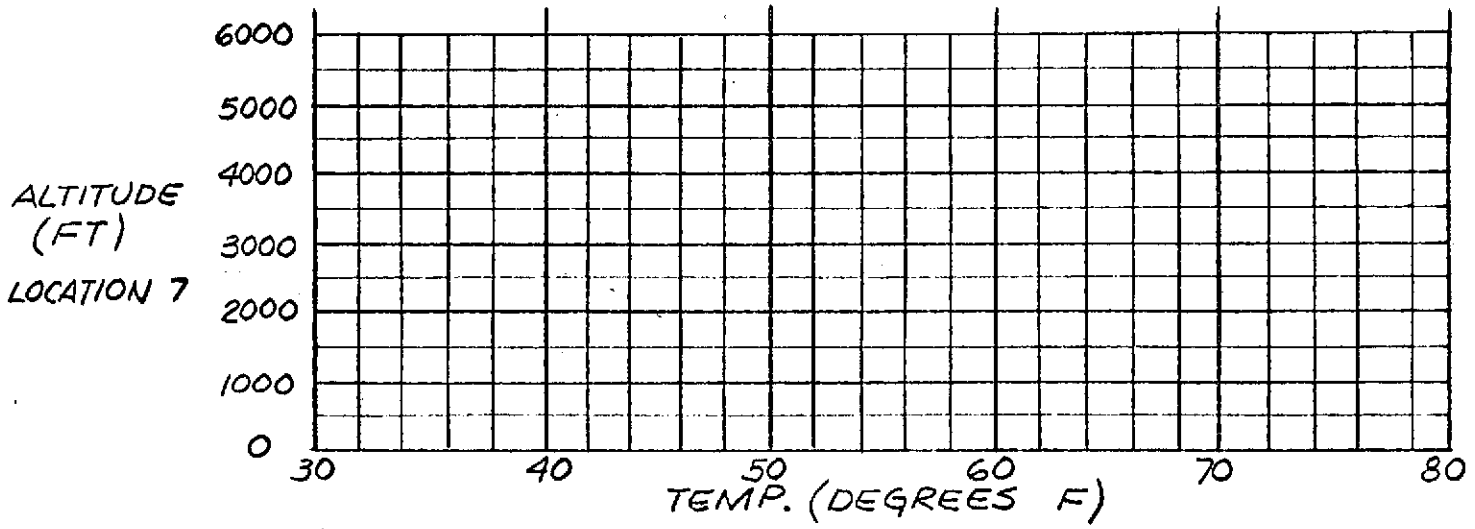

SOLAR AUREOLE BRIGHTNESS (WATTS/cm² STER)					
LOCATION	SOLAR ELEVATION ANGLE (DEG)	DISTANCE FROM THE CENTER OF THE SOLAR DISC ALONG THE ALMUCANTAR			
		0 DEG	1 1/2 DEG	3 DEG	6 DEG

Table A-II (Cont.)

DATE: 6 FEB 1973 TIME: 10:00 AM P.S.T.

LOCATION	VISIBILITY (MILES)	RELATIVE HUMIDITY (%)	PARTICULATE DENSITY (Km x 10)	NO (PPHM)	NO_2 (PPHM)	O_3 (PPHM)	HYDRO-CARBONS (PPM)	CH_4 (PPM)	CO (PPM)	SO_2 (PPHM)
1	6	97								
2	7	97								
3										
4	3	90								
5										
6	5	80								
7										
8	20	90								
9										
A	8	82	28	11	4	2	2	1	4	2
B			13	1	1	2	2	2	1	1
C			13	5	4	2	2	2	3	1
D			22	11	7				4	1
E			30	4	3				3	1
F			17	5	5	3	3	3	2	1
G			15	3	3	2	2	2	4	1
H			26	17	4	2	2	2		
I				7	5	3	3		4	2
J			2	3	3	2	2	2	2	1
K			5	1	1	2	2	2	2	2
L			9	3	4	2	2	2	3	1

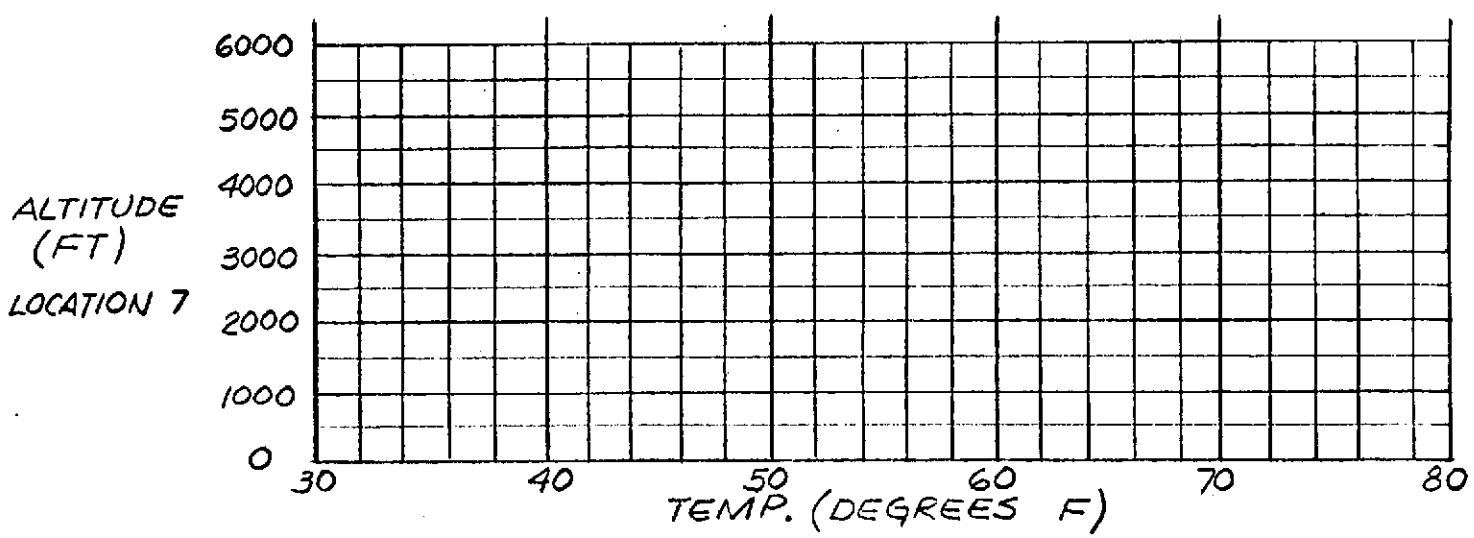

SOLAR AUREOLE BRIGHTNESS (WATTS/cm² STER)					
LOCATION	SOLAR ELEVATION ANGLE (DEG)	DISTANCE FROM THE CENTER OF THE SOLAR DISC ALONG THE ALMUCANTAR			
		0 DEG	1 1/2 DEG	3 DEG	6 DEG

Table A-II (Cont.)

DATE: 24 FEB 1973 TIME: 10:00 AM P.S.T.

LOCATION	VISIBILITY (MILES)	RELATIVE HUMIDITY (%)	PARTICULATE DENSITY (Km x 10)	NO (PPHM)	NO_2 (PPHM)	O_3 (PPHM)	HYDRO-CARBONS (PPM)	CH_4 (PPM)	CO (PPM)	SO_2 (PPHM)
1	4	87								
2	3	80								
3										
4	3	69								
5										
6	6	77								
7										
8	10	71								
9										
A	5	72	15	1	5	2	2	1	3	1
B			34	5	8	3	3	3	3	2
C			15	5	6	2	2	2	3	2
D			13	3	7				5	1
E			24	4	5				1	1
F			17	2	7	3	3	3	2	1
G			12	6	4	2	2	3	4	1
H			20	16	6	3	3	2	4	3
I				2	4	2	2	2	2	3
J			13	1	4	2	2	2	2	1
K			7	1	1	2	2	2	2	1
L			33	4	8	3	3	2	4	2

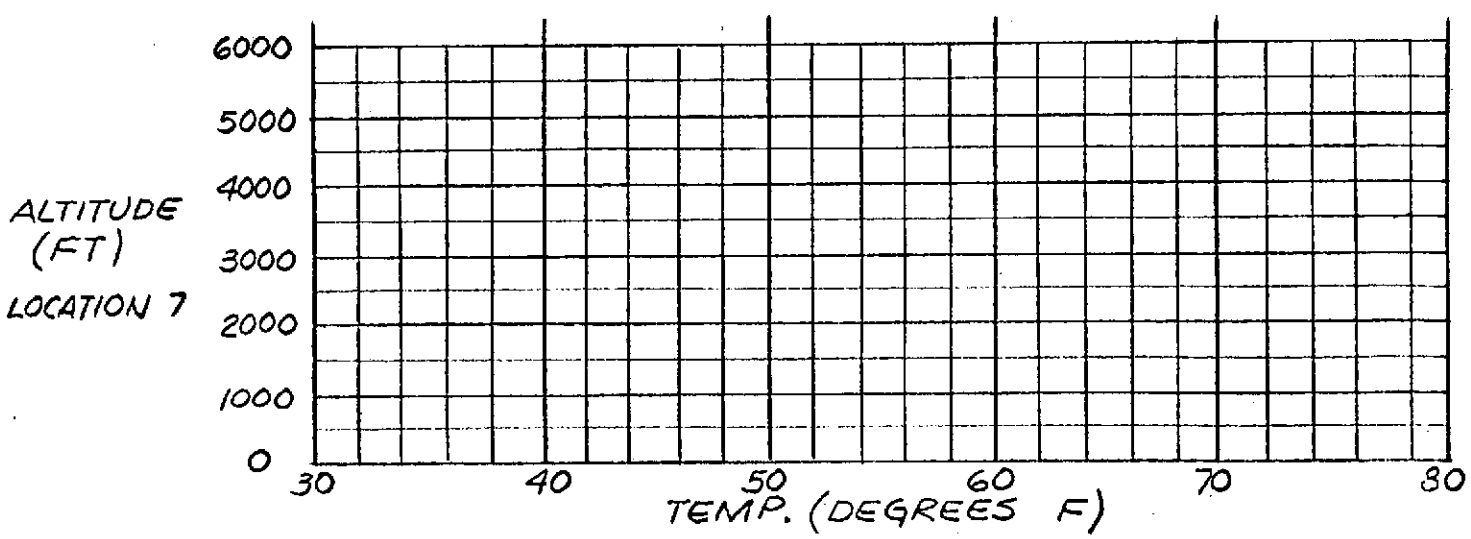

SOLAR AUREOLE BRIGHTNESS (WATTS/cm² STER)					
LOCATION	SOLAR ELEVATION ANGLE (DEG)	DISTANCE FROM THE CENTER OF THE SOLAR DISC ALONG THE ALMUCANTAR			
		0 DEG	1 1/2 DEG	3 DEG	6 DEG

Table A-II (Cont.)

DATE: 14 MAR 1973 TIME: 10:00 AM P.S.T.

LOCATION	VISIBILITY (MILES)	RELATIVE HUMIDITY (%)	PARTICULATE DENSITY (Km x 10)	NO (PPHM)	NO_2 (PPHM)	O_3 (PPHM)	HYDRO-CARBONS (PPM)	CH_4 (PPM)	CO (PPM)	SO_2 (PPHM)
1	50	25								
2	40	25								
3	25									
4	55	26								
5	>15									
6	50	36								
7										
8	35	37								
9	20									
A	30	32	9	1	1	3	2	1	2	1
B			6	1	1	2	2	2	2	1
C			2	3	2	1	2	2	2	2
D			7	1	2	2			3	1
E			25	1	3	3			1	1
F			9	1	2	3	3	3	1	1
G			12	5	3	2	2	2	4	1
H			10	10	4	1	2	1	2	1
I				2	2	3	2	2	2	1
J			8	1	1	3	2	2	4	1
K			6	1	1	4	2	2	2	
L			7	1	2	3	2	2	1	1

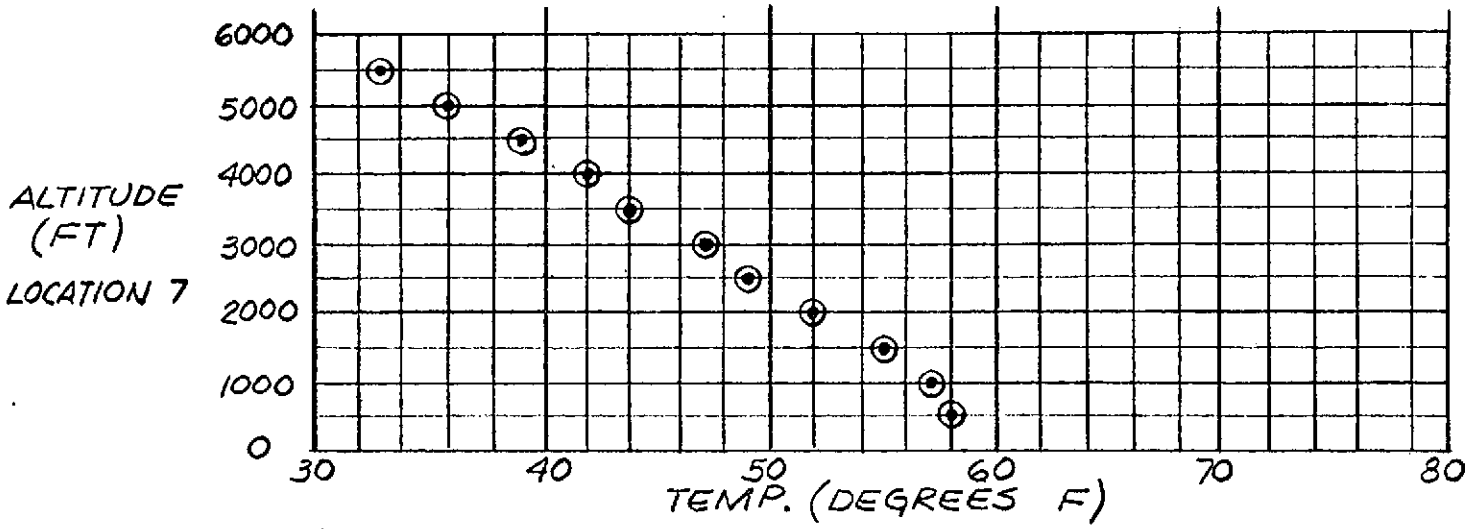

SOLAR AUREOLE BRIGHTNESS (WATTS/cm² STER)					
LOCATION	SOLAR ELEVATION ANGLE (DEG)	DISTANCE FROM THE CENTER OF THE SOLAR DISC ALONG THE ALMUCANTAR			
		0 DEG	1 1/2 DEG	3 DEG	6 DEG
1	44	4.3×10^{2}	2.9×10^{-3}	2.8×10^{-3}	2.6×10^{-3}

Table A-II (Cont.)

DATE: 1 APRIL 1973 TIME: 10:00 AM P.S.T.

LOCATION	VISIBILITY (MILES)	RELATIVE HUMIDITY (%)	PARTICULATE DENSITY (Km x 10)	NO (PPHM)	NO_2 (PPHM)	O_3 (PPHM)	HYDRO-CARBONS (PPM)	CH_4 (PPM)	CO (PPM)	SO_2 (PPHM)
1	25	49								
2	50	21								
3	25									
4	7	55								
5	10									
6	30	38								
7	30									
8	30	47								
9	8									
A		27	6	1	1	4	1	1	1	1
B			13	1	3	3	2	2	2	2
C			24	1	1	3	2	2	1	1
D			7	1	2	4			2	1
E			13	1	4	2			1	2
F			3	1	2	3	3	3	1	1
G			6	2	3	3	2	2	4	1
H			7	1	2	3	3	2		1
I				1	1	3	2	2	1	1
J			25	2	2	3	2	2	2	2
K			3	1	1	4	2	2	2	1
L			7	1	2	4	2	2	2	1

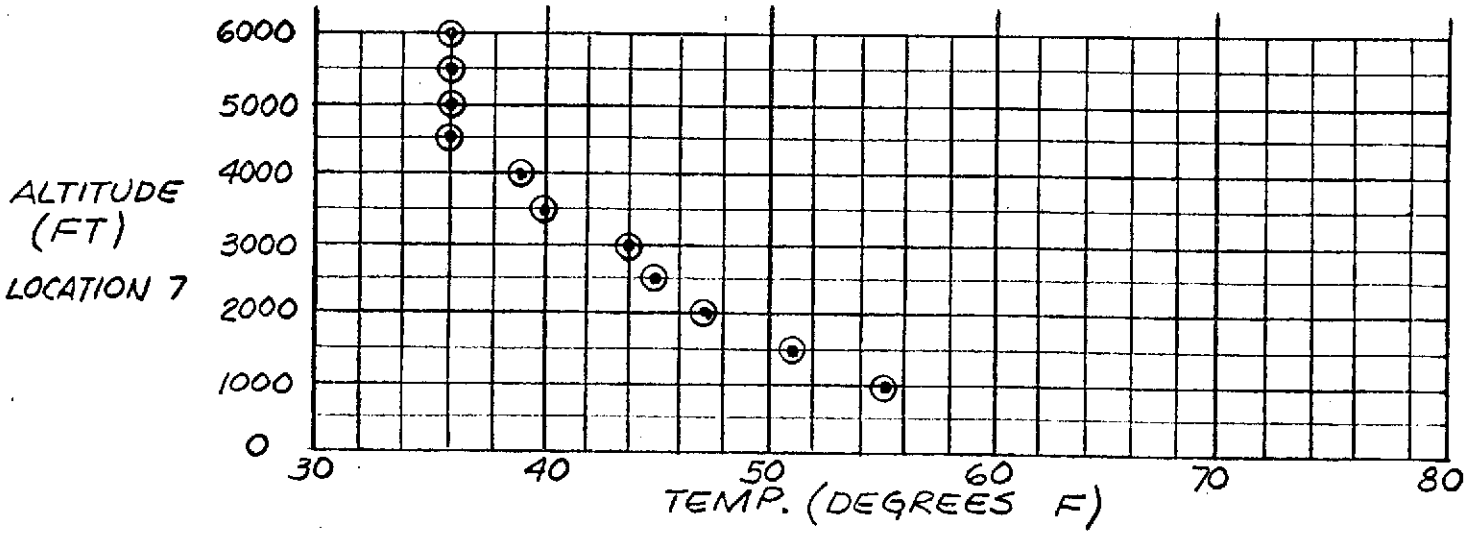

SOLAR AUREOLE BRIGHTNESS (WATTS/cm² STER)					
LOCATION	SOLAR ELEVATION ANGLE (DEG)	DISTANCE FROM THE CENTER OF THE SOLAR DISC ALONG THE ALMUCANTAR			
		0 DEG	1 1/2 DEG	3 DEG	6 DEG
1	50	3.8×10^{2}	1.8×10^{-2}	1.5×10^{-2}	1.0×10^{-2}

Table A-II (Cont.)

DATE: 19 APRIL 1973 TIME: 10:00 AM P.S.T.

LOCATION	VISIBILITY (MILES)	RELATIVE HUMIDITY (%)	PARTICULATE DENSITY (Km x 10)	NO (PPHM)	NO2 (PPHM)	O3 (PPHM)	HYDRO-CARBONS (PPM)	CH4 (PPM)	CO (PPM)	SO2 (PPHM)
1	10	60								
2	50	38								
3	>15									
4	7	53								
5	10									
6	8	54								
7										
8	30	42								
9	20									
A		59	29	6	8	2	2	2	5	2
B			8	1	4		3	2	1	1
C			10	1	4	2	3	3	2	1
D			10	1	4	3			2	2
E			20	4	6	2			3	1
F			7	1	2	4	3	3	2	1
G			16	2	3	3	2	2	4	1
H			10	3	6	1	2	1	2	6
I				1	5	3	2	2	2	1
J			7	1	1	3	2	2	2	2
K			5	1	1	4	2	2	2	1
L			12	2	5	4	2	2	2	1

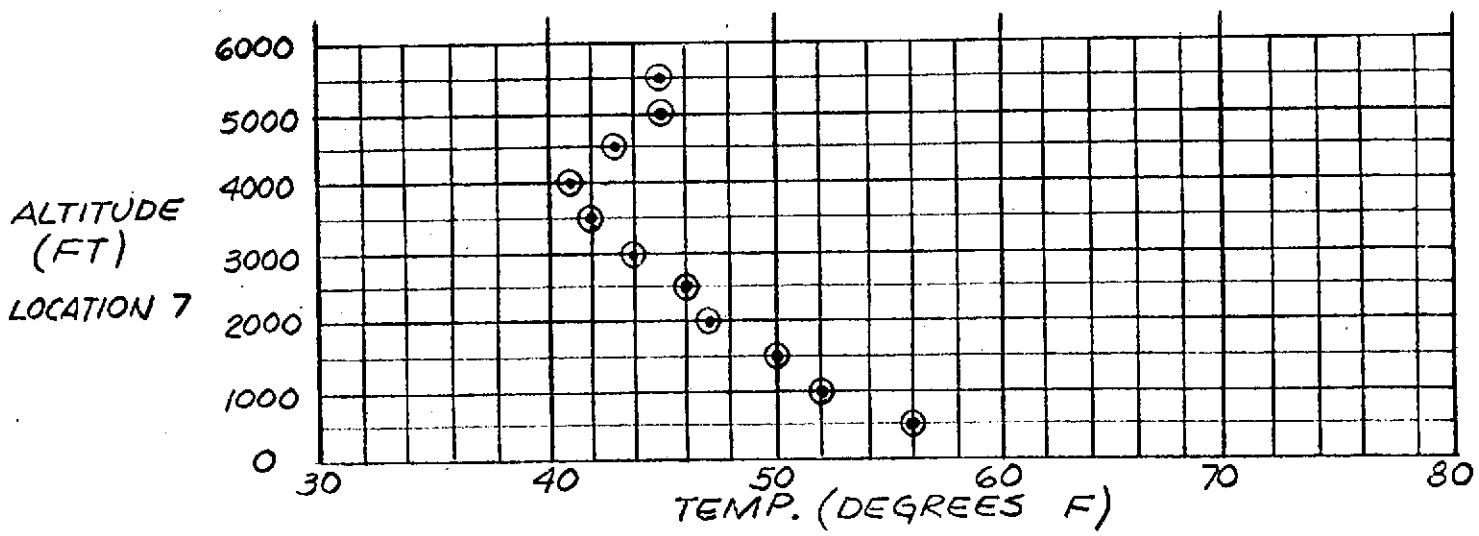

SOLAR AUREOLE BRIGHTNESS (WATTS/cm² STER)					
LOCATION	SOLAR ELEVATION ANGLE (DEG)	DISTANCE FROM THE CENTER OF THE SOLAR DISC ALONG THE ALMUCANTAR			
		0 DEG	1 1/2 DEG	3 DEG	6 DEG
1	56	3.7×10^{2}	2.0×10^{-2}	1.5×10^{-2}	1.1×10^{-2}
5	56	3.7×10^{2}	2.3×10^{-2}	1.6×10^{-2}	1.0×10^{-2}

Table A-II (Cont.)

DATE: 7 MAY 1973 TIME: 10:00 AM P.S.T.

LOCATION	VISIBILITY (MILES)	RELATIVE HUMIDITY (%)	PARTICULATE DENSITY (Km x 10)	NO (PPHM)	NO_2 (PPHM)	O_3 (PPHM)	HYDRO-CARBONS (PPM)	CH_4 (PPM)	CO (PPM)	SO_2 (PPHM)
1	7	73								
2	7	63								
3	7									
4	1.5	52								
5	5									
6	6	56								
7	6									
8	30	27								
9	20									
A		59	37	1	11	6	3	2	5	
B			30	1	6		3	3	3	1
C			38	1	15	7	3	3	5	2
D			10	1	5	3			2	1
E			24	9	13	1			3	4
F			20	2	12	7	3	3	3	1
G			28	1	8	8	2	2	5	2
H			10	3	8	1	2	2	2	5
I						7	2	2	3	
J			30	1	5	8	2	2	5	4
K			4	1	1	5	2	2	2	1
L			24	2	11		3	3	3	1

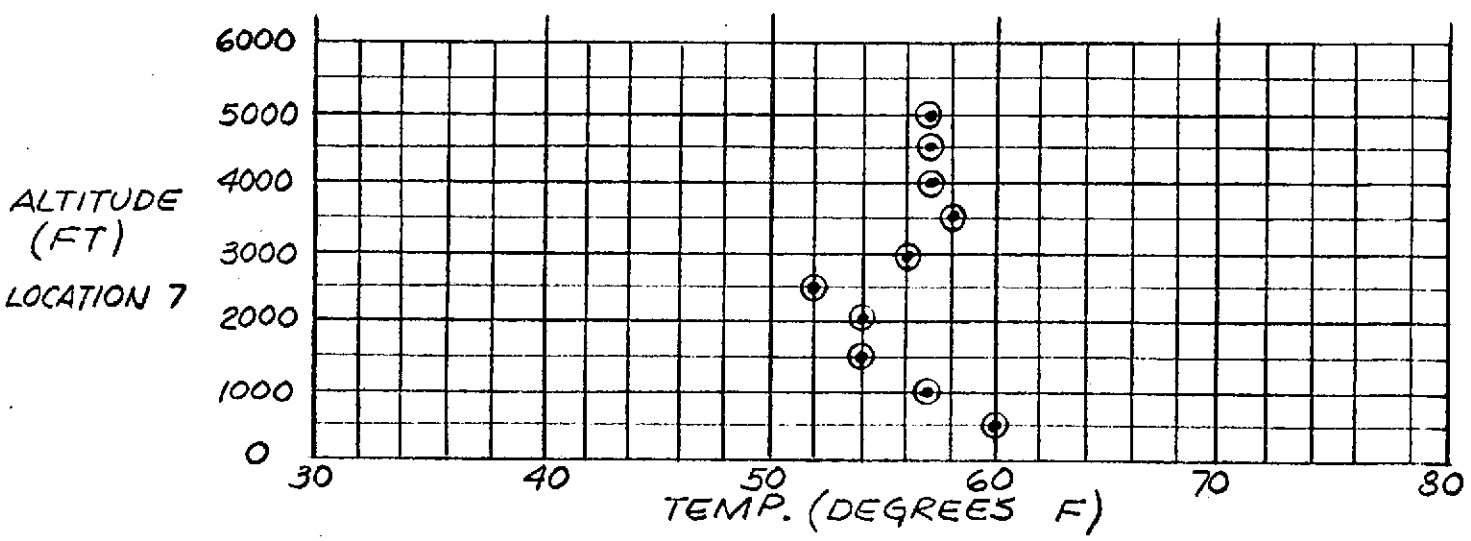

SOLAR AUREOLE BRIGHTNESS (WATTS/cm² STER)					
LOCATION	SOLAR ELEVATION ANGLE (DEG)	DISTANCE FROM THE CENTER OF THE SOLAR DISC ALONG THE ALMUCANTAR			
		0 DEG	1 1/2 DEG	3 DEG	6 DEG
1	60	3.4×10^{2}	3.9×10^{-2}	3.2×10^{-2}	2.7×10^{-2}
A	60	3.6×10^{2}	3.7×10^{-2}	2.2×10^{-2}	1.7×10^{-2}

Table A-II (Cont.)

DATE: 25 MAY 1973 TIME: 10:00 AM P.S.T.

LOCATION	VISIBILITY (MILES)	RELATIVE HUMIDITY (%)	PARTICULATE DENSITY (Km x 10)	NO (PPHM)	NO_2 (PPHM)	O_3 (PPHM)	HYDRO-CARBONS (PPM)	CH_4 (PPM)	CO (PPM)	SO_2 (PPHM)
1	5	70								
2	3	81								
3	3									
4	2	69								
5	6									
6	6	64								
7										
8	15	54								
9	10									
A	4	72	25	8	10	2	2	1	4	1
B			17	1	3		2	2	3	1
C			18	2	5	3	3	3	4	1
D			20	2	7	3			4	
E			31	8	8	1			1	2
F			23	2	7	2	3	3	2	1
G			20	3	5		2	2	5	1
H			21			1	3	2	4	2
I				2	6	3	2	1	3	1
J			23	1	5	4	2	2	4	1
K			4	1	1	4	2	2	1	
L			23	2	7	3	3	3	3	1

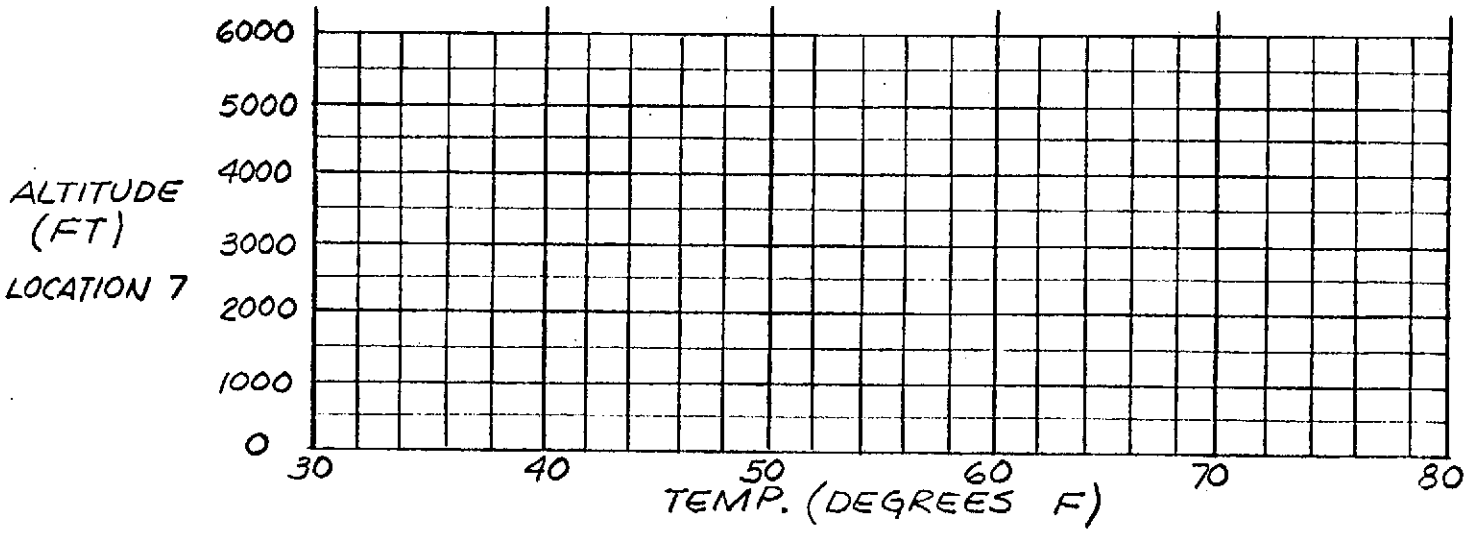

SOLAR AUREOLE BRIGHTNESS (WATTS/cm² STER)					
LOCATION	SOLAR ELEVATION ANGLE (DEG)	DISTANCE FROM THE CENTER OF THE SOLAR DISC ALONG THE ALMUCANTAR			
		0 DEG	1 1/2 DEG	3 DEG	6 DEG

Table A-II (Cont.)

DATE: 12 JUNE 1973 TIME: 10:00 AM P.S.T.

LOCATION	VISIBILITY (MILES)	RELATIVE HUMIDITY (%)	PARTICULATE DENSITY (Km x 10)	NO (PPHM)	NO_2 (PPHM)	O_3 (PPHM)	HYDRO-CARBONS (PPM)	CH_4 (PPM)	CO (PPM)	SO_2 (PPHM)
1	4	70								
2	5	65								
3										
4	2	65								
5										
6	3	61								
7										
8	30	19								
9										
A	4	71	25			5	2	2	4	3
B			28	1	6	6	3	3	3	1
C			31	2	11	4	2	2	6	2
D			13			5			3	
E			21			1			3	3
F			27	1	6	8	3	3	3	1
G			26				3	3	5	1
H			15	2	6	1	3	2	2	3
I				2	8	5	3	2	4	5
J			28	1	7	8	3	2	4	1
K			6	1	1	7	2	2	2	
L				2	13	7	3	2	4	2

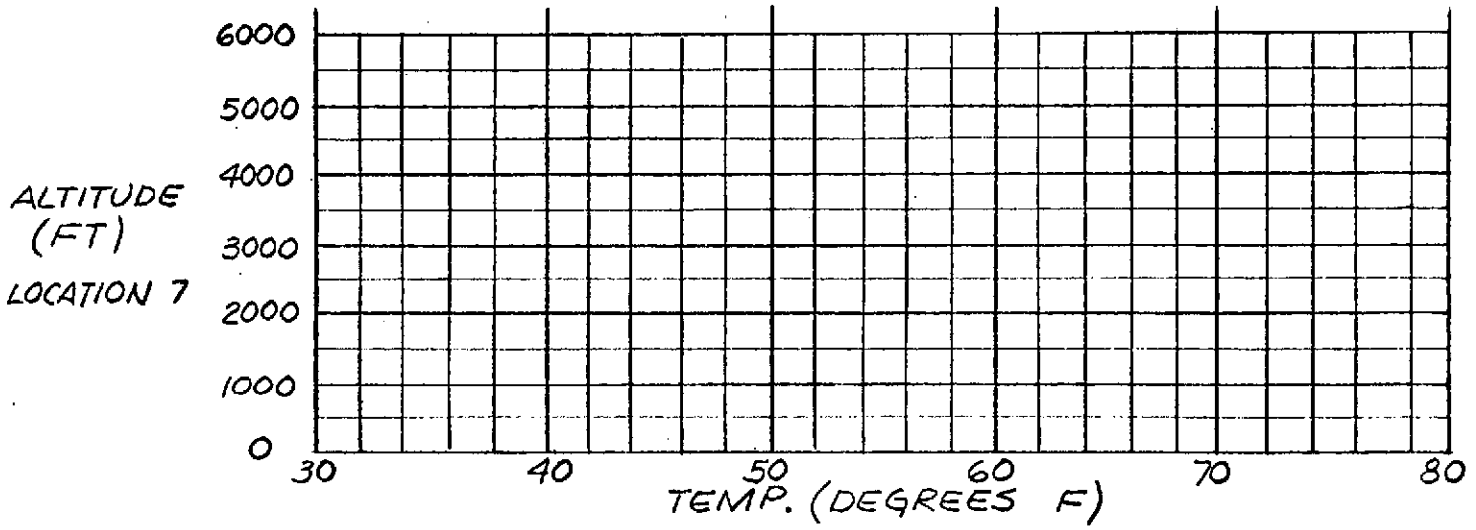

SOLAR AUREOLE BRIGHTNESS (WATTS/cm² STER)					
LOCATION	SOLAR ELEVATION ANGLE (DEG)	DISTANCE FROM THE CENTER OF THE SOLAR DISC ALONG THE ALMUCANTAR			
		0 DEG	1 1/2 DEG	3 DEG	6 DEG

Table A-II (Cont.)

DATE: 30 JUNE 1973 TIME: 10:00 AM P.S.T.

LOCATION	VISIBILITY (MILES)	RELATIVE HUMIDITY (%)	PARTICULATE DENSITY (Km x 10)	NO (PPHM)	NO_2 (PPHM)	O_3 (PPHM)	HYDRO-CARBONS (PPM)	CH_4 (PPM)	CO (PPM)	SO_2 (PPHM)
1	2.5	78								
2	1.5	93								
3										
4	1	68								
5										
6	4	76								
7										
8	35	18								
9										
A	2.5	88	20	1	6	2	2	2	3	2
B			28	1	8	5	3	3	4	1
C			31	2	8	4	4	3	4	3
D			15	4	8	1			3	3
E			15	1	4	1			2	1
F			23	3	8	5	4	3	2	1
G			23	3	9	6	3	3	5	2
H			11	4	5	1	2	2	3	3
I				2	3	4	2	2	1	1
J			31	2	9	10	3	2	4	2
K			2	1	1	7	2	2	2	
L			22	1	8	6	3	2	3	1

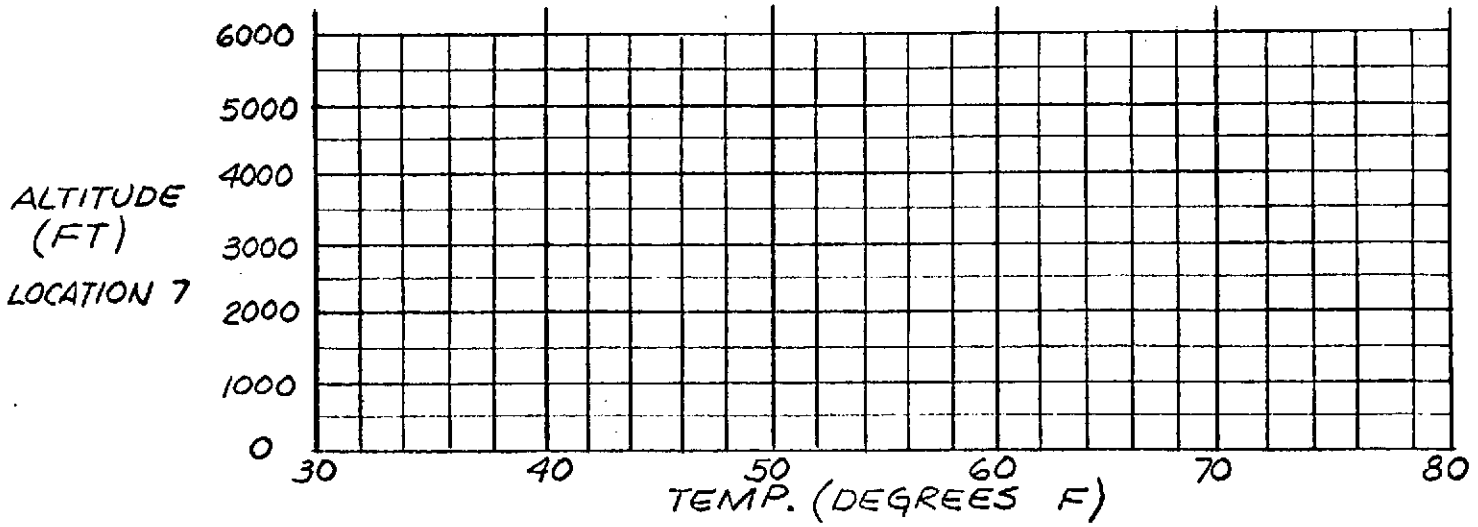

SOLAR AUREOLE BRIGHTNESS (WATTS/cm² STER)					
LOCATION	SOLAR ELEVATION ANGLE (DEG)	DISTANCE FROM THE CENTER OF THE SOLAR DISC ALONG THE ALMUCANTAR			
		0 DEG	1 1/2 DEG	3 DEG	6 DEG

Table A-II (Cont.)

DATE: 18 JULY 1973 TIME: 10:00 AM P.S.T.

LOCATION	VISIBILITY (MILES)	RELATIVE HUMIDITY (%)	PARTICULATE DENSITY (Km x 10)	NO (PPHM)	NO2 (PPHM)	O3 (PPHM)	HYDRO-CARBONS (PPM)	CH4 (PPM)	CO (PPM)	SO2 (PPHM)
1	7	70								
2	6	70								
3	7									
4	2.5	58								
5	6									
6	7	59								
7	5									
8	20	28								
9	25									
A	3	68	32	1	10	5	2	2	5	3
B			35	1	13	8	3	3	4	3
C			31	4	13	5	4	3	6	3
D			15	3	8	2			3	3
E			20	5	7	1				3
F			23	2	8	6	3	3	2	2
G			28	3	11	7	3	3	6	2
H			14	7	5	1	3	2	3	10
I				1	4	4	2	1		1
J			17	1	4	12	3	2	3	2
K			6	1	1	9	2	2	2	
L			32	3	15	7	3	2	3	3

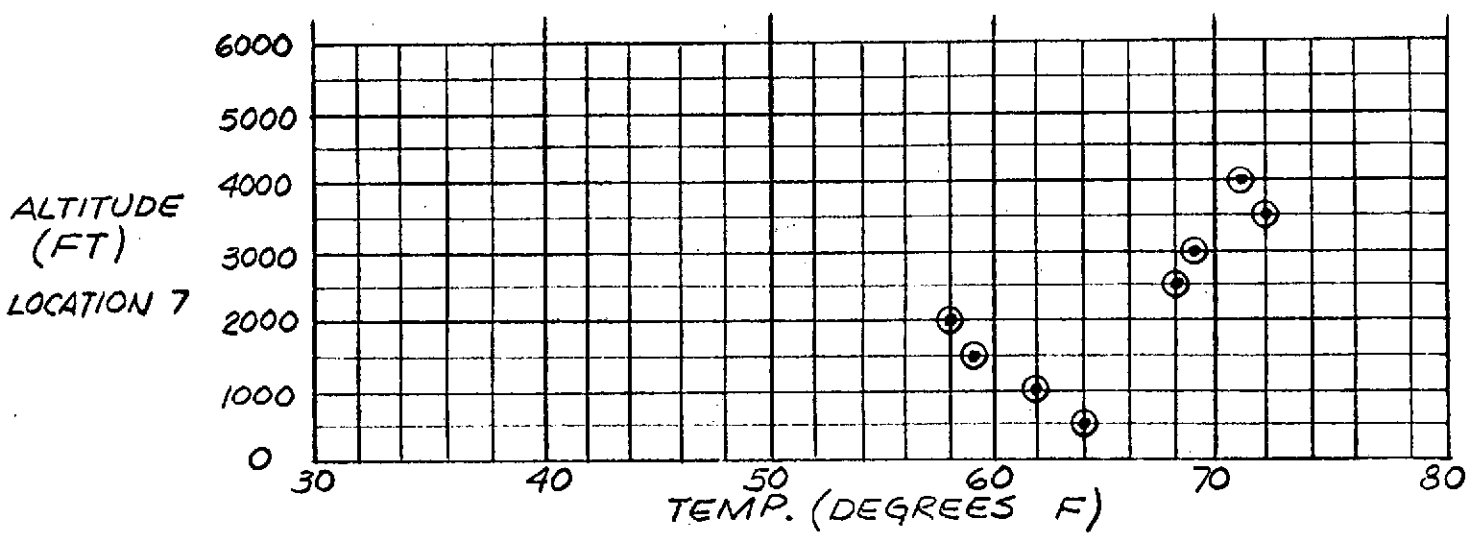

SOLAR AUREOLE BRIGHTNESS (WATTS/cm² STER)					
LOCATION	SOLAR ELEVATION ANGLE (DEG)	DISTANCE FROM THE CENTER OF THE SOLAR DISC ALONG THE ALMUCANTAR			
		0 DEG	1 1/2 DEG	3 DEG	6 DEG

APPENDIX B

SOLAR AUREOLE MONITOR

The solar aureole monitor measured the aureole brightness at angular distances of 1.5, 3.0, and 6.0 deg from the center of the solar disc along the almucantar, i.e., along a line parallel to the horizon, in a spectral band extending from 0.6 μm to 1.0 μm.

A sketch of this instrument is shown in Fig. 24. The incoming sunlight passed through the entrance aperture, A. A pinhole image of the solar disc passed through the solar disc aperture, O, into the light trap. Pinhole images of the aureole were detected at angles of 1.5, 3, and 6 deg from the center of the solar disc by the detectors, which were 1 mm diameter silicon diodes. A Wratten #29 filter was mounted on the face of each diode to block wavelengths less than 0.6 μm.

Typical aureole intensities are in the range of 10^{-4} to 10^{-6} of the brightness of the solar disc. Thus, the primary technical difficulty in constructing an aureole monitor is insuring that a negligible amount of the large flux of the solar disc scatters or diffracts into the aureole detectors. A pinhole was chosen for the entrance aperture rather than a lens, because a lens at that position would need to be inherently a very low scatter fabrication and would need to be kept extremely clean. Diffraction of light from the pinhole into the aureole detectors can be calculated, and thus designed to be negligibly small. The ratio of diffracted to incident light is given by (Ref. 12)

$$I/I_o = \left[\frac{2J_1(x)}{(x)}\right]^2$$

where

$$x = \frac{\pi D \sin\theta}{\lambda}$$

J_1 is the first order Bessel function

D is the diameter of the aperture

θ is the angle of diffraction

λ is the wavelength of light

I/I_o has numerous maxima and minima. Its maximum value falls below 10^{-6} for $x \approx 150$, and continues to fall as x increases.

For

$D = 0.095'' = 2.413 \times 10^3 \mu m$

$\lambda = 0.75 \mu m$

$x = 150$

$\theta = 51$ min.

The solar disc subtends a half angle of 16 min. This is smeared by the finite size of the entrance aperture to 21 min. at the detector plane. Thus light diffracted into the 1-1/2 deg detector is much less than 10^{-6} even from the edge of the solar image, next to that detector. The light diffracted into the 3 and 6 deg detectors is much less even than that scattered into the 1-1/2 deg detector. Therefore, diffraction from the entrance aperture is negligible compared with the aureole signal in this system.

The solar disc aperture, O, allows the intense flux of the solar image to pass into the light trap. The diameter of the solar disc at this point is 0.28 inch. This is blurred to a diameter of 0.375 inch by the finite size of the entrance aperture. It is smeared even farther to about 0.40 inch by diffraction from the entrance aperture. The diameter of the aperture O of 0.52 inch allows some margin. A separate unit, boresighted with the aureole monitor, was used to keep the solar image centered in the solar disc aperture. This also maintained the aureole detectors at the proper angles. The design of the light trap, baffles, etc., limits the light from the solar disc that scatters inside the instrument into the aureole detectors to $\sim 2 \times 10^{-10}$ of the intensity of the image of the solar disc.

A separate unit, boresighted with the aureole monitor, was added to measure the brightness of the center of the solar disc in the same wavelength band as that used to monitor the aureole brightness. Figure 25 shows a solar aureole monitor in operation.

APPENDIX C

IBM BYTE TO CDC WORD CONVERSION PROGRAM.

This routine for use on Control Data 6000-7000 series computers converts information from records generated on 8 bit byte oriented computers such as XDS computers or IBM 360-370 computers to convenient CDC formats. The routine is written in the CDC assembler language, COMPASS, and is compatible with CDC RUN Fortran.

Depending on the source of bytes for the conversion to CDC format the routine may be used in any of three modes.

Mode 1	Bytes are supplied by the user in the argument array.
Mode 2	Bytes are supplied by the user in a separate array.
*Mode 3	Bytes are supplied by the user as blocks on a file.

The different modes are indicated to the routine by the values in the single array which is the argument of the subroutine for all calls. The specific values will be discussed later.

The specific type of conversion desired is indicated by the entry point of the routine which is called. These entries are:

NXBYTE This entry returns bytes to the user as directed by the argument array. Bytes are right justified with zero fill. The bit pattern is exactly that appearing in the desired bytes. No conversions are made.

---

*In mode 3 the file reading is done by the routine employing the Record Manager under the CDC SCOPE 2.0 operating system on the 7600 computer. Use of Mode 3 under different operating systems might require some modifications to the routine. Modes 1 and 2 are believed to be independent of operating system.

IHEX — The CDC display code corresponding to the hexidecimal equivalent of the bytes desired is returned right justified and blank filled.

IEBCDC — The CDC display code corresponding to the byte is returned right justified with blank fill. Upper and lower case letters are not distinguished. For the assignment of symbols in the CDC character set to the IBM hex codes and symbols see Table C-I. The symbol ∨ (display code 66_8) is returned for all bytes which do not correspond to a letter, a number, or one of the symbols defined in Table C-I.

INT2 — The 1's complement integer corresponding to the 16 bit 2's complement integer provided in two bytes will be returned.

INT4 — The 1's complement integer corresponding to the 32 bit 2's complement integer provided in four bytes will be returned.

REAL4 — The CDC floating point number corresponding to the 32 bit IBM floating point number contained in four bytes will be obtained and returned.

REAL8 — The single precision CDC floating point number obtained from the 64 bit IBM format floating point number contained in 8 bytes by rounding the 56 bit IBM fraction to 48 bits and converting to CDC format is returned.

SKPRCD — No value is returned. This entry reads a new block from the file (Mode 3 operation) and initilizes the pointers so that the next call for bytes in sequence will start at the beginning of the new block.

Except for SKPRCD, which returns no values, all entry points are used as Fortran functions. All of the entries are called with one

argument, an array of at most 10 words. (Mode 1 requires only a 2 word array.) The significance of the various words in the array is as follows:

Word 1 The byte location or bytes to be converted.

If word 2 is positive (mode 2 or 3) --

This word indicates the location of the next byte desired.

If word 1 is positive --

This word is the number of the first byte desired from the array or block for this conversion. The first byte of the array or block is numbered 1.

If word 1 is negative --

The next bytes in sequence will be obtained. On the first call the first byte of the block or array will be returned except in mode 2 operation a negative value is not allowed on the first call.

In both cases this word will be set to -1 on return to the user.

If word 2 is negative (mode 1) --

Word 1 contains the bytes to be converted to CDC format right justified with zero fill. The contents of word 1 will not be changed.

Word 2 The mode of operation and the number of bytes desired for conversion.

For NXBYTE this must be between 1 and 7, otherwise only one byte will be returned.

For IHEX if this word is positive the bytes are taken from the block or array being converted and the value of this word should be brtween 1 and 5. If it's value is 6 or 7, then 6 or 7 bytes will be extracted from the array or block but only the 6th or 7th byte will be converted. For values greater than 7 only one byte will be extracted and converted.

If the value of this word is between -1 and -5 the right hand number of bytes from word 1 of the argument array will be converted. If it is zero or less than -5 only the rightmost byte of word 1 of the argument array will be converted.

For REAL8 if this word is positive it's value will be ignored and it will be set to 7 on return.

If this word is negative the most significant byte of the 8 required (the IBM sign-exponent byte) will be taken as the righthand 8 bits of the complement of this word. The other 7 bytes will be taken from the right-hand 56 bits of word 1 of the argument array.

For all other entries only the sign of this word is important. If the sign is positive the required bytes are drawn from the block or array being converted and word 2 will be set to the number of bytes required for that particular conversion.

If the sign of word 2 is negative the value of word 2 is ignored and the number of bytes required for the conversion are taken from word 1 of the argument array.

If bytes are being extracted from a block or array (word 2 positive, mode 2 or 3 operation) and if bytes beyond the end of the block or array are required by the combination of values appearing in words 1 and 2 then mode 3 operation is assumed and an attempt will be made to read a new block into the array.

The rest of the words in the argument array are needed only for mode 2 or 3 operation. See the discussion of the modes to determine which should be set by the user in each of the modes of operation.

Word 3 This word contains the length of the array or block in bytes.

Word 4 This word contains the number of bytes remaining in the array or block.

Word 5 This word contains the bit position in the word corresponding to the next byte to be obtained. This quantity is maintained by the routine and should not be modified externally.

Word 6 This word contains the address of the word in the array in which the next byte begins. This quantity is maintained by the routine and should not be modified externally.

Word 7 This word is not used at present.

Word 8 This word indicates the name of the file from which blocks are obtained for mode 3 operation. It may be an integer, n, from 1 to 99 to indicate the file name in the usual Fortran convention of TAPEn. It may also contain a file name in left justified zero filled display code. In either case the file name must be mentioned on the program card. No file card is required in the control cards. The file is defined by the routine to be RT=U, BT=K and RB=1 and so does not have the usual Fortran file definition.

Word 9 This word contains the address of the first word of the buffer array which contains the block or array to be converted in modes 2 and 3 operation. (This may be obtained conveniently with the Fortran function LOCF. See the examples.)

In mode 2 operation this buffer is filled by the user with the array he desires to make conversions from.

In mode 3 operation this buffer is filled from the file defined by word 8, one block at a time. The buffer

must be long enough to contain the longest block expected. That length will be 8 times the maximum number of bytes expected divided by 60 and rounded to the next highest integer.

Word 10 This word contains a flag which indicates the status of the file after the most recent call to the routine. Possible values are:

0 No change has occurred in the file or buffer, or a new block was read in successfully from the file by SKPRCD.

1 Bytes beyond the end of the current array or block were requested. A new record was satisfatorily read in but no data has been extracted from it. The word and byte pointers are set so that the next call to the routine will start at the beginning of the block or array if word 1 of the argument array is negative at that time.

2 An end of section, end of partition or end of information was encountered on the read. The type of end of data will be indicated by a message in the OUTPUT file.

3 A parity error was encountered on the last read.

4 All other record manager detected errors detected on the last read are indicated by the value 4. The RM error number will be indicated in a error message put into the OUTPUT file.

The various modes of operation, which depend on the source of bytes for conversion, are indicated to the routine as described below.

Mode 1 The bytes to be converted are supplied by the user right justified in word 1 of the argument array. This mode is indicated by a negative sign in word 2 of the argument

array. The value of word 2 is ignored except for two cases. For REAL8 conversion word 2 is the complement of the most significant byte of the word. For IHEX conversion word 2 is the complement of the number of bytes to be converted.

Mode 2 The bytes to be converted are extracted by the routine from an array supplied by the user. In this mode the following words are set, at least initially by the user.

Word 1 On the first call this word cannot be negative. A specific byte location must be specified. Subsequent calls may specify the byte desired explicitly or may obtain the bytes in sequence by setting (or leaving) this word set to a negative value.

Word 2 This word must be positive. See the word description for limitations on its value.

Word 3 This must be set by the user to the length, in bytes, of the array from which the bytes will be drawn. This must be done before the first call to the routine and need not be reset unless a new byte string of different length is put into the array by the user.

Word 4 This must be set by the user, before the first call to the routine, to the length, in bytes, of the array from which the bytes will be drawn, i.e., it is set to the same value as word 3. It shouldn't be reset by the user thereafter unless a byte string of different length is put into the array by the user.

Word 9 This word must contain the address of the first word of the array containing the bytes to be converted.

Words 5, 6, 7, 8 and 10 are not set by the user.

Mode 3 The bytes are extracted from blocks obtained from a file. In this mode the following words are set, at least initially by the user. In addition the file name must be mentioned in the main program card.

Word 1 This word may have any value allowed in the word description on any call.

Word 2 This word must be positive. See the word discription for limitations on its value.

Word 4 This word should be set to a negative value on the first call of the program to assure reading the first block into the buffer. Thereafter this word need not concern the user.

Alternatively the first block may be input with the SKPRCD function and this word always ignored.

Word 8 This must indicate the file name from which the records will be obtained. See the word description for a discussion of possible forms.

Word 9 This word contains the address of the first word of a storage area used to store blocks as they come in from the file. The length required is discussed in the word description.

Words 3, 5, 6, 7, and 10 are not set by the user but may contain information of interest to him as described under the various word descriptions.

Length: The subprogram is 415_8 words long.

Other Routine s Required: No other routines unavailable with a normal RUN Fortran job are called. Several RUN Fortran Library routines are called however in Mode 3 operation.

Error Mes sages: Error Messages are writtin on the OUTPUT file whenever a record manager error occurs or when an end of data is encountered in mode 3 operation.

Notes and Examples

1) IEBCDC can conveniently be combained with the routine STRMOV to transform long strings of EBCDIC characters into display code character strings. For example we assume the mode of the subprogram will be 2. (User supplied arrays.) Assume that a user written function routine, IBYTES, is used to fill the array IAR with the bit pattern to be converted and that the function returns as its value the length in bytes of the array filled. Assume that in this particular array there is a string of 108 EBDCIC characters starting with byte 325. It is desired to transform that string to display code, store it in an array ITST and print it out.

The following coding will fill the buffer array by means of the here undescribed routine IBYTES, set up all required words for mode 2 use, convert the string of characters desired and print it.

```
      COMMON IAR(512)
      DIMENSION ICONT(10),ITST(11),ITTM(2)
      ICONT(3) = IBYTES(IAR)
      ICONT(4) = ICONT(3)
      ICONT(9) = LOCF(IAR)
      ICONT(1) = 325
      ITST(11) = 1H
      DO 105 I=1,108
      CALL STRMOV(IEBCDC(ICONT),10,1,ITST,I)
  105 CONTINUE
      WRITE (6,2) ITST
    2 FORMAT (* ITST = *,6A10,/8X,5A10)
```

The *results are:*

```
ITST = THIS ISA MESSAGE. NUMBERS - 0123456789876543210 SYMBOLS ≥.<(
       +↓↑v$*);≤-/,%#>^:Ξ( )=≠  END OF CHARACTER STRING.
```

2) For calls to NXBYTE and IHEX the number of bytes to be converted may be, within limits, specified. The results of varying the number of bytes even beyond the allowed limits is indicated by the following coding, again applied to the character string of the preceeding example. This example also illustrates the use of a mode 1 call. This example presupposes the initialization coding of example 1.

```
      ICONT(1) = 325
      ITST(2) = -5
      DO 135 I = 1,9
      ICONT(2)=I-1
      ITST(1) = NXBYTE(ICONT)
      ITST(3) = IHEX(ITST)
      WRITE (6,5)  ITST(1),ITST(3),ITST(3)
    5 FORMAT (' ITST = ',O20,5X,A10,5X,O20)
  135 CONTINUE
      ICONT(1) = 325
      DO 140 I=1,6
      ICONT(2)=I
      IOUT = IHEX(ICONT)
      WRITE (6,5) IOUT,IOUT
  140 CONTINUE
```

The results of executing this are:

```
 ITST = 0000000000000000343     00000000E3     3333333333333330536
 ITST = 0000000000000000310     00000000C8     3333333333333330343
 ITST = 0000000000000144742     000000C9E2     3333333333303440535
 ITST = 0000000000020144742     000040C9E2     3333333337303440535
 ITST = 0000000030120152305     00C140D4C5     3333033437330437040
 ITST = 0000016134260343705     E2E2C1C7C5     0535053503403420340
 ITST = 0002264032571152302     40D5E4D4C2     3733044005370437033
 ITST = 0305663611003004036O    E2406040F0     0535373413337330633
 ITST = 0000000000000000361     00000000F1     3333333333333330634
 ITST = 5555555555555550536           E3
 ITST = 5555555555503430344           C8C9
 ITST = 5555555503537330344           E240C9
 ITST = 5555053503437330437           E2C140D4
 ITST = 0340053503503340342           C5E2E2C1C7
 ITST = 5555555555555550437             D4
```

3) These examples illustrates the use of calls for number conversion. Assume the array of the previous examples has a sequence of 14 single IBM precision (32 bit) floating point words starting at byte number 121. The following coding will extract these numbers and convert them to CDC floating point format. The other numerical conversions may be applied in exactly the same way, changing only the entry point name used to obtain the various conversions. This example presupposes the initialization coding of example 1.

```
      ICONT(1) = 121
      DO 110 I=1,14
      OUT = REAL4(ICONT)
      WRITE(6,3) OUT,OUT
    3 FORMAT (* OUT = *,E20.10,5X,O20)
  110 CONTINUE
```

The results of executing this are:

```
 OUT =      .1000000000E+01     1720400000000000000
 OUT =     -.1000000000E+01     6057377777777777777
 OUT =      .1492500000E+03     1727452400000000000
 OUT =     -.1492500000E+03     6050325377777777777
 OUT =     0.                   0000000000000000000
 OUT =     -.5000000000E+00     6060377777777777777
 OUT =      .1562500000E-01     1712400000000000000
 OUT =     -.1562500000E-01     6065377777777777777
 OUT =     -.1500000000E+02     6054037777777777777
 OUT =      .1500000000E+02     1723740000000000000
 OUT =      .5397605347E-78     1314400000000000000
 OUT =     -.5397605347E-78     6463377777777777777
 OUT =      .7237005146E+76     2314777777700000000
 OUT =     -.7237005146E+76     5463000000077777777
```

Table C-1. IEBCDC Symbol Conversion Code

HEX Value	IBM Symbol	CDC Display Code (Octal)	CDC Symbol
40	space	55	blank
4A	¢	75	≥
4B	.	57	.
4C	<	72	<
4D	(	51	(
4E	+	45	+
4F	|	71	↓
50	&	70	↑
5A	!	66	∨
5B	$	53	$
5C	*	47	*
5D	)	52	)
5E	;	77	;
5F	¬	74	≤
60	-	46	-
61	/	50	/
6B	,	56	,
6C	%	76*	¬*
6D	—	65	⌜
6E	>	73	>
6F	?	67	∧
7A	:	63	:
7B	#	60	≡
7C	@	61	⊏
7D	'	62	⊐
7E	=	54	=
7F	"	64	≠

*Octal 76 prints % on 200 terminals and ¬ on high speed Line printers.